Investigation of electron-beam deposition and related damage in p-Si by means of Laplace and conventional deep-level transient spectroscopy

By

Helga Tariro Danga

Submitted in partial fulfilment of the requirements for the degree

Philosophiae Doctor (Physics)

in the Faculty of Natural and Agricultural Science

Department of Physics

University of Pretoria

Pretoria

Supervisor: Prof W.E. Meyer

Co-supervisor: Prof F.D. Auret

July 2019

Investigation of electron-beam deposition and related damage in p-Si by means of Laplace and conventional deep-level transient spectroscopy

Helga Tariro Danga

The study of defects in semiconductors has been on-going for over 50 years. During this time, researchers have been studying the origins and identity of process induced defects, a task which has proved to be very demanding. While defects in silicon, the most widely used semiconductor, have been widely studied, there is more literature on n-type silicon than on p-type silicon. Compared to n-type silicon, p-type silicon is challenging to work with when it comes to making good Schottky diodes. A good rectifying device is essential for the performing of electrical characterisation techniques such as deep-level transient spectroscopy. In spite of this challenge p-silicon cannot be ignored. Many of the electronic devices are a combination of both n- and p-silicon therefore the need to understand the electronic properties of both materials.

In this thesis, defects introduced in p-Si by electron beam deposition (EBD) were investigated. In order to understand these defects better, defects introduced by conditions of electron beam deposition (EBD) without metal deposition, were investigated. This process will be referred to as electron beam exposure (EBE). Finally, the defects were compared to defects induced by alpha-particle irradiation.

EBD defects, introduced during electron beam deposition (EBD) of titanium (Ti) contacts on p-Si were investigated. The Schottky contacts were annealed within a temperature range of 200–400 °C. Current-voltage (*I-V*) measurements were conducted to monitor the change in electrical characteristics with every annealing step. Deep-level transient spectroscopy (DLTS) and Laplace-DLTS techniques were employed to identify the defects introduced after EBD and isochronal annealing of the Ti Schottky contacts. DLTS revealed that the main defects introduced during metallisation were hole traps with activation energy of 0.05 eV, 0.23 eV and 0.38 eV. Depth profiles of these defects showed that the formed close to the interface within a depth of 0.4 μm.

Defects induced by EBE were studied by exposing samples for 50 minutes after which nickel (Ni) Schottky contacts were fabricated using resistive deposition. Only one defect with an activation energy of 0.55 eV was observed. This activation energy is similar to that of the I-

defect. DLTS depth profiling revealed that the defect could be detected up to a depth of 0.8μm below the junction, which is significantly deeper than EBD defects.

Defects induced when p-Si was irradiated by alpha particles from a 5.4 MeV americium (Am) 241 foil radioactive source with a fluence rate of 7×10^{6} cm^{-2} s^{-1} at room temperature were investigated. After exposure at a fluence of 5.1×10^{10} cm^{-2}, hole traps with the following activation energies were observed: 0.10 eV, identified as a tri-vacancy related defect, 0.33 eV, the interstitial carbon (C_i), 0.52 eV, a B-related defect and 0.16 eV. Low temperature irradiation experiments were also carried out using alpha- particles with the same fluence rate. Measurements were taken between 35 K and 120 K. The defect levels were at 0.10 eV, 0.14 eV and 0.18 eV. These levels were attributed to the boron-substitutional vacancy complex, the mono-vacancy and a vacancy-related defect, respectively. We conclude that EBD and EBE induced more complex defects than those induced by alpha-particle irradiation.

Key words: Schottky contact, defects, Laplace deep-level transient spectroscopy, p-type silicon, low temperature irradiation, electron beam deposition, alpha-particle induced defects, electron beam exposure

Declaration

I Helga Tariro Danga declare that this thesis, which I hereby submit for the degree of Philosophiae Doctor (PhD) in Physics at the University of Pretoria, is my own work and has not been previously submitted by me for a degree at this or any other tertiary institution.

Signature:

Student number: 12374718

Date: July 2019

For my boys

“hope that is seen is no hope at all. Who hopes for what they already have? But if we hope for what we do not yet have, we wait for it patiently’’.

Romans 8:24-25 New International Version

Acknowledgements

- My supervisor Prof Walter E. Meyer for his guidance, patience and support.
- My co-supervisor Prof Danie Auret for guiding me throughout my postgraduate studies.
- Mr Johan van Rensburg and Mr Matshisa Legodi for helping me with all the technical aspects of this work.
- I would like to extend many thanks to the members of the thin films group for all the encouragement.
- I would like to especially thank Dr S.M Tunhuma, Miss N. Mrwetyana, Dr F.Taghizadeh, Mr K. Ostvar, Mr W.A. Barnard, Dr P.N.N Ngoepe, Mr A. Mayimele, Prof J.M. Nel, Dr E. Omotoso and Dr A.T. Paradzah.
- I would like to thank the head of department Prof. Chris Theron for affording me the opportunity to work part-time in the department.
- The University of Pretoria for funding.
- My friends and family for their support and encouragement.
- My mother for her unwavering love and support.
- Above all, I thank God for the grace and mercy He continuously shows me.

Contents

1 Introduction 1
References 3
2 Theory 4
2.1 General properties of silicon 4
2.1.1 Crystal structure 4
2.1.2 Growth methods 5
2.1.3 The band structure of silicon 8
2.1.4 Electrical properties 9
2.2 Theory of metal–semiconductor junctions 10
2.2.1 The depletion region 10
2.2.2 Barrier formation 12
2.2.3 Reverse and forward bias 12
2.3 Defect theory 13
2.3.1 Point defects 15
2.3.2 Capture and emission by electronic defect states 16
2.4 Defect introduction mechanisms 21
2.4.1 Process induced defects 21
2.4.2 Radiation-induced defects 22
References 25
3 Experimental Techniques 29
3.1 Sample preparation 29
3.1.1 Silicon wafer cleaning procedure 29
3.1.2 Schottky contact fabrication 29
3.1.3 Ohmic contact fabrication 31
3.2 Electron beam exposure (EBE) 31
3.3 Sample annealing 32
3.4 Atomic force microscopy (AFM) 33
3.5 Sample irradiation 34
3.6 Electrical characterisation techniques 35
3.6.1 Current-voltage measurements 35
3.6.2 Capacitance-voltage measurements 35
3.6.3 Deep-level transient spectroscopy (DLTS) 36
3.6.4 The concepts of DLTS 39

3.6.5 Laplace-DLTS ... 41
3.6.6 The concepts of Laplace-DLTS ... 41
3.6.7 Deep level transient spectroscopy measurement set-up ... 43
References ... 45
4 Results and discussion ... 47
4.1 Process induced defects ... 47
4.1.1 Annealing studies of electron beam deposition induced defects ... 47
4.1.2 Electron beam exposure ... 53
4.2 Radiation-induced defects ... 57
4.2.1 Alpha-particle irradiation at room temperature ... 57
4.2.2 Low temperature alpha-particle irradiation ... 61
4.3 General discussion ... 65
4.3.1 Differences in defects formed during EBD of Ti and Ni ... 65
4.3.2 Alpha- particle irradiation ... 67
References ... 69
5 Conclusion ... 71
5.1 Electron beam deposition and electron beam exposure induced defects ... 71
5.2 Room-and low-temperature alpha-particle induced defects ... 72
5.3 Future work ... 72
6 Appendix ... 73

List of figures

Figure 2-1 A picture showing a 3 inch Czochralski-grown Si wafer used in this study............4
Figure 2-2 The diamond structure of Si generated by Crystal Explorer 3.1, using data from the inorganic crystal structure data base taken from ref [1]..5
Figure 2-3: Figure 2-3: The Czochralski method of growing Si [6]...6
Figure 2-4: The Float-zone method of growing Si [6]..7
Figure 2-5: Schematic of an oxide-MBE set-up that shows the epitaxial integration of perovskite-based oxides on Si by means of a means of metallic evaporation under oxygen [9]. 8
Figure 2-6: Direct and indirect electron transitions in semiconductors : (a) direct transition with accompanying phonon and (b) indirect transition through a defect level [3]...................9
Figure 2-7:Visualisation of acceptor action of boron using the bonding model redrawn from ref [13]. 10
Figure 2-8: Schottky barrier between a p-type semiconductor and a metal: (a) band diagrams before contact; (b) band diagram for the junction at equilibrium redrawn from [10, 17]. 11
Figure 2-9: Energy-band diagrams of metal on p-type semiconductors under different biasing conditions. (a) forward bias (b) thermal equilibrium (c) reverse bias [10, 18].......................13
Figure 2-10: Common point defects in semiconductors. Substitutional and interstitial defects involve a foreign atom, whereas self-interstitials are due to an original atom [23]................16
Figure 2-11: Representation of electron (n), hole (p), emission (e) and capture (k) processes between level ET and the conduction and valence bands [28]. 17
Figure 2-12: Illustration of lattice displacement after irradiation using a charged alpha-particle [44]...23
Figure 3-1: Schematic of the resistive deposition system set-up at the University of Pretoria. 30
Figure 3-2: Schematic diagram of the EBD system at the University of Pretoria..................31
Figure 3-3 A sketch of the annealing furnace used in this study at the University of Pretoria. 33
Figure 3-4: Illustration of the AFM set-up after reference [6]...34
Figure 3-5: diagram showing alpha-particle irradiation of a silicon sample. 35
Figure 3-6: A block diagram of I-V and C-V station set up at the University of Pretoria. 36
Figure 3-7: The variation of the depletion region width and capacitance after the application of a voltage bias and filling pulse sequence for a hole trap in an p-type semiconductor [11].38
Figure 3-8: A schematic diagram showing (a) the change in the shape of the DLTS transient with increasing temperature and (b) the DLTS signal obtained from the transients as a function of sample temperature [12]...40
Figure 3-9: A block diagram of DLTS set up at the University of Pretoria. 44
Figure 4-1 :The forward and reverse bias I-V characteristics of Ti/Si and Ni/Si Schottky contacts fabricated using EBD...66
Figure 4-2: The DLTS spectra of (a) Ti/Si Schottky contacts and (b) Ni/Si Schottky contacts. 67
Figure 4-3: All defects measured in the current study using conventional and Laplace –DLTS. 68

1 Introduction

Silicon (Si) is the building block of much of the advanced technology of today. This is because Si is abundant, durable, stable and non-toxic. Moreover, Si processing is well controlled at the industrial level, and the electronic properties and defect physics of this element are theoretically well understood [1, 2].

Si has a large impact on the economy of the modern world and is of fundamental importance in the technological field, particularly in the solar cell industry. Due to the decreasing resource of fossil fuels and demand of reducing carbon emission during energy production, exploration of new clean energy is of great interest and fundamental importance [2]. There are other materials which can be used for solar cell fabrication for example gallium arsenide but Si solar cells using mono-crystalline, polycrystalline, or amorphous Si in the form of wafers or thin-films still dominate the current photovoltaic market share. According to Sunil Kumar Singh, a lead semiconductor equipment analyst from Technavio, "Consumer electronic products have transformed substantially in recent times with vendors introducing new age electronic gadgets with smart features including touch displays, keypads, in-built memory-based appliances, and automated coffee machines. After these developments, the need for silicon wafers has become more evident as they are used in almost all the home appliances."[3].

Although much work has been done on the electrical properties of defects in Si, there are still several loose ends that need to be tied. In literature, there are more reports on n-type Si than p-type Si - this is because of the technical constraint of p-type material [4, 5]. Compared to n-Si, p-Si is challenging to work with when it comes to making a good rectifying Schottky diode device. For one to carry out electrical characterisation techniques such as deep-level transient spectroscopy (DLTS), a good rectifying device is essential. In spite of this challenge p-Si cannot be ignored. Many of the electronic devices are a combination of both n- and p-Si therefore the need to understand the electronic properties of both materials.

Defects can be beneficial or deleterious to the electronic properties of semiconductors, depending on application. Defects are often unintentionally introduced into semiconductors during material growth. With most material growth methods defects are unavoidable. The study of defects in Si has been going on for over 50 years but an understanding of their nature and

existence is still not clear. The study of the electrical properties of defects has been helpful for the defect engineering field. Researchers have been able to determine useful characteristics of some defects for example the temperatures at which defects are eliminated or introduced into the material. A good example is rapid thermal annealing experiments with fast cooling rates carried out on Si wafers to investigate the influence of the free vacancy concentration on oxygen precipitation. By heating the wafers to above 1150°C, detectable concentrations of Frenkel pairs are created in the wafer bulk [6].

In this thesis, electron-beam deposition and radiation-induced defects were studied by means of conventional and Laplace-DLTS. Chapter 2 covers the theoretical aspects of the study. Chapter 3 gives an account of the experimental techniques used in this study. Chapter 4 gives a detailed discourse of the present work in the form of publications from 2016 to 2019. Chapter 5 is the conclusion and a brief discussion on future work.

References

[1] S. Botti, J.A. Flores-Livas, M. Amsler, S. Goedecker, M.A.L. Marques, *Low-energy silicon allotropes with strong absorption in the visible for photovoltaic applications*, Physical Review B, **86** (2012) 121204-121201.

[2] Q. Wang, B. Xu, J. Sun, H. Liu, Z. Zhao, D. Yu, C. Fan, J. He, *Direct Band Gap Silicon Allotropes* Journal of the American Chemical Society, **136** (2014) 9826−9829.

[3]https://www.businesswire.com/news/home/20170608006155/en/Global-Semiconductor-Silicon-Wafer-Market---Competitive, *Global Semiconductor Silicon Wafer Market 2017-2021*, in, 2017.

[4] B.L. Smith, E.H. Rhoderick, *Schottky barriers on p-type silicon* Solid-State Electronics, **14** (1971) 71-75.

[5] C. Nyamhere, F. Cristiano, F. Olivie, E. Bedel-Pereira, Z. Essa, *Electrical and optical characterization of extended defects induced in p-type Si after Si ion implantation* Physica Staus Solidi c, **11** (2014) 146–149.

[6] W.v. Ammon, A. Sattler, G. Kissinger, *Defects in Monocrystalline Silicon* in: S. Kasap, P. Capper (Eds.) *Springer Handbook of Electronic and Photonic Materials*, Springer International Publishing AG 2017.

2 Theory

This chapter presents some of the important background knowledge regarding Si and semiconductors in general. The crystal structure and electrical properties of Si as well as the theory of defects in semiconductors are discussed. There is also a brief discussion on defect introduction mechanisms in semiconductors.

2.1 General properties of silicon

In 1787 Antoine Lavoisier postulated about the existence of Si, the 14th element in the periodic table. The name silicon stems from the Latin word *silex*, meaning hard stone, describing its strong but rather brittle nature. Si is the eighth most common element in the universe and second most common in the Earth's crust, with over 90% of the lithosphere composing of silicate minerals [1]. At room temperature, Si exists as amorphous or crystalline. Si single crystals have a greyish, metallic appearance as shown in Figure 2-1.

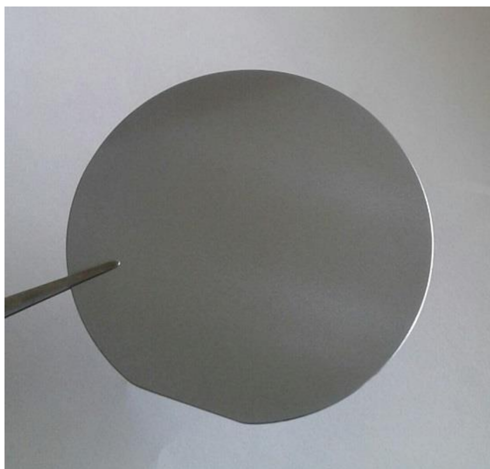

Figure 2-1: A picture showing a 3 inch Czochralski-grown Si wafer used in this study.

2.1.1 Crystal structure

Si, a group IV element, crystallises in the diamond cubic lattice structure [2]. Each Si atom has four bonds, one to each of its four nearest neighbours as illustrated in Figure 2-2. This lattice structure can be constructed from two interpenetrating face-centred cubic lattices displaced from each other along the body diagonal by a distance equal to one-fourth of its length [3].

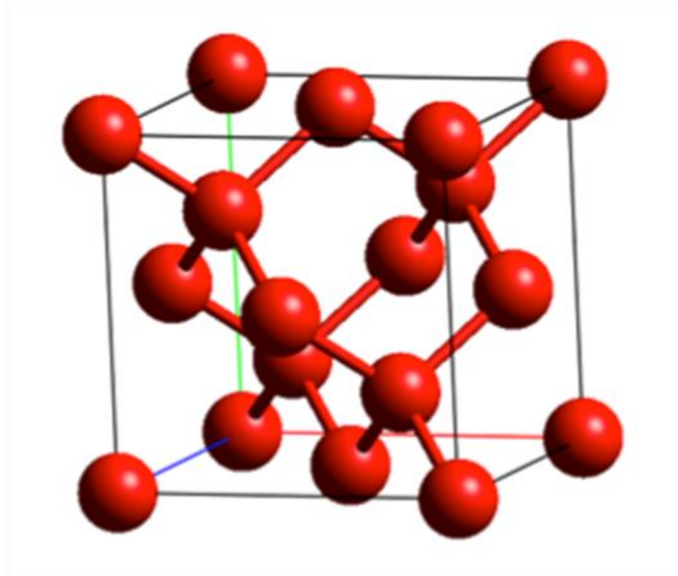

Figure 2-2: The diamond structure of Si generated by Crystal Explorer 3.1, using data from the inorganic crystal structure data base taken from ref [1].

2.1.2 Growth methods

The raw material for Si crystal is silicon dioxide (SiO_2). SiO_2 is reacted with C in the form of coke in an arc furnace at very high temperatures (approximately 1800°C) to reduce SiO_2 to Si and CO. This forms metallurgical-grade Si (MGS) which has impurities such as Fe, Al and heavy metals at levels of several hundred to several thousand parts per million (ppm). The MGS is refined further to yield semiconductor-grade or electronic-grade Si (EGS), in which the levels of impurities are reduced to parts per billion (ppb) [3].

2.1.2.1 Czochralski

The design of this technique was based on pulling fibres of different metals from their melts. The obtained metallic wires proved to be single crystals. The results of these experiments were published by Czochralski in Zeitschrift für Physikalische Chemie in 1918 [4]. This method allowed him to obtain good quality single crystals of pure metals like Sn, Pb, Zn grown in air. Later on, a modified Czochralski method was adopted for crystal growth of semiconductors and oxides for electronic applications [5]. Figure 2-3 shows the Czochralski process.

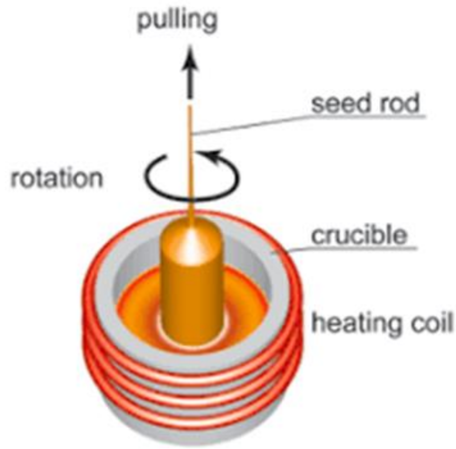

Figure 2-3: Figure 2-3: The Czochralski method of growing Si [6].

2.1.2.2 Float Zone

The Float Zone (FZ) crystal growth method produces silicon crystals of higher purity and longer minority carrier lifetime compared to the Czochralski technique. These properties are beneficial to the solar cells giving value to the cells, PV modules and solar farms. However, there are also some extra costs associated with the feedstock needed for the FZ process, and although the crystal growth process is cheaper and more efficient than the dominating Czochralski crystal growth method, it seems that these overall benefits cannot fully compensate for the extra expenses of raw materials [7]. Figure 2-4 gives an idea of the float zone process.

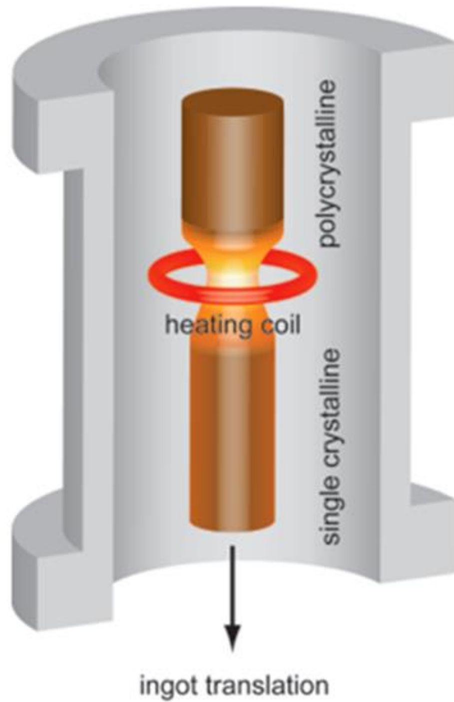

Figure 2-4: The Float-zone method of growing Si [6].

2.1.2.3 Epitaxy

Epitaxy is the technique of depositing an ultra-pure mono-crystalline layer on a mono-crystalline substrate [8]. The deposited film is called the epitaxial layer or epitaxial film. The epitaxial layer can be grown from gaseous or liquid precursors. The substrate acts as a seed crystal therefore the deposited film takes on the lattice structure and orientation of the substrate. The epitaxial growth technique enables the growth of a variety of crystals for device applications, having properties specifically designed for the electronic or optoelectronic device being made [3]. There are a variety of epitaxy techniques used for crystal growth. These include chemical vapour deposition (CVD), metal oxide chemical vapour deposition (MOCVD), liquid phase epitaxy (LPE) and molecular beam epitaxy (MBE) [3]. Figure 2-5 gives an idea of how the oxide-molecular beam epitaxy process is carried out.

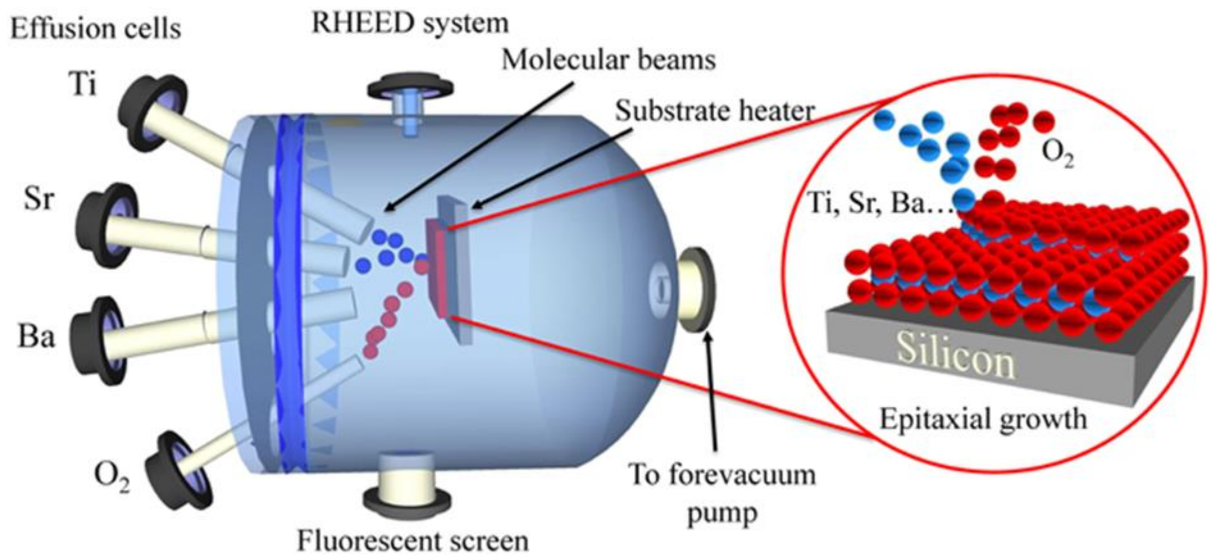

Figure 2-5: Schematic of an oxide-MBE set-up that shows the epitaxial integration of perovskite-based oxides on Si by means of a means of metallic evaporation under oxygen [9].

2.1.3 The band structure of silicon

A direct band gap semiconductor is a material where the conduction band minimum and valence band maximum occur at the same wave number k. What happens is that an electron moves from the conduction band minimum to the valence band maximum without a change in momentum and the energy lost in the transition can be emitted as a photon. A material in which the conduction-band minimum appears at a different point to the valence-band maximum, is called an indirect-gap semiconductor [10]. An electron in the conduction band minimum of an indirect semiconductor such as Si cannot fall directly to the valence band maximum but must undergo a momentum change as well as changing its energy. For example, it may go through some defect state E_T within the band gap as depicted in Figure 2-6. In an indirect transition which involves a change in k, part of the energy is generally given up as heat to the lattice rather than as an emitted photon [3].

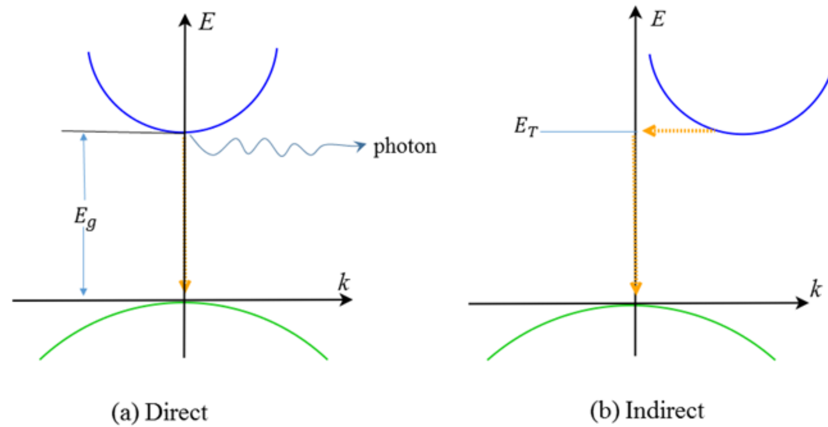

Figure 2-6: Direct and indirect electron transitions in semiconductors : (a) direct transition with accompanying phonon and (b) indirect transition through a defect level [3].

Complete energy band diagrams of semiconductors are quite complex. The detailed energy band diagrams of silicon have been presented extensively in literature [3, 10, 11]. The value of the band gap of silicon at room temperature and under normal pressure is 1.12 eV [12].

2.1.4 Electrical properties

Si is a Group 4 semiconductor. It can either be doped using Group 5 elements or Group 3 elements, depending on whether n- or p-type Si [10] material is required. Adding dopants in controlled quantities to semiconductor materials increases either electron or hole concentration. If a Si atom is replaced by a boron atom, or another atom from column 3 of the periodic table, the impurity atom contributes only three valence electrons. These three electrons form valence bonds with three of the neighbouring silicon atoms. In the fourth bond there is a missing electron, or hole. An electron from a neighbouring bond may move into this hole with very little spending of energy, leaving a hole behind [13], as shown in Figure 2-7.

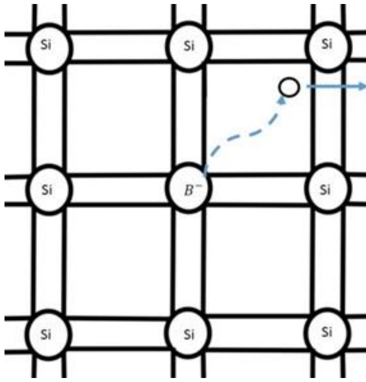

Figure 2-7:Visualisation of acceptor action of boron using the bonding model redrawn from ref [13].

2.2 Theory of metal–semiconductor junctions

Metal-semiconductor contacts have been intensively studied since the 1960s. This was greatly encouraged by their importance in semiconductor technology, both as rectifying elements and as low resistance contacts [14]. The Schottky-barrier model describes the formation of a potential barrier at the interface between a metal and a semiconductor. [10].When a metal contact is evaporated onto the surface of a semiconductor, a potential barrier is formed at the metal–semiconductor interface. This is called a Schottky contact. In this work, only the case for a p-type semiconductor will be considered.

2.2.1 The depletion region

When a semiconductor is placed in contact with a metal, an electrical double layer is set up, either between the metal and the semiconductor, or in the semiconductor itself [15].The potential barrier which forms arises from the separation of charges at the metal-semiconductor interface such that a region without mobile carriers is formed and is referred to as the depletion region W. The earliest model put forward to explain the barrier height is that of Schottky and Mott. According to this, model the barrier results from the difference in the work functions of the metal, ϕ_m and the semiconductor, ϕ_s [16].

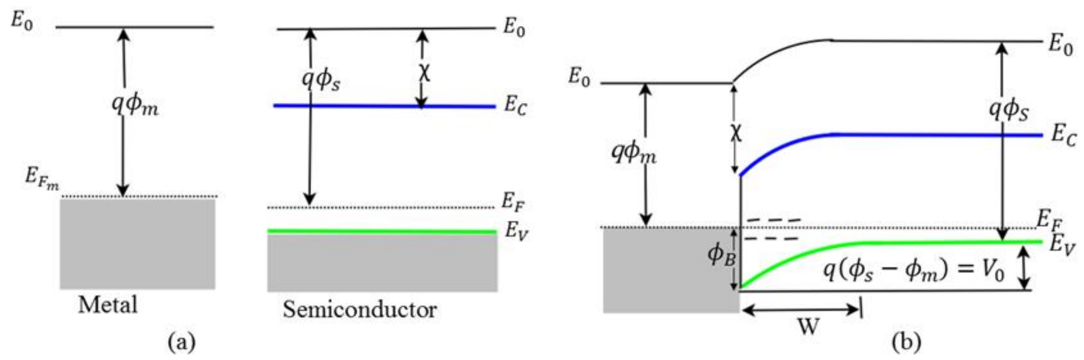

Figure 2-8: Schottky barrier between a p-type semiconductor and a metal: (a) band diagrams before contact; (b) band diagram for the junction at equilibrium redrawn from [10, 17].

2.2.2 *Barrier formation*

The energy band diagrams for p-type material in the case where the metal work function, ϕ_m is smaller than the electron affinity, χ, and the two materials are separate as shown in Figure 2-8(a). When the two are brought into intimate contact, electrons flow from the metal into the semiconductor until the Fermi level on the two sides are aligned. These electrons are minority carriers in the p-type semiconductor. After reaching the semiconductor they recombine with holes giving rise to a space charge layer of ionized acceptors as shown in Figure 2-8(b). The concentration of holes in the space charge region is very small compared to the acceptor concentration. Therefore, on the semiconductor side of the contact the space charge region consists of a depletion layer whose thickness W_0 depends on the concentration of ionized acceptor atoms. Because the current in a p-type semiconductor is carried by holes we have to look for barrier for holes in the band diagram of Figure 2-8(b). The barrier height ϕ_B for holes is given by the relation

$$\phi_B = \chi + E_g - \phi_m \qquad 2.1$$

where E_g represents the band gap of the semiconductor. Looking at Figure 2-8, it can be deduced that, according to this theory, a metal–p-type semiconductor contact is non-rectifying if the metal work function is larger than the electron affinity. Experimental results have shown that a large majority of metal-semiconductor combinations form rectifying contacts with potential barriers.

Moreover, Schottky barrier contacts on semiconductors in general have smaller barrier heights to p-type semiconductors compared to n-type semiconductors, which is why they are not frequently used in devices [16].

2.2.3 *Reverse and forward bias*

For Schottky diodes on p-type material, forward voltage V is when the semiconductor is biased positively with respect to the metal. Forward current increases as this voltage lowers the potential barrier V_0 to $V_0 - V$ and holes flow from the semiconductor to the metal. Of course, a reverse voltage increases the barrier for hole flow and the current becomes negligible that is, the Schottky barrier diode is rectifying, with easy current flow in the forward direction and little current in the reverse direction. We also note that the forward current in each case is due to the injection of majority carriers from the semiconductor into the metal. The absence of

minority carrier injection and the associated storage delay time is an important feature of Schottky barrier diodes. Although some minority carrier injection occurs at high current levels, these are essentially majority carrier devices. Their high-frequency properties and switching speed are therefore generally better than typical p-n junctions [3].

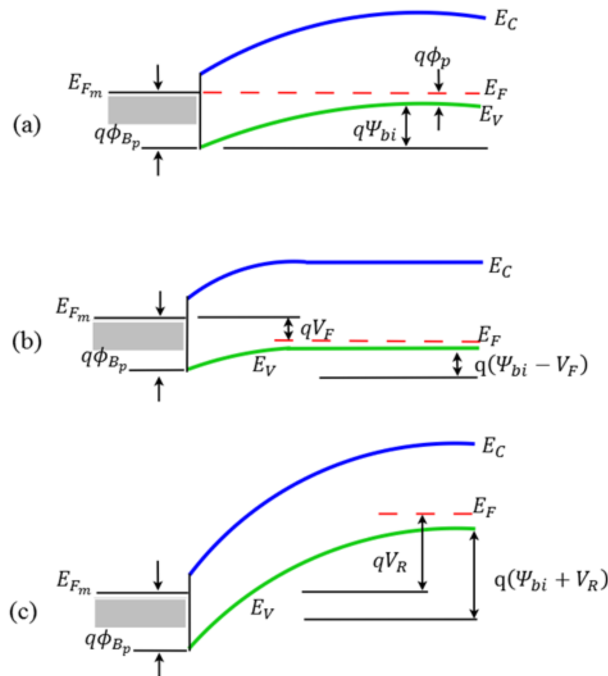

Figure 2-9: Energy-band diagrams of metal on p-type semiconductors under different biasing conditions. (a) forward bias (b) thermal equilibrium (c) reverse bias [10, 18].

2.3 Defect theory

The fabrication and development of efficient semiconductor devices requires sufficient knowledge of the identity, nature and properties of the deep levels that are native and those which are induced in the semiconductor. Depending on the application of the semiconductor, defects can be detrimental to device operation or they may enhance the operation of the device. Defects with deep states in the band gap (E_g) are usually referred to as traps, recombination centres, generation centres or deep level defects [19].

Defects in crystalline Si are often detrimental to devices notably affecting dopant diffusion during processing and finally causing leakage current. In general, defects are created as a

“response” of the crystals to strong “out-of-equilibrium” conditions generated by the processes used to fabricate the devices. More precisely, defects provide a solution to the system to lower its energy, to relax, from an excessively high-energy state toward a lower energy configuration. Consequently, it is important to know the characteristics of the defects to understand their origin. Knowledge of their features is also required to determine, on a quantitative basis, the effect of process parameters for example, annealing conditions, on their sizes and densities, thereby guiding the search for optimised process conditions [20].

2.3.1 Point defects

Point defects are defects that are localised at or around a lattice point. Point defects include vacancies which are formed when an atom is missing from its lattice site and interstitials which occur when an atom is in an irregular position in the lattice structure [21]. There are also impurities which are foreign atoms found isolated inside the lattice [22] and Frenkel-pairs where a vacancy and an interstitial are in close proximity as shown in Figure 2-10. This occurs when an atom vacates its original position in the lattice and occupies an interstitial position in the crystal [23].

Using the Gibbs potential, defects can be classified as equilibrium defects or non-equilibrium defects:

- Equilibrium defects decrease the free energy causing the material to be more thermodynamically stable. This is because their production results in an increase in configurational enthalpy. They usually arise in the lattice during material growth [24].
- Non-equilibrium defects increase the free energy causing the material to be less stable. The increase in enthalpy dominates the increase in entropy. In the presence of sufficient thermal energy the system will tend to minimise these defects, for example, irradiation induced defects [25].

Thermodynamics shows that the free energy of a crystal depends on its internal energy E, entropy S, temperature T, pressure P and volume V. A decrease in self-interstitials and vacancies reduces the crystal's internal energy because the crystal takes on a more ordered structure. From thermodynamics we find that the free energy, G sometimes called the Gibbs free energy, is given by [26]

$$G = U + PV - TS. \qquad 2.2$$

Leaving out the PV product, the free energy is proportional to the difference between the internal energy E and TS- a term proportional to the entropy. Assuming negligible change in volume, we do not consider the PV term in this work thus, Equation 2.2 can be written as

$$\Delta G = \Delta H - T\Delta S \qquad 2.3$$

where ΔH is the enthalpy. The equilibrium state of the crystal corresponds to a minimum in the free energy which, at temperatures above 0 K, requires a certain amount of disorder. Recall that entropy is a measure of disorder. In other words, the most favorable free energy state of the crystal is a compromise between crystal perfection and disorder.

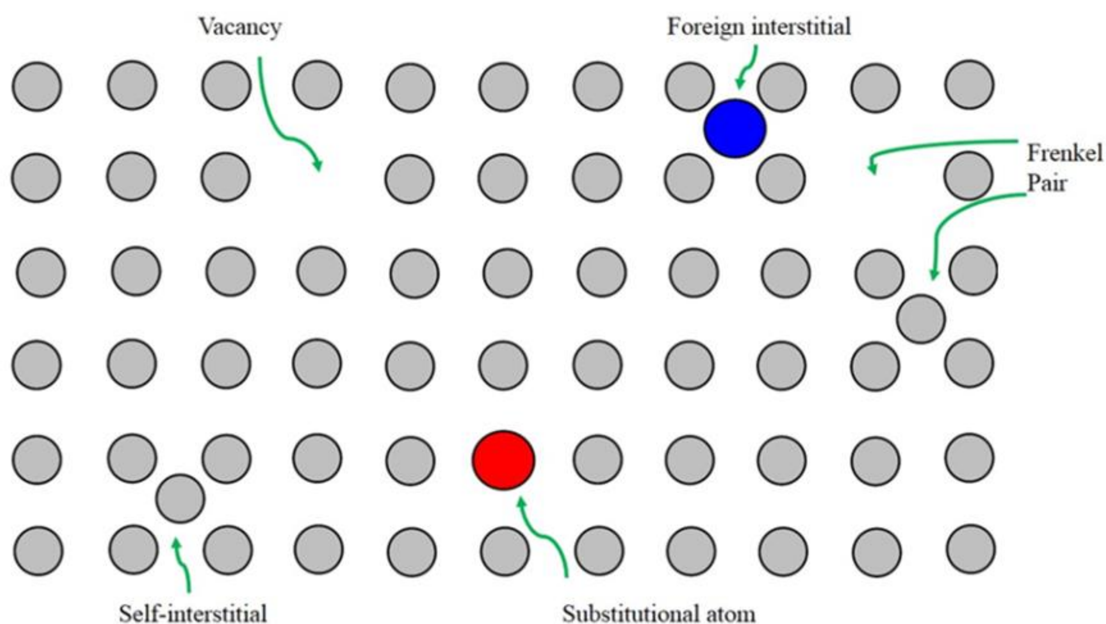

Figure 2-10: Common point defects in semiconductors. Substitutional and interstitial defects involve a foreign atom, whereas self-interstitials are due to an original atom [23].

2.3.2 Capture and emission by electronic defect states

Defect states may influence the mobility of charge carriers by scattering, and cause various features in the optical absorption and emission spectrum of the semiconductor. The most important electrical effect of deep levels in the band gap of a semiconductor is the emission and capture of charge carriers. These processes cause various transitory effects and cause defects to act as recombination and trapping centres, influencing the carrier lifetimes in semiconductors [27].

The kinetics of emission and capture of carriers from defect levels has been discussed extensively in the literature [19, 28]. In this section, the case of a single level with two charge states in a non-degenerate semiconductor is discussed, similarly to the approach followed by [28].

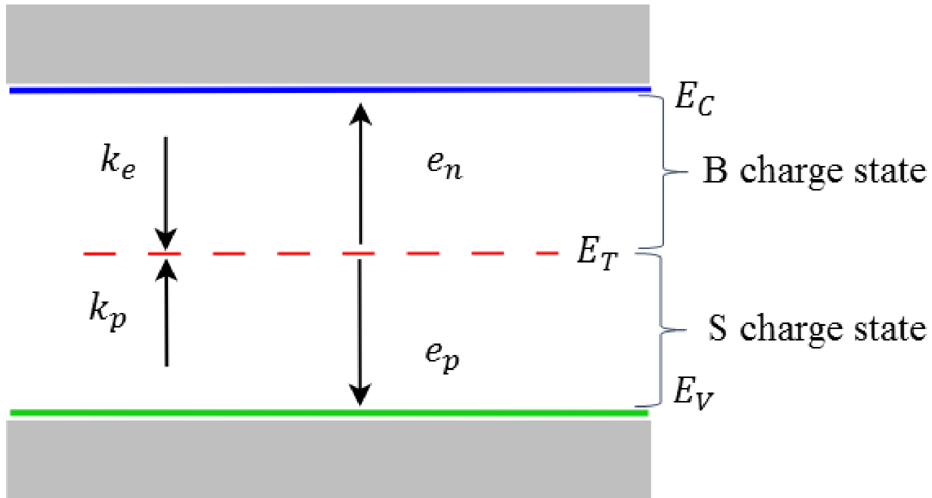

Figure 2-11: Representation of electron (n), hole (p), emission (e) and capture (k) processes between level E_T and the conduction and valence bands [28].

The probability per unit time k_p that a defect captures a hole from the valence band and changes its charge state from B to S, is proportional to the concentration of holes in this band is given by

$$k_p = c_p p \qquad 2.4$$

where c_p is the capture coefficient of the holes and p is the hole concentration in the valence band. The capture coefficient $c_n$has the dimensions of volume per unit time and can be written as

$$c_p = \sigma_p v_{th,p} \qquad 2.5$$

where σ_p is the hole capture cross-section and $v_{th,p}$ is the hole carrier velocity.

The velocity corresponds to a thermal average obtained from

$$\frac{1}{2}m_p^* v_{th,p}^2 = \frac{3}{2}kT \quad 2.6$$

where m_p^* is the hole effective mass.

Carrier emission from the defect to a band takes place with a probability per unit time e_p for hole emission that is, S→B. The quantity e_p depends on the number of empty states in the bands, equal to the total number of states minus p. However, p is usually small compared to the number of empty states so that they can be neglected. Therefore, e_p can be considered as independent of the free carrier concentration.

The total rate, that is, the change in concentration per unit time, for the different processes are the products of the probability per unit time (k_p, e_p) multiplied by the concentration *s* or *b* of the defect in the corresponding initial charge state (S or B). These rates are given by:

$k_p = c_p p b$ for hole capture

$e_p s$ for hole emission 2.7

The coefficients $c_p$and e_p are not independent since at thermal equilibrium, $k_p^0 b^0 = e_p^0 s^0$ (the superscript 0 indicates thermal equilibrium). By combining 2.4 and 2.7 we get

$$e_p = c_p p \frac{b^0}{s^0} \quad 2.8$$

From Lanoo *et al.* [29] we know that the ratio s^0/b^0 is given by

$$\frac{s^0}{b^0} = \gamma \exp\left(\frac{E_T - E_F}{kT}\right), \quad 2.9$$

where E_T is the negative free energy of ionisation of the defect corresponding to the change in its charge state from B to S. The factor γ is the degeneracy factor equal to the ratio $Z(S)/Z(B)$ where Z is the internal degeneracy [29]. To obtain a symmetrical expression for e_p we write

$$p^0 = n_i \exp\left(\frac{E_i - E_T}{kT}\right). \qquad 2.10$$

Here n_i is the intrinsic carrier concentration of the semiconductor and E_i is the intrinsic Fermi-level position. Substituting for p and $\frac{b^0}{s^0}$ in Equation 2.8 we get

$$e_p = \frac{c_p}{\gamma} n_i exp\left(\frac{E_i - E_T}{kT}\right) \qquad 2.11$$

Equation 2.11 can be re-written by replacing c_p with its expression from Equation 2.6 and also using the quantity

$$n_i \exp\left(\frac{E_i - E_F}{kT}\right) = N_v \exp\left(\frac{E_v - E_F}{kT}\right), \qquad 2.12$$

where E_v is the valence band limit and N_v is the effective number of states in the non-degenerate situation. The expression

$$e_p = \frac{\sigma_p v_{th,p}}{\gamma} N_v exp\left(\frac{E_v - E_T}{kT}\right) \qquad 2.13$$

results from the thermodynamic considerations and the quantity $E_v - E_T$ is the free energy of ionisation [29] of a hole in the valence band. Thus, equation 2.13 can be re-written as

$$e_p = v_{th,p} \sigma_p N_v \exp\left(\frac{\Delta S}{k}\right) \exp\left(-\frac{\Delta H}{kT}\right). \qquad 2.14$$

Here the free energy has been split into its entropy part ΔS and its enthalpy part ΔH. The degeneracy factor $1/\gamma$ has been included in the entropy. This defines the entropy and enthalpy

of ionization of holes from a given defect. In the following equation, the interest is on temperature dependence of e_p. Recall that N_v behaves as $T^{3/2}$, while $v_{th,p}$ is proportional to $T^{1/2}$, which allows us to write

$$e_p = v_{th,p} T^2 \sigma_p(T) \exp\left(\frac{\Delta S}{k}\right) \exp\left(-\frac{\Delta T}{kT}\right). \quad 2.15$$

If it is assumed that the capture cross-section of the defect is independent of temperature, it follows that an Arrhenius plot of $\ln(e_n/T^2)$ as a function of $1/T$ should yield a linear relationship from which the defect's energy E_T and capture cross-section σ_p may be calculated. These two values are frequently referred to as the defect's signature. The defect signature is one of the important parameters used to identify a defect during electrical measurements.

It is, however, necessary to note that the capture cross-section calculated from an Arrhenius plot is subject to a number of assumptions, for example, that the capture cross-section of the defect is not temperature dependent. Therefore, the capture cross-section calculated from the Arrhenius plot is frequently referred to as the apparent capture cross-section and indicated by $\sigma_{p,a}$ so as to distinguish it from the capture cross-section determined by more direct means. For the same reason the energy level of the defect calculated from the Arrhenius plot, might differ from values obtained under different conditions or by other techniques. The differences between values obtained using different techniques, might give important information about the nature of the defect involved [27].

2.4 Defect introduction mechanisms

There is a large overlap between process-induced defects and those produced during irradiation. In sputter deposition, for example, substrates are exposed to high energy electrons, heavy particle bombardment, x-ray and ultraviolet radiation [30].

2.4.1 Process induced defects

A process-induced defect in a semiconductor can be defined as any defect, including point and an extended defects, that is introduced during operations such as epitaxial film growth, dopant-diffusion, implantation and metallisation [30]. These defects have been reported extensively in the literature [20, 31-37].

2.4.1.1 Electron beam deposition

The electron beam deposition (EBD) method is used for the fabrication of metal contacts on Si for the purpose of electrical characterisation in the current study. In this technique a hot filament discharges electrons which are then accelerated by electric and magnetic fields onto the crucible containing the metal to be deposited. As a result, the metal melts and evaporates and energetic particles reach the semiconductor [38]. The deposition rate is controlled by the filament current. The EBD system can be used to deposit any metal but it may introduce defects on or below the surface of the sample on which the contacts are made.

2.4.1.2 Electron beam exposure

Electron beam exposure (EBE) is a technique whereby a semiconductor material is exposed to EBD conditions without metal deposition. This technique was specifically used to investigate EBD induced damage. Energetic particles that cause EBD damage are present during EBE but interact directly with the semiconductor whereas during EBD this interaction mostly occurs via the metal used as a contact [39]. During EBE, without metal deposition, the samples are exposed for 50 minutes; while the beam heats a tungsten source using a beam current of 100 mA, this current being insufficient to evaporate tungsten, thus exposing the samples to EB conditions comparable to those experienced during deposition.

2.4.2 Radiation-induced defects

The term "radiation-induced defects" refers to relatively stable lattice imperfections, produced by high-energy particles [40]. Extensive studies on the influence of high-energy radiation on semiconductors [19, 29, 31, 41-43] have been carried out for over fifty years. Many of the investigations are concerned not only with general problems of semiconductor physics, but also with practical problems, for example, the study of the radiation stability of solar silicon cells used in space explorations [40].

When irradiation is carried out there are two types of damage: ionisation damage and displacement damage. Displacement damage is the focus in this work.

When an energetic particle travels through a solid-state material it loses energy. The rate at which energy is deposited not only depends on the projectile mass but also on the target material's mass and atomic number. For suitably high particle energies, the energy transferred during an elastic or inelastic nuclear collision may be large enough to knock an atom from its lattice site as shown in Figure 2-12. This creates a vacancy and an atom in the interstitial position. For Si, the exact configuration depends on the charge state of the point defect. These primary radiation defects are highly mobile at room temperature and will therefore move a long distance. These defects can either disappear from the material by recombination at the substrate or other sinks or become trapped by impurity atoms giving rise to more stable secondary defects or defect complexes [43].

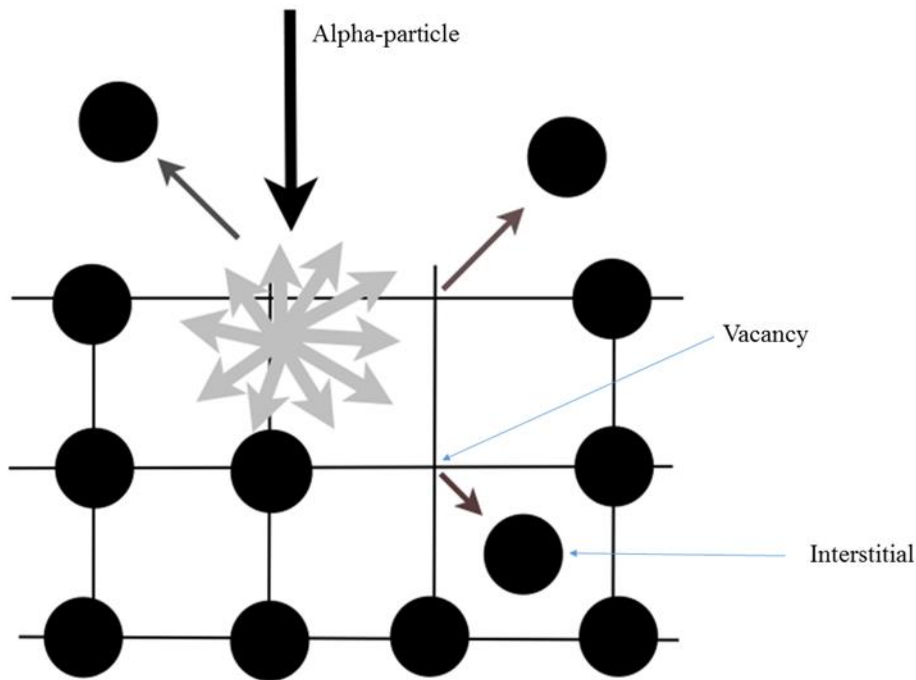

Figure 2-12: Illustration of lattice displacement after irradiation using a charged alpha-particle [44].

Displacement damage in a semiconductor can have a significant impact on its electrical properties through the creation of stable radiation-induced defects which have one or more levels in the band gap [43]. Following displacement damage the following electrical degradation effects can be observed:

- generation of electron-hole pairs by radiation-induced defects
- recombination of electron-hole pairs by radiation-induced defects
- trapping of carriers by radiation-induced defects
- tunnelling of carriers

After irradiation an increase in the resistivity is mostly observed, which results from a combination of two effects [45, 46]. Firstly, the removal of the free carriers due to either the removal of dopants from active lattice sites by interaction with the vacancies and interstitials created, giving rise to stable point defect complexes or to dopants at a neutral lattice sites. Well known examples for Si are the creation of the Group V donor-vacancy pairs or the creation of the interstitial boron (B_i). Furthermore, the presence of deep level defects changes the charge balance in the material and through Fermi-Dirac statistics, the position of the Fermi level, which impacts on the free carrier density. The carrier removal rate, K_n in n- and p-type Si has been studied by Pease *et al.* [47] and is defined by

$$n(\Phi) = n(0) - K_n\Phi, \quad 2.16$$

where $n(0)$ and $n(\Phi)$ are the free carrier concentration before and after exposure to a fluence Φ. K_n is a constant for low Φ, to first approximation, so that n decreases linearly with the fluence. In addition it is about two times larger in p-type Si compared to n-type Si, for 1 MeV equivalent neutron or high-energy proton irradiation [47].

References

[1] J. Adamson, J. Archbold, J. Auckett, S. Batten, J. Bevitt, J. Binns, H. Brand, W. Brant, S. Callori, H. Chevreau, J. Christian, J. Clegg, B. Collins, M. Warren, K. White, K. Wood, *Silicon – an element that is everywhere!*, in: H. Maynard-Casely (Ed.), 2014.

[2] O. Madelung, Semiconductors: Data Handbook, 3rd ed., Springer, Germany, 2004.

[3] B.G. Streetman, S.K. Banerjee, *Solid State Electronic Devices*, 6th ed., Prentice Hall, 2005.

[4] J. Czochralski, *A new method for measuring the crystallization rate of the metals*, Journal of Physical Chemistry, **92** (1918) 219.

[5] E. Talik, M. Oboz, Czochralski Method for Crystal Growth of Reactive Intermetallics Acta Physica Polonica A, 124 (2013).

[6] https://www.alineason.com/en/knowhow/crystal-growth/, Crystal growth, in.

[7] J. Vedde, T. Clausen, J. Borregaard, P. Kringhøj, *Float-Zone Crystal Growth For PV – Where Is The Future?* , in, 2008.

[8] http://www.slideshare.net/HrishikeshGhewande/epitaxial-crystal-growth-method, *Epitaxial Crystal Growth Method*, in, 2016.

[9] J.M. Vila-Fungueiriño, R. Bachelet, G. Saint-Girons, M. Gendry, M. Gich, J. Gazquez, E. Ferain, F. Rivadulla, J. Rodriguez-Carvajal, N. Mestres, A. Carretero-Genevrier, Integration of functional complex oxide nanomaterials on silicon, Frontiers of Physics, 3 (2015).

[10] S.M. Sze, K.K. Ng, *Physics of Semiconductor Devices*, 3 ed., John Wiley & Sons, Inc., New Jersey, 2007.

[11] W.M. Bullis, R.B. Herring, L.P. Hunt, T.D. Kamins, R.L. Lane, H.M. Liaw, W.C. O'Mara, L.C. Rogers, D.K. Schroder, R.A. Seilheimer, *Handbook Of Semiconductor Silicon Technology*, Noyes Publications, United States of America, 1990.

[12] S.M. Sze, K. K.Ng, Physics of Semiconductor Devices, 3rd ed., John Wiley and Sons (WIE), 2007.

[13] R.F. Pirret, *Semiconductor fundamentals*, 2 ed., Addison-Wesly, New York, 1988.

[14] E.H. Rhoderick, *Metal-semiconductor contacts*, Oxford, Claredon, 1978.

[15] N.F. Mott, *Note on the contact between a metal and an insulator or semiconductor*, Mathematical Proceedings of the Cambridge Philosophical Society, **34** (1938) 568.

[16] M.S. Tyagi, *Physics of Schottky Barrier Junctions*, in: B. L.Sharma (Ed.) *Metal-Semiconductor Schottky Barrier Junctions and Their Applications*, Plenum Press, New York, 1984, pp. 1-379.

[17] A.D. Bartolomeo, *Graphene Schottky diodes: An experimental review of the rectifying graphene/semiconductor heterojunction*, Physics Reports, **606** (2016) 1.
[18] M. Grundmann, *Diodes*, in: *The Physics of Semiconductors: An Introduction Including Nanophysics and Applications* Springer-Verlag, Heidelberg, 2010, pp. 864.

[19] F.D.Auret, *Electrical Characterisation of Defects Introduced in Epitaxially Grown GaAs by Electron-, Proton- and He-Ion Irradiation*, in: K. Wada, S.W. Pang (Eds.) *Optoelectronic Properties of Semiconductors and Superlattices*, Gordon and Breach Science Publishers, Netherlands, 2001, pp. 265.
[20] N. Cherkashin, A. Claverie, Characterization of Process-Induced Defects, in: A. Claverie (Ed.) Transmission Electron Microscopy in Micro-nanoelectronics ISTE Ltd and John Wiley & Sons, Inc. , Great Britain and the United States 2013, pp. 165-193.
[21] J. Jimenez, J.W. Tomm, Spectroscopic Analysis of Optoelectronic Semiconductors, Springer Series in Optical Sciences, Switzerland, 2016.
[22] K. Kuitunen, in: School of Science and Technology, Alto University, Finland, 2010.
[23] C. Nyamhere, *Characterizaton of process and radiation induced defects in Si and Ge using conventional deep level transient spectroscopy (DLTS) and Laplace-DLTS*, in: Physics, University of Pretoria, Pretoria, 2009.
[24] Z.E. Smith, S. Wagner, *Band tails, entropy, and equilibrium defects in hydrogenated amorphous silicon*, Physical Review Letters, **59** (1987) 688.
[25] H. Ryoken, I. Sakaguchi, N. Ohashi, T. Sekiguchi, S. Hishita, H. Haneda, *Non-equilibrium defects in aluminum-doped zinc oxide thin films grown with a pulsed laser deposition method*, Journal of Material Research, 20 (2005) 2866.
[26] D.K. Schroder, *Carrier Lifetimes in Silicon*, in: W.C. O'Mara, R.B. Herring, L.P. Hunt (Eds.) *Handbook of Semiconductor Silicon Technology* Noyes Publications, United States of America, 1990, pp. 795.
[27] W.E. Meyer, *Digital DLTS studies on radiation induced defects in Si, GaAs and GaN* in: Physics, University of Pretoria, Pretoria, 2006 pp. 108.
[28] J. Bourgoin, M. Lannoo, *Point Defects in Semiconductors II Experimental Aspects* Springe-Verlag Berlin Heidelberg and New York, 1983.

[29] M. Lannoo, J.C. Bourgoin, *Point Defects in Semiconductors I: Theoretical Aspects*, Springer Series in Solid-State Sciences, Berlin, Heidelberg, New York 1981.

[30] S.M.M. Coelho, Electrical characterization of process induced defects in germanium, in: Physics, University of Pretoria, Pretoria, 2015, pp. 173.
[31] F.D. Auret, S.A. Goodman, *Radiation and processed induced defects in GaN* in: M.O. Manasreh (Ed.) *III-V Nitride Semiconductors: Defects and Structural Properties* Elsevier, Amsterdam, 2000, pp. 448.
[32] B.N. Mukashev, K.A. Abdullin, Y.V. Gorelkinskii, Interactions of primary defects with impurities in silicon, Nuclear Instruments and Methods in Physics Research B, 186 (2002) 83-87.
[33] P.J.v. Rensburg, F.D. Auret, V. Matias, A. Vantomme, *Electrical characterization of rare-earth implanted GaN*, Physica B: Condensed Matter, 404 (2009) 4411-4414.
[34] C. Nyamhere, F. Cristiano, F. Olivie, E. Bedel-Pereira, Z. Essa, Electrical and optical characterization of extended defects induced in p-type Si after Si ion implantation Physica Staus Solidi c, 11 (2014) 146–149.
[35] A.T. Paradzah, F.D. Auret, M.J. Legodi, E. Omotoso, M. Diale, Electrical characterization of 5.4 MeV alpha-particle irradiated 4H-SiC with low doping density, Nuclear Instruments and Methods in Physics Research Section B: Beam Interactions with Materials and Atoms, 356 (2015) 112-116.
[36] S.M. Tunhuma, F.D. Auret, M. Legodi, M. Diale, Electrical characterisation of 5.4 MeV alpha-particle irradiated; low doped, n-type gallium arsenide, in: South African Institute of Physics, Port Elizabeth, 2015.
[37] S.M. Tunhuma, F.D. Auret, M.J. Legodi, J. Nel, M. Diale, Electrical characterization of defects introduced during sputter deposition of tungsten on n type 4H-SiC, Materials Science in Semiconductor Processing, 81 (2018) 122-126.
[38] F. Auret, S. Coelho, J. Nel, W. Meyer, *Electrical characterization of defects introduced in n- Si during electron beam deposition of Pt*, Physica Status Solidi (a), 209 (2012) 1926-1933.
[39] H.T. Danga, F.D. Auret, S.M.M. Coelho, M. Diale, Electrical Characterisation of electron beam exposure induced Defects in silicon, Physica B: Condensed Matter, 480 (2016) 206-208.
[40] V.S. Vavilov, N.A. Ukhin, *Radiation Effects in Semiconductors And Semiconductor Devices*, Consultants Bureau, New York, 1977
[41] M.-A. Trauwaert, J. Vanhellemont, H.E. Maes, A.-M.V. Bavel, G. Langouche, P. Clauws, *Low temperature anneal of electron irradiation induced defects in p type silicon*, Materials Science and Technology, 14 (1998) 1295-1298.

[42] G. D.Watkins, *Intrinsic defects in silicon*, Materials Science in Semiconductor Processing, **3** (2000) 227-235.

[43] C. Claeys, E. Simoen, Radiation Effects in Advanced Semiconductor Materials and Devices, Springer, Berlin, 2002.

[44] E.H. Ibe, *Terrestrial Radiation Effects In Ulsi Devices And Electronic Systems* John Wiley & Sons Singapore Pte. Ltd., Singapore, 2015

[45] P.G. Piva, S. Charbonneau, I.V. Mitchell, R.D. Goldberg, *Effect of implantation dose on photoluminescence decay times in intermixed GaAs/AlGaAs quantum wells*, Applied Physics Letters, 68 (1998).

[46] M.B. Johnston, M. Gal, N. Li, Z. Chen, X. Liu, N. Li, W. Lu, S.C. Shen, *Interdiffused quantum-well infrared photodetectors for color sensitive arrays*, 75 (1999).

[47] R.L. Pease, E.W. Enlow, G.L. Dinger, P. Marshall, *Comparison of Proton and Neutron Carrier Removal Rates*, EEE Transactions on Nuclear Science, **34** (1987) 1140

3 Experimental Techniques

In this chapter the experimental techniques used for sample preparation, contact fabrication, electrical characterisation and surface analysis are described. The Schottky contact electrical characterisation methods include: current-voltage I-V, capacitance-voltage (C-V) and deep-level transient spectroscopy (DLTS). Surface topology analysis was carried out using atomic force microscopy (AFM).

3.1 Sample preparation

Before metallisation, Si was cut and cleaned using a chemical cleaning process to remove organic materials such as oils, waxes and fingerprints, ionic substances such as sodium and potassium, and trace metals [1]. Immediately after cleaning, metallisation follows to prevent further oxidation of the silicon surface.

3.1.1 Silicon wafer cleaning procedure

The cleaning steps were used sequentially as follows:

(1) A three step degrease for the removal of dust particles and grease using:

- Trichloroethylene (TCE)
- Isopropanol
- Methanol

Samples were placed in an ultrasonic bath for 5 minutes for each degreasing step.

(2) The samples were then etched in dilute 40% hydrofluoric acid (HF) for 1 minute. This was done to remove the native oxide, SiO_2.

(3) The samples were then dried using flowing Nitrogen gas.

3.1.2 Schottky contact fabrication

Immediately after the chemical cleaning procedure, Schottky contacts were fabricated on p-type Si on the polished side through a mechanical mask with circular holes 0.60 mm in diameter. This was done by resistively depositing the metal of choice after evacuating the chamber to 2×10^{-6} mbar. The schematic diagram of the resistive deposition system is shown

in Figure 3-1. In this technique, a current flows through the crucible containing the metal to be deposited until the metal reaches its melting point. The metal then evaporates and deposits on the sample mounted above the crucible. The deposition rate is monitored by a crystal monitor and controlled by adjusting the current until the desired deposition rate is reached. The resistive deposition method is used for metals with low melting points that is, below 1600°C. In this study, the metals which were deposited using this method were aluminium and nickel.

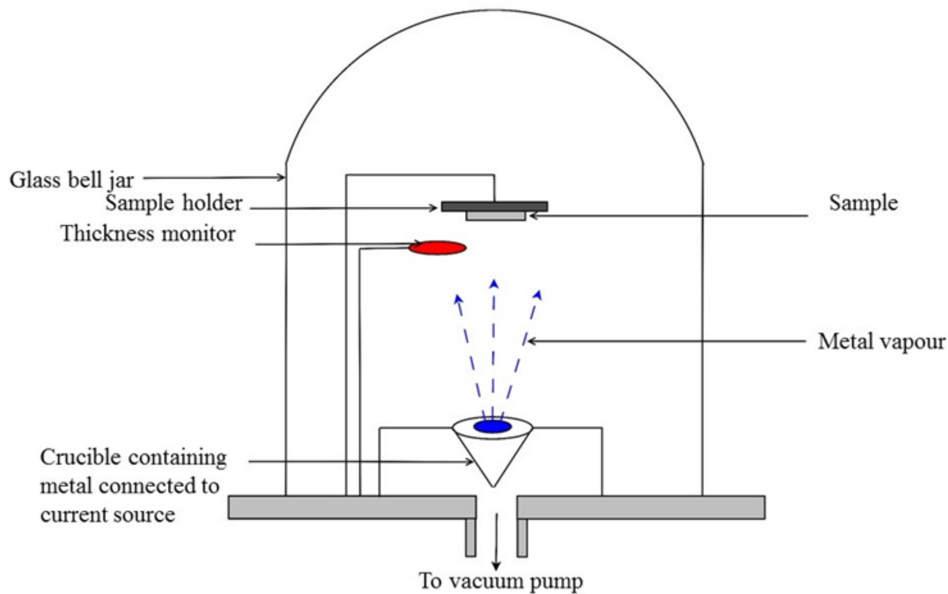

Figure 3-1: Schematic of the resistive deposition system set-up at the University of Pretoria.

Schottky contacts with a thickness of 100nm were fabricated on Si wafers by evaporating Titanium on the polished side through a mechanical mask with circular holes 0.60 mm in diameter. The contacts were deposited using electron beam deposition. In this technique a hot filament discharges electrons which are then accelerated by electric and magnetic fields, onto the crucible containing the metal to be deposited. As a result, the metal melts and evaporates and deposits onto the sample. The deposition rate is controlled by the filament current. The EBD system can be used to deposit any metal but it may introduce defects on or below the surface of the sample on which the contacts are made. Figure 3-2 shows a schematic diagram of the EBD system. After metallisation of the sample, electrical characterisation techniques are carried out on it.

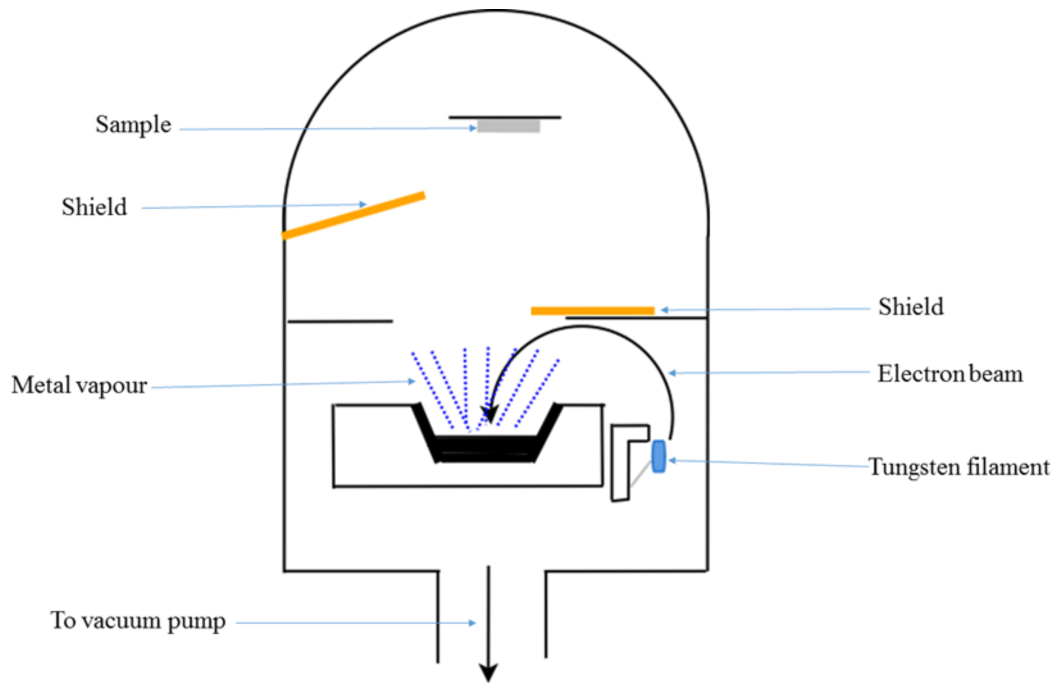

Figure 3-2: Schematic diagram of the EBD system at the University of Pretoria.

3.1.3 Ohmic contact fabrication

Indium-gallium eutectic was used as the ohmic contact. This was achieved by painting the back of the sample using the eutectic after Schottky contact fabrication.

3.2 Electron beam exposure (EBE)

The main aim of developing the EBE technique was to see if EBD induced defects can be introduced in a controlled way. Excessive exposure (time and beam current) would reduce the usefulness of diodes for further study thus putting a limit on how much damage could be introduced. Energetic particles that cause EBD damage are present during EBE but interact directly with the semiconductor whereas during EBD this interaction mostly occurs via the metal used as a contact [2].

Vacuum pumping was carried out by a dry pump in series with a turbo molecular pump and to lower the H_2 concentration, tungsten (W) was evaporated in the chamber with the sample rotated away from the evaporation source. While the pre-deposition vacuum was typically 5×10^{-7} mbar, this soon went up to approximately 3×10^{-6} mbar during the evaporation. As the

vacuum conditions vary greatly during EBD, forming gas H15 with a composition of N_2:H_2 of 85%:15% by volume was also used to raise the pressure in the vacuum chamber to 10^{-4} mbar which was kept constant during processing of selected samples. EBE of samples and EBD of contacts were fabricated using a 10 kV source (MDC model e-Vap 10CVS) with the samples positioned 50 cm above the crucible [3].

During EBE, without metal deposition, the samples were exposed for 50 minutes; while the beam heated a tungsten source using a beam current of 100 mA. This current being insufficient to evaporate tungsten, thus exposing the samples to EB conditions comparable to those experienced during deposition. Gold and nickel diodes were used for all the other samples prepared for this study as it can be evaporated resistively, a process that is known to not introduce defects in concentrations measurable by deep-level transient spectroscopy (DLTS) [3].

3.3 Sample annealing

Annealing can sometimes help reduce defects in semiconductors and in some cases introduce them. The purpose of the annealing is three-fold: Firstly, to achieve epitaxial growth or oxidation or during the fabrication of contacts, heating is necessary to obtain the required chemical reaction at the surface. Secondly, it is to increase the diffusion coefficient of some defect so that it has sufficient mobility to migrate the required distance during the time of the treatment. Thirdly, following irradiation of samples by high-energy particles which leads to the displacement of atoms from lattice sites, it is usually necessary that the damage should subsequently be removed. It is not so much a matter of making primary defects more mobile, but of allowing metastable configurations involving perhaps clusters of vacancies to dissociate and annihilate with interstitials which may be clustered elsewhere in the crystal [4].

The samples were annealed in a Lindberg Hevi-duty furnace in a quartz tube. A gas cylinder was connected to the tube so that it provided the required ambient – in this work argon was used. A thermocouple placed in the furnace just below the sample was used to monitor the annealing temperature. Argon was supplied at a constant rate of 2.0 ℓ/min for the whole annealing period. Figure 3-3 shows the set-up of the furnace.

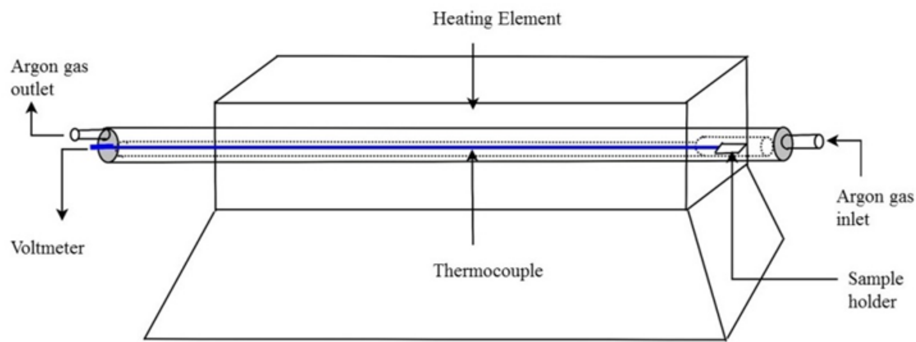

Figure 3-3 A sketch of the annealing furnace used in this study at the University of Pretoria.

3.4 Atomic force microscopy (AFM)

From the time when atomic force microscopy (AFM) was developed in 1986 by Binnig many experimental studies on nano-scale phenomena have utilized atomic force microscopy (AFM) to image the atomic topography and measure interacting forces. AFM has been used in a variety of research fields including physics, chemistry, biology and engineering [5].

AFM uses a very small device called a cantilever, which is basically a tiny record player needle made of silicon. The machine taps the tip of this cantilever along the surface of the sample being characterised and generates an image based on the interactions of the cantilever tip with the sample. The movements of this cantilever are measured by bouncing a laser off the back of it and measuring how the deflection of the laser changes using a photo-detector. When the laser goes over a bump the laser will also move and a photo-detector which collects this light records this change [6]. Figure 3-4 gives a picture of the measurement set-up.

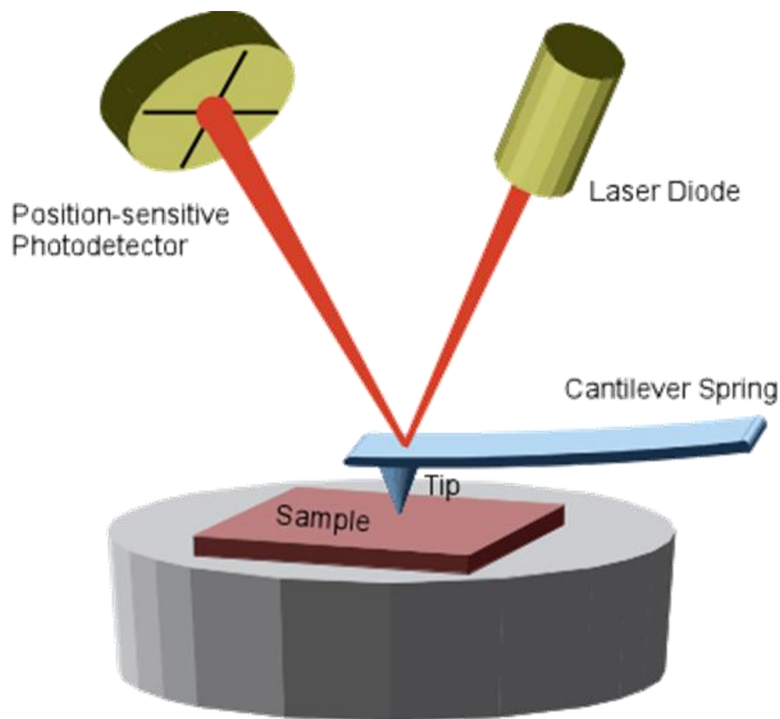

Figure 3-4: Illustration of the AFM set-up after reference [6].

3.5 Sample irradiation

Contacts fabricated on the p-type Si samples were irradiated with alpha particles using an Americium 241 foil at room temperature with a fluence rate of $7 \times 10^{6}\ \mathrm{cm^{-2}s^{-1}}$. The sample was first irradiated for 30 minutes to a fluence of $6.4 \times 10^{9}\ \mathrm{cm^{-2}}$. *I-V*, *C-V* measurements and DLTS were done after each irradiation. Figure 3-5 gives illustrates how the alpha-particles impinge on the sample.

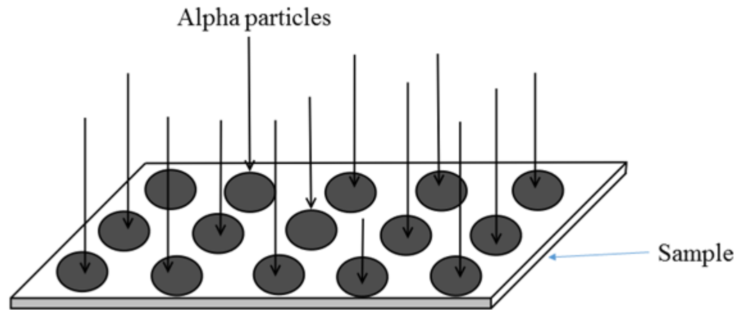

Figure 3-5: diagram showing alpha-particle irradiation of a silicon sample.

3.6 Electrical characterisation techniques

Current-voltage *(I-V)* and capacitance-voltage *(C-V)* measurements were conducted on the samples to monitor the quality and electrical characteristics of the diodes while annealing of the samples was carried out. Deep-level transient spectroscopy (DLTS) was used to characterise the defects in the semiconductor band gap after annealing, irradiation and electron beam exposure.

3.6.1 Current-voltage measurements

The *I-V* measurement technique is ideal for checking the quality of the Schottky contacts on each sample after preparation. Measuring the current that flows through the contact under forward and reverse bias conditions enables the deduction of whether a contact is a good rectifier or it is ohmic. The properties of diodes that are extracted from *I-V* measurements are: series resistance R_s, ideality factor n, reverse leakage current I_R (measured at −1 V reverse bias) and barrier height Φ_B. These diode properties determine whether the sample can be used for DLTS measurements. A good diode suitable for DLTS measurements should have a high barrier height, low leakage current (less than 10^{-4} A) and a low series resistance (less than 200Ω) [7]. The *I-V* characteristics were measured using an HP 4140B pA meter/DC voltage source with the capability to measure currents as low as 10^{-14} A.

3.6.2 Capacitance-voltage measurements

The *C-V* technique is used to deduce important parameters of the contact which include; the barrier height, built-in-voltage, and free carrier concentration. The *C-V* characteristics of the

contacts are determined using an HP 4192A LF impedance analyser. The *I-V* and C-V contacts were carried out in the dark. A schematic diagram of the I-V and C-V measurement set up is shown in Figure 3-6.

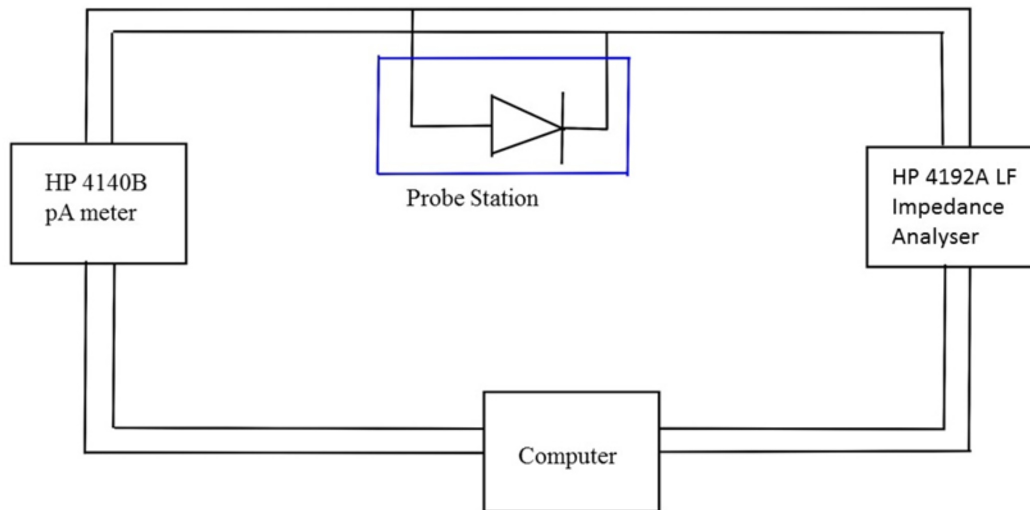

Figure 3-6: A block diagram of I-V and C-V station set up at the University of Pretoria.

3.6.3 Deep-level transient spectroscopy (DLTS)

Deep level transient spectroscopy (DLTS) is a unique and powerful tool used for the study of electrically active point defects in semiconductor materials. DLTS measures the electrical effects of defect states in the depletion region of a p-n junction or a metal-semiconductor junction [8, 9]. In DLTS a defect is observed by monitoring the effect of emission of a carrier from a deep level to the corresponding band edge in the depletion region of a reversed biased semiconductor junction. A lattice defect, such as a vacancy, an interstitial, a dislocation; an impurity, or a complex, introduces an electronic energy state into the band gap of the semiconductor. Intentionally processed dopants produce shallow states within the energy gap and control the majority carrier concentration in the material. The deep states measured in this spectroscopy are those whose energy levels fall deeper in the bandgap than the dopant levels. The deep levels in silicon emit thermally within the temperature range of 40 to 350 K for typical DLTS measurements systems. In n-type samples, the observed defects will emit electrons to the conduction band and will lie above the middle of the gap. In p-type semiconductors, the defect states are below the mid gap and the holes are emitted to the valence band [8].

By making use of DLTS, defects in semiconductors are analysed by probing the space charge region which exists in both a p-n junction and a Schottky barrier diodes. The width, W, of the depletion region of a SBD or p-n junction varies with applied voltage according to:

$$W = \sqrt{\frac{2\varepsilon(V_{bi}+V)}{qN}}, \tag{3.1}$$

where $\varepsilon =$ dielectric constant of the depleted semiconductor

$V_{bi} =$ built-in-voltage of the junction

$V =$ externally applied voltage

$q =$ charge on the electron

$N =$ density of ionised impurities due to the dopants and other imperfections.

The junction capacitance due to the depletion layer is:

$$C = \frac{\varepsilon A}{W} = A\sqrt{\frac{q\varepsilon N}{2(V_{bi}+V)}} \tag{3.2}$$

where A = area of the junction.

From equations 3.1 and 3.2 it can be seen that if *N* changes in the depletion region, W and C will also change, and so junction capacitance is a direct measure of the total charge. If the concentration of electrons or holes trapped at deep levels is changed by the thermal or optical emission of carriers to the conduction or valence bands, this change can be monitored by measuring the variation in junction capacitance at constant applied voltage. The variation in the temperature dependant variation of N forms the basis of capacitance-based DLTS [10, 11]. The processes of carrier capture and emission are shown in Figure 3-7 for a Schottky barrier diode having a hole trap in the lower half of the bandgap. During the DLTS measurement, free carriers are removed from the junction depletion region by the application of a reverse bias V_r. Thereafter, a forward pulse, V_p, is applied and it collapses this depletion region, filling the deep

level states with carriers. When the pulse is removed the filled states emit the captured carriers during a thermal process with a characteristic time constant dependant on the defect's position in the forbidden gap and the available thermal energy [8].

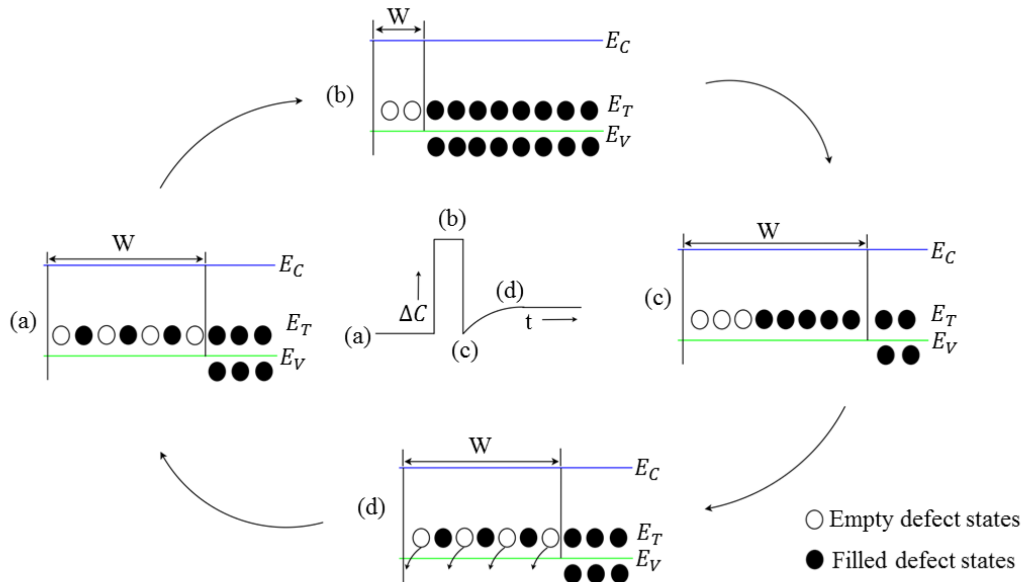

Figure 3-7: The variation of the depletion region width and capacitance after the application of a voltage bias and filling pulse sequence for a hole trap in an p-type semiconductor [11].

Before applying a reverse voltage, the traps in the depletion region above the Fermi level are empty as shown in (a). Reducing the applied voltage to $V - V_P$ reduces the width of the depletion region, allowing carrier to be trapped by deep levels, as depicted in (b). Hole capture into an initially empty trap is given by

$$N_0(t) = N_T\left[1 - exp\left(-c_p t\right)\right] \quad 3.3$$

where N_0 is the density of traps filled with holes, N_T is the trap density and c_p is the capture rate.

Part (c) shows the point when the voltage is returned to is steady-state value, V, where the filled traps lie within the depletion region. When holes are emitted into the valance band by the traps, where they are immediately swept away by the electric field in the junction. This is observed as a majority carrier capacitance transient as shown in (d).

Using this experimental approach, the hole emission rate can be determined from the time constant of the capacitance transient. Assuming all the traps were filled by the filling pulse, the density of the occupied traps at time *t* after removing the pulse is:

$$N_0(t) = N_T exp(-e_p t). \qquad 3.4$$

Here e_p is the thermal emission rate and N_T is the trap concentration. From equations 3.4 and 3.1 it can be shown that change in trap population gives rise to a corresponding diode capacitance which is dependent on time. Furthermore, if $N_T \ll N_D$, it can be expressed as:

$$C(t) = C_O - \Delta C_O \exp(-e_p t)\ , \qquad 3.5$$

where C_O is the equilibrium capacitance at reverse bias and ΔC_O is the change in capacitance from before to directly after the filling pulse.

3.6.4 The concepts of DLTS

DLTS is a highly sensitive capacitance technique. It is a technique that is capable of distinguishing different traps from each other. During a DLTS temperature scan, an emission rate window is set which is the emission rate at which the measurement apparatus responds maximally to a transient. While temperature scanning takes place, taking into consideration that the thermal emission process is strongly temperature dependant, the emission rate of a defect changes. The maximum signal on the DLTS spectrum is reached at the temperature at which the emission rate of the defect is equal to the rate window. The boxcar method is often used for accurate determination of the emission rate window and signal averaging, therefore improving the signal to noise ratio [12]. Figure 3-7 shows how the double boxcar method works.

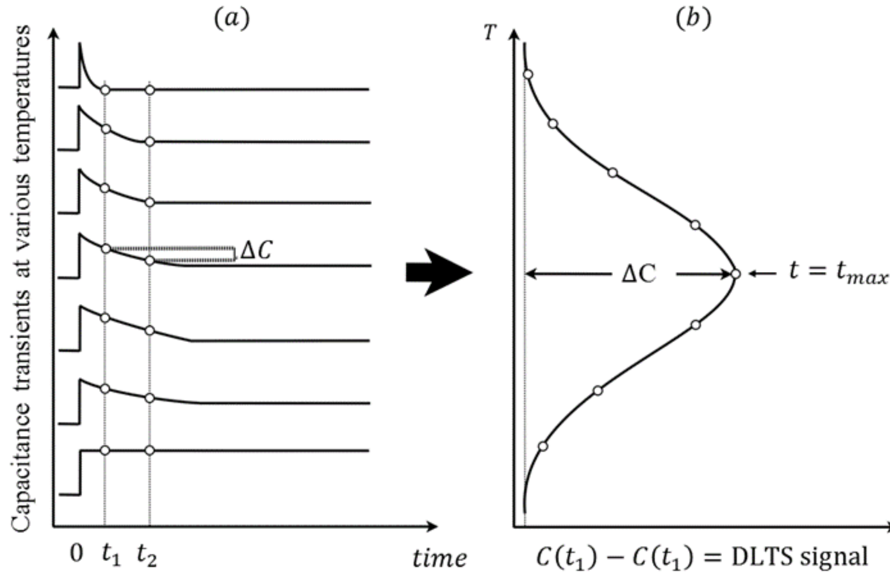

Figure 3-8: A schematic diagram showing (a) the change in the shape of the DLTS transient with increasing temperature and (b) the DLTS signal obtained from the transients as a function of sample temperature [12].

The transient figures shown in Figure 3-8 (a) are fed through the double boxcar with pre-set times, t_1 and t_2. The average difference between the capacitances at t_1, C(t_1) and at t_2, C(t_2) are plotted as a function if temperature as shown in Figure 3-8(b). The rate window for the thermal scan is determined by t_1 and t_2. The peak is formed when the decay constant $\boldsymbol{\tau}$ falls within the order of $t_2 - t_1$. The value of $\boldsymbol{\tau}$ at the maximum of the $C(t_2) - C(t_1)$ vs T for a particular trap, τ_{max} can be related to the gate positions t_1 and t_2. This is achieved by normalising the DLTS signal in Figure 3-7 to define S (T) given by

$$S(T) = [C(t_1) - C(t_2)]/\Delta C(0) \qquad 3.6$$

where ΔC(0) is the capacitance due to the pulse change at t = 0. Now for exponential transients,

$$S(T) = \left[\exp\left(^{-t_1}/_{\tau}\right)\right] - \left[\exp\left(^{-t_2}/_{\tau}\right)\right] \qquad 3.7$$

which can also be written as

$$S(T) = \exp\left(-t_2/_{\tau}\right)\left[1 - \exp\left(-\Delta t/_{\tau}\right)\right] \qquad 3.8$$

where $\Delta t = t_2 - t_1$. Therefore the relationship between τ_{max}, t_1 and t_2 can be obtained by differentiating S(T) with respect to τ and equating the result to zero:

$$\tau_{max} = \frac{t_1 - t_2}{ln\left(\frac{t_1}{t_2}\right)}. \qquad 3.9$$

Therefore the emission rates of the peak of DLTS signal can be obtained accurately. Carrying out a thermal scan using many different rate windows enables one to identify the peak positions and the temperature at which they occur. This information can be used to calculate the activation enthalpy and the apparent capture cross-section [13].

3.6.5 Laplace-DLTS

Deep level transient spectroscopy has been a valuable tool in characterising electrically active deep level states in semiconductors since its invention in the 70s by Lang [9]. Unfortunately, this technique has limitations as far as its emission rate resolution is concerned. The lock-in-amplifier or the double boxcar filter used in DLTS shows good sensitivity but poor time-constant resolution. This poor time-constant resolution that makes DLTS unsuitable for separating closely spaced transients and therefore its inability to study defect fine structure.

Dobaczewski *et al.* [14] developed an improved a high resolution version of DLTS in 1990. They called it Laplace-DLTS. Laplace-DLTS uses a regularised inverse Laplace transform instead of the boxcar analysis. This results in an order of magnitude improvement in emission rate resolution in the studies of the thermal emission of carriers from deep states. Consequently, Laplace-DLTS can separate closely spaced transients when a number of defects with similar emission characteristics are present. Laplace-DLTS can also probe very narrow regions of the semiconductor and selectively study the active regions of devices.

3.6.6 The concepts of Laplace-DLTS

In DLTS there are two main classes of transient processing methods, analogue and digital signal processing. Analogue signal processing is a real-time process using analogue electronics which extract the DLTS signal from the capacitance transients as the temperature is ramped.

The digital signal processing involves digitising the transient output of the capacitance meter, normally done with a sample held at a fixed temperature and averaging many of these digitalised transients to reduce noise. If the transient is digitised it is easier to apply signal processing tasks, even complex ones. The concept of digitising the capacitance transient at a constant temperature and extracting the time constant is the basis of high resolution Laplace-DLTS.

Within the context of DLTS using digitised transients, various schemes have been published and various degrees of success reported. Among the range of approaches that are of importance is the method of moments technique as used by Ikossi-Anastasiou and Roenker [15]. Nolte and Haller [16] used the Gaver-Stehfest algorithm to effect a Laplace transform although achieving a substantial increase in resolution found the approach to be unstable in the presence of experimental noise levels. Eiche *et al.* [17] use Tikhonov regularization to separate the constituent exponentials in a photo-induced current transient spectroscopy signal with an approach very similar to that which has been adopted for the work described in this work.

In order to give a quantitative description of the non-exponential nature observed in the capacitance transients, one assumes that they are characterized by a spectrum of emission rates [18]

$$f(t) = \int_0^\infty F(s)\, e^{-st} ds \qquad 3.10$$

where $f(t)$ is the recorded transient and $F(s)$ is the spectral density function. Equation 3.10 gives a mathematical Laplace transform of the true spectra of the emission rates. To get the real spectra of the emission rates, an algorithm is used that performs an inverse Laplace transform of the function $f(t)$. As a result, a spectrum of delta-like peaks is expected to be obtained for mono- and multi-exponential transients or a broad spectrum with no fine structure for a continuous distribution [18].

In the Laplace DLTS system, three different software procedures are used for the numerical calculations. All of them are based on the Tikhonov regularization method. However, they differ in the way the criteria for finding the regularization parameters are defined. The first one (CONTIN) is in the public domain and has been obtained from a software library and modified in order to integrate it with the system [19]. The outline code of the second one (FTIKREG) is distributed by the same library but it has been substantially modified by the original authors

for operation within the LDLTS system [19]. The last one (FLOG), has been specifically developed for the system. The parallel use of three different software packages substantially increases the level of confidence in the spectra obtained [20]. Additionally, for preliminary data analysis a discrete (multi-exponential) deconvolution method can be used. This method is based on a simple integration procedure [21].

3.6.7 Deep level transient spectroscopy measurement set-up

The set-up of the DLTS and Laplace-DLTS system used in this work consists of the following:

(a) A cryostat in which the sample to be characterised is mounted. A closed cycle cryostat is used in the cooling from high to low temperatures. A heater is located at the tip of the cryostat which raises the temperature from low to high values. The temperature of the cryostat is controlled by a Lakeshore 340 temperature controller which is used in the range 40K to 350K in this study.

(b) A Boonton 7200 capacitance meter with 100 mV, 1 MHz ac voltage signal used to monitor the thermal emission of carriers after excitation by a pulse generator.

(c) A Laplace DLTS card with an internal pulse generator for producing the appropriate quiescent reverse bias voltage and pulses. The Laplace card also contains the hardware used for data collection and averages transients before the spectra is processed for both conventional and Laplace- DLTS. The Laplace card was also used to record the capacitance-temperature (CT) scans.

(d) A HP 33120 15 MHz waveform external generator, which produced the desired quiescent bias and filling pulse in measurements that required shorter filling pulse widths.

Conventional and Laplace-DLTS sample excitation parameters are set up using the Laplace program. In the conventional-DLTS mode the capacitance meter measures the capacitance transient after excitation. The transients are then processed by the Laplace card. Ramping up or down the temperature using a particular rate window, a DLTS spectrum is displayed on the computer. Figure 3-9 shows the schematic of the DLTS set-up.

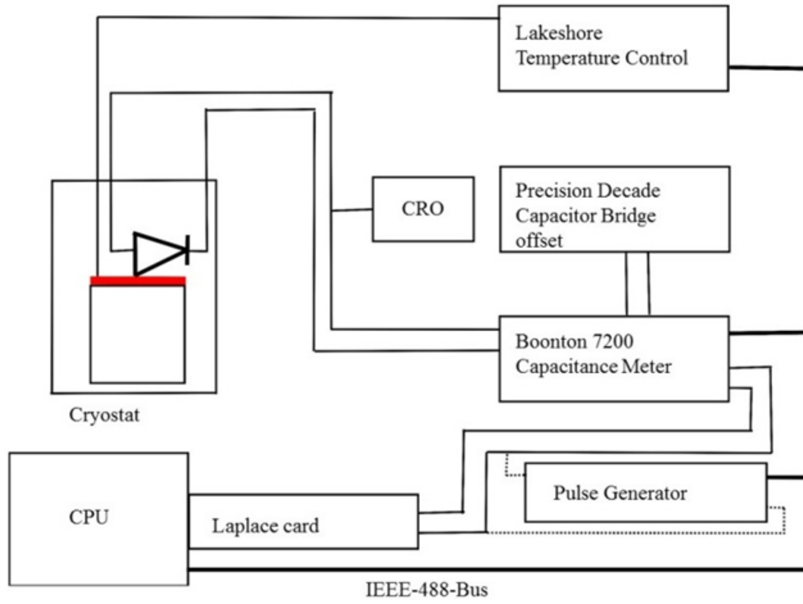

Figure 3-9: A block diagram of DLTS set up at the University of Pretoria.

References

[1] W.M. Bullis, R.B. Herring, L.P. Hunt, T.D. Kamins, R.L. Lane, H.M. Liaw, W.C. O'Mara, L.C. Rogers, D.K. Schroder, R.A. Seilheimer, *Handbook Of Semiconductor Silicon Technology*, Noyes Publications, United States of America, 1990.

[2] S.M.M. Coelho, Electrical characterization of process induced defects in germanium, in: Physics, University of Pretoria, Pretoria, 2014.

[3] S.M.M. Coelho, F.D. Auret, P.J.J.v. Rensburg, J.M. Nel, *Electrical characterization of defects introduced in n-Ge during electron beam deposition or exposure*, Journal of Applied Physics, **114** (2013) 173708.

[4] R.C. Newman, *Defects in silicon*, Reports on Progress in Physics, **45** (1982) 1163.

[5] Y. Seo, W. Jhe, *Atomic force microscopy and spectroscopy*, Reports on Progress in Physics, **71** (2008) 23.

[6] https://undergrad.research.ucsb.edu/2014/03/atomic-force-microscope-tiny-record-player/, *Atomic Force Microscope: A Tiny Record Player*, in: D. Myers (Ed.), 2014.

[7] C. Nyamhere, *Characterizaton of process and radiation induced defects in Si and Ge using conventional deep level transient spectroscopy (DLTS) and Laplace-DLTS*, in: Physics, University of Pretoria, Pretoria, 2009.

[8] J. L.Benton, *Characterization of defects in semiconductors by deep level transient spectroscopy*, Journal of Crystal Growth, **106** (1990) 116.

[9] D.V. Lang, *Deep level transient spectroscopy: A new method to characterize traps in semiconductors*, Journal of Applied Physics, **45** (1974) 3023.

[10] F.D.Auret, *Electrical Characterisation of Defects Introduced in Epitaxially Grown GaAs by Electron-, Proton- and He-Ion Irradiation*, in: K. Wada, S.W. Pang (Eds.) *Optoelectronic Properties of Semiconductors and Superlattices*, Gordon and Breach Science Publishers, Netherlands, 2001, pp. 265.

[11] G.L. Miller, D.V. Lang, L.C. Kimerling, *Capacitance Transient Spectroscopy*, Annual Review of Materials Science, **7** (1977) 377-448.

[12] D.K. Schroder, *Carrier Lifetimes in Silicon*, in: W.C. O'Mara, R.B. Herring, L.P. Hunt (Eds.) *Handbook of Semiconductor Silicon Technology* Noyes Publications, United States of America, 1990, pp. 795.

[13] W. Mtangi, *Electrical characterisation of process, annealing and irradiation induced defects in ZnO,* in, University of Pretoria, 2012.

[14] L. Dobaczewski, A.R. Peaker, K.B. Nielsen, Laplace-transform deep-level spectroscopy: The technique and its applications to the study of point defects in semiconductors Journal of Applied Physics, (2004) 41.

[15] K. Ikossi-Anastasiou, K.P. Roenker, *Refinements in the method of moments for analysis of multiexponential capacitance transients in deep‐level transient spectroscopy*, Journal of Applied Physics, **61** (1987).

[16] D.D. Nolte, E.E. Haller, *Optimization of the energy resolution of deep level transient spectroscopy*, Journal of Applied Physics, **62** (1988) 592.

[17] C. Eiche, D. Maier, M. Schneider, D. Sinerius, J. Weese, K.W. Benz, J. Honerkamp, J. Phys.: Condensed Matter, **4** (1992) 6131.

[18] L. Dobaczewski, P. Kaczor, I.D. Hawkins, A.R. Peaker, Laplace transform deep-level transient sectroscopic studies of defects in semiconductors American Institute of Physics, 76 (1994).

[19] J. Weese, *A regularization method for nonlinear ill-posed problems*, Computer Physics Communications, **77** (1993) 429.

[20] http://info.ifpan.edu.pl/Dodatki/WordPress/laplacedlts/?page_id=330, *Laplace DLTS*, in, 1998.

[21] K. Tittelbach-Helmrich, *An integration method for the analysis of multiexponential transient signals*, Measurement Science and Technology, **4** (1993) 1323.

4 Results and discussion

This chapter focuses on the results obtained using the techniques described in Chapter 3. The results are presented as a series of articles that have been published from 2016 to 2019. These papers investigate process induced defects due to electron beam deposition (EBD) as well as alpha-particle induced defects during irradiation at both room temperature low temperatures.

In order to better understand EBD defects observed after deposition of Ti (Section 4.1.1) a study comparing EBD and EBE using Ni contacts, which could be evaporated resistively, was conducted (Section 4.1.2). This led to some differences between EBD of Ti and Ni contacts being observed, as discussed in the general discussion Section 4.3.

In order to correlate these defects with intrinsic defects induced by particle irradiation, the defects induced during room temperature and low-temperature irradiation were investigated (Section 4.2.1 and 4.2.2) and compared to process-induced defects in Section 4.3.

4.1 Process induced defects

Processes such as epitaxial film growth, dopant diffusion, implantation and metallisation[1] may inadvertently induce defects. Metallisation can be done using electron beam deposition (EBD), sputter deposition (SD) and resistive evaporation. EBD is frequently used to deposit high melting point materials. Resistive evaporation does not induce damage, but both EBD and SD induce damage[1]. In this thesis, EBD induced damage is investigated.

4.1.1 Annealing studies of electron beam deposition induced defects

In this study we investigated the defects induced by EBD and we also looked at the effects of annealing on the defects observed soon after metal deposition. Knowledge about the thermal stability of the defects is useful so that they can be reproducibly introduced, avoided or eliminated depending on the application [2].

As discussed in Chapter 3, annealing can often help reduce defects in semiconductors. This can be due to either diffusion or breaking up of complex defects. However, due to defect reactions, annealing can in some cases introduce new defects. After irradiation of samples using high-energy particles which leads to the displacement of atoms from lattice sites, it is usually necessary that the damage should afterwards be removed by annealing [3].

The samples were annealed in a quartz tube under argon at a flow rate of 2 ℓ/min. A thermocouple placed in the furnace just below the sample was used to monitor the annealing temperature. During each annealing step morphological changes of the metal contact were observed. Atomic force microscopy (AFM) was employed for this part of the study.

A paper written by the present author entitled "Thermal stability of defects introduced by electron beam deposition on p-type silicon" [4] discusses the electronic properties of the defects introduced by EBD and the results of isochronal annealing are presented. DLTS revealed that the main defects introduced during metallisation were hole traps H(0.05), H(0.23) and H(0.38).The three hole traps were characterised using Laplace-DLTS. The *I*-*V* characteristics showed that the quality of the Schottky diode deteriorated with increase in annealing temperature. After annealing at 300°C, two of the EBD-induced defects were removed; however the third defect remained stable up to 400°C. For comparison, a sample exposed to electron beams, a process known as electron beam exposure (EBE) was characterised. Ni contacts were fabricated using EBD. One prominent broad peak was observed when DLTS was performed on the EBE+EBD contacts. Laplace-DLTS suggests that there is more than one level within that peak. AFM was used to monitor the surface topology of the contacts with each annealing step and showed some surface roughening.

The present author took part in the planning, the sample preparation, performed the electrical characterisation and analysis and wrote the draft manuscript for proof-reading and discussion with co-authors. E. Omotoso assisted with EBE and EBD while the AFM was done by S.M. Tunhuma.

Nuclear Instruments and Methods in Physics Research B 409 (2017) 46–49

Contents lists available at ScienceDirect

Nuclear Instruments and Methods in Physics Research B

journal homepage: www.elsevier.com/locate/nimb

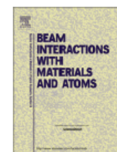

Thermal stability of defects introduced by electron beam deposition in p-type silicon

H.T. Danga *, F.D. Auret, S.M. Tunhuma, E. Omotoso, E. Igumbor, W.E. Meyer

Department of Physics, University of Pretoria, Pretoria 0002, South Africa

ARTICLE INFO

Article history:
Received 9 December 2016
Received in revised form 23 March 2017
Accepted 11 April 2017
Available online 18 April 2017

Keywords:
Silicon
Laplace-DLTS
Electron beam deposition
Annealing

ABSTRACT

The electronic and thermal properties of defects introduced during electron beam deposition (EBD) followed by isochronal annealing of titanium (Ti) contacts on p-Si were investigated. In this work, EBD-deposited Ti Schottky contacts were annealed within a temperature range of 200–400 °C. Current-voltage (*I-V*) measurements were conducted to monitor the change in electrical characteristics with every annealing step. A barrier height of 0.55 eV was measured on the as-deposited sample. Deep level transient spectroscopy (DLTS) and Laplace-DLTS techniques were employed to identify the defects introduced after EBD and isochronal annealing of the Ti Schottky contacts. DLTS revealed that the main defects introduced during metallization were hole traps H(0.05), H(0.23) and H(0.38). Annealing at 300 °C removed the two hole traps H(0.05) and (0.38). Atomic force microscopy (AFM) was performed on the contacts to monitor their surface topology. The surface of the contacts became rougher as the annealing temperature increased. The slight increase in root-mean-square roughness of the contacts with increasing annealing temperature may be attributed to outdiffusion of Si into Ti layers.

© 2017 Elsevier B.V. All rights reserved.

1. Introduction

Metallization is a fundamental practice in silicon technology. Electron beam deposition (EBD) of metals is often used due to its ability to deposit high melting point metals and because this can be done at accurately controlled rates. It has, on the other hand, been shown that EBD of metals on semiconductors introduces electrically active defects at and beneath the semiconductor surface [1]. The origin of the defects was shown to be energetic particles accelerated from the vicinity of the electron filament onto the sample by the electric and magnetic fields present in the locality of the metal source [2]. These defects usually have an adverse effect on device performance, but may in some cases be beneficial [3].

The electrical properties of defects introduced in Si by EBD of metals have been previously reported. Some data is also available on the annealing of these defects, e.g. for Mo-Si contacts [1]. Annealing studies are usually hampered by the fact that Schottky contacts become too leaky for electrical measurements after annealing above 500 °C. However, a complete annealing study involving the removal of all defects, is vital in order to determine processing conditions for obtaining a defect-free space charge region below Schottky contacts formed by EBD.

In this study, we have investigated the thermal stability (in the range 200–400 °C) of Ti Schottky contacts and of the defects introduced in p-Si during electron beam deposition (EBD) of these contacts.

2. Experimental procedure

A p-type, boron-doped Si wafer with a carrier density of $3.4 \times 10^{16}\ cm^{-3}$ was used for this study. Samples were prepared for metal deposition by cleaning them using a three step degrease in trichloroethylene, isopropanol and methanol for three minutes each in an ultrasonic bath. Hereafter, the samples were dipped in clean de-ionised water then in 40% HF for ten seconds and finally a rinse in de-ionised water. The samples were blow-dried with nitrogen and then immediately loaded into the vacuum chamber which was then evacuated to a pressure below 1×10^{-6} mbar to prevent oxidization before metallization.

Deposition of Ti was carried out using electron beam deposition (EBD). A mechanical mask was used for depositing well-defined circular dots of diameter 0.6 mm and a spacing of 1 mm between dots. A Varian 10 kW e-Gun in a high vacuum evaporation chamber was used for this process. The electron-gun has been designed with a 270° deflection angle for the electron beam and so that no contaminants from the heated tungsten filament can be deposited on the substrate. The crucible was water cooled to ensure safe

* Corresponding author.
E-mail address: helga.danga@up.ac.za (H.T. Danga).

http://dx.doi.org/10.1016/j.nimb.2017.04.037
0168-583X/© 2017 Elsevier B.V. All rights reserved.

operation even at full power. At the completion of the deposition process, the sample was removed from the vacuum chamber and prepared for *I-V* and *C-V* measurements.

Ti Schottky contacts with a thickness of 100 nm were deposited. These contacts were annealed in Ar at temperatures of up to 400 °C in 100 °C steps for 20 min periods. *I-V* and *C-V* measurements were used to monitor the quality of the Schottky contacts. Conventional and high-resolution Laplace-DLTS (L-DLTS) [4] was performed after each annealing cycle to monitor the presence of the EBD-induced defects and to obtain their electronic properties (activation enthalpy, E_T, and apparent capture cross section for carriers, σ_a). For comparison, a sample exposed to electron beams, a process known as electron beam exposure (EBE), was also characterised. During EBE, without metal deposition, the samples were exposed for 50 min; while the beam heated a tungsten source using a beam current of 100 mA, this current being insufficient to evaporate tungsten, thus exposing the samples to electron beam conditions comparable to those experienced during deposition [5]. Nickel (Ni) diodes were then fabricated on the sample using EBD. AFM analysis was performed on the as-deposited and annealed samples using the Bruker Dimension Icon Nanoscope 5 with ScanAsyst scanning probe microscope.

3. Results and discussion

3.1. Thermal stability of the Ti Schottky contacts

As-deposited metal-semiconductor contacts display non-ideal *I-V* characteristics. The experimental data were best fitted by the thermionic emission equation [6] which is given by

$$I = I_s\left[exp\left(\frac{qV}{nk_BT}\right) - 1\right] \quad (1)$$

where I is the measured current, I_s is the saturation current, V is the applied voltage, q is the electronic charge, n the ideality factor, k_B is the Boltzmann constant and T is the absolute temperature. The saturation current, I_s is given by

$$I_s = A^*AT^2 \exp\left(-\frac{q\phi_B}{k_BT}\right) \quad (2)$$

I_s is determined from the extrapolated intercept of log I versus V curve on the y-axis.

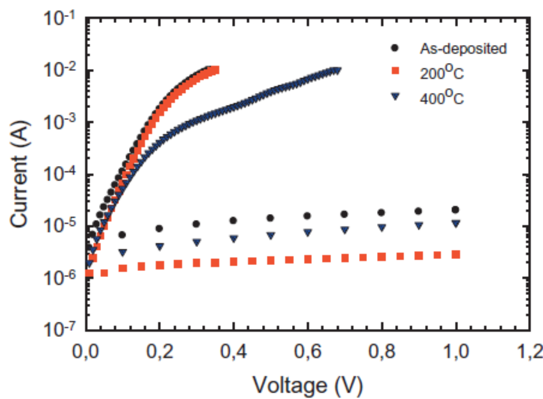

Fig. 1. The forward and reverse bias *I-V* characteristics of a Schottky contact after metallization (as-deposited), after isochronal thermal annealing for 20 min at a temperature of 200 °C and 400 °C, measured at room temperature.

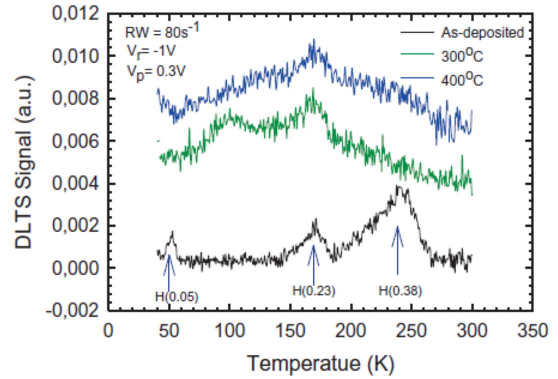

Fig. 2. The DLTS spectra of the as-deposited sample, after annealing at 300 °C and at 400 °C measured at a rate window (RW) of 80 s^{-1}.

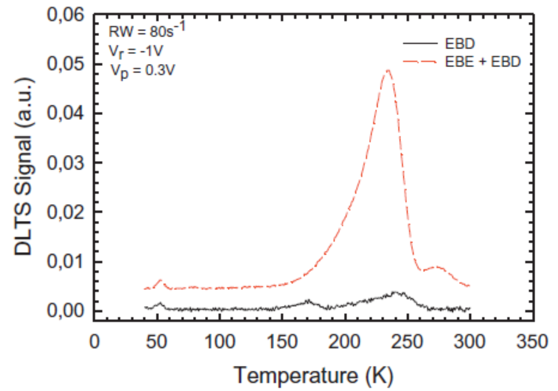

Fig. 3. The DLTS spectra of the EBD and EBE + EBD as-deposited samples measured at a rate window (RW) of 80 s^{-1}.

$$\phi_B = \left(\frac{k_BT}{q}\right)ln\left(\frac{A^*A^2}{I_s}\right) \quad (3)$$

where A^*, A and ϕ_B are the Richardson constant, the contact area and the Schottky barrier height respectively. Putting this value of

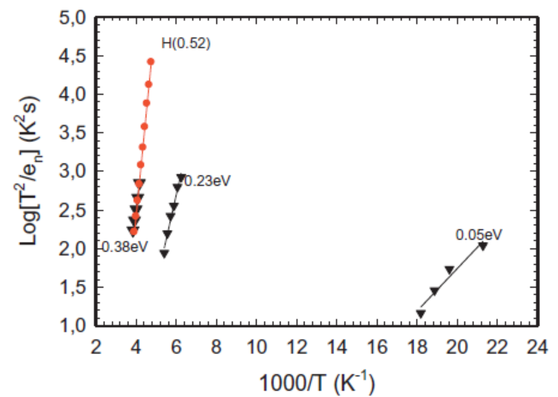

Fig. 4. The Arrhenius plot showing the defects present after: metallization (triangles) and electron beam exposure with electron beam deposition thereafter (circles).

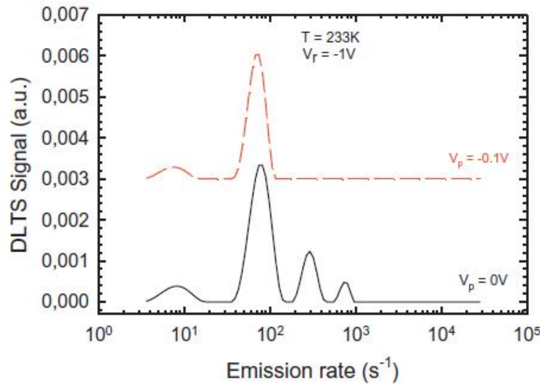

Fig. 5. The Laplace-DLTS spectrum clearly separating the signal of the EBE + EBD peak.

I_s in Eq. (3), the value of SBH is evaluated. From *I-V* measurements it was found that the barrier heights of Ti contacts directly after EBD were 0.55 eV. Fig. 1 shows that the Ti contact was affected by series resistance as the annealing temperature was increased. After annealing at 400 °C the Ti Schottky contacts degraded due to oxidation [7]. The barrier height of the Ti contact remained at 0.55 eV after annealing at 400 °C.

3.2. Electronic properties of EBD induced defects

DLTS revealed (Fig. 2) that the main defects introduced during metallization are H(0.05), H(0.23) and H(0.38). In this notation "H" means "hole trap" and the number after H is the activation enthalpy, in eV, obtained from an Arrhenius plot of log (T^2/e_n) vs 1000/T. Here e_n is the emission rate at temperature T. Annealing at 300 °C removed H(0.38) and H(0.05), while a new peak was introduced. The peak height was too small for resolution using L-DLTS as a result the peak's identity is not clear.

Two of the defects seen here are related to well-known radiation induced defects in Si. H(0.23) is the 0/+ charge state of the divacancy [8]. H(0.38) is introduced during electron irradiation, that was originally proposed by Mooney et al. to be associated with the carbon-oxygen-vacancy complex (V-O-C) also known as the K centre [8,9]. A defect at H(0.35) with a similar annealing behaviour has also been reported by Auret et al. after electron irradiation of p-Si, as well as after EBD of contacts on p-Si [1]. However, Trombetta et al. strongly demonstrated that this level is associated with the interstitial-substitutional carbon complex C_i-O_i [10]. The origin of H(0.05) is still the subject of speculation.

The conventional-DLTS spectra of the Ti contacts fabricated using EBD and the Ni contacts fabricated after EBE using EBD (EBE + EBD) are shown in Fig. 3. The EBE + EBD spectrum exhibits one prominent broad peak at 233 K and a small peak at 54 K which suggests that it is the EBD defect, H(0.05). In this study, the defects' electronic properties were extracted from the Arrhenius plots shown in Fig. 4. The activation energy calculated for the peak at 233 K was H(0.52).This defect may have been an EBD process induced defect. The defect's structure is still under investigation as are the rest of the peaks revealed by L-DLTS. Fig. 5 shows the high resolution L-DLTS spectra measured around the broad peak at −1 V reverse bias (V_r). L-DLTS separates the signals of the levels within that peak. The number of peaks was reduced by varying the filling pulse (V_p).

The aim of depth profiling was to find the defect concentration as a function of depth for individual defects. Fixed bias-variable pulse L-DLTS depth profiling [11,12] was used to measure the depth distribution of the defects investigated in this study. For each defect, the temperature was kept constant and the reverse bias of −2.5 V was maintained while varying the filling pulse. L-DLTS depth profiling showed that the concentration of all the defects reduced from the surface into the Si away from the junction. This was as a result of the fact that EBD introduces defects at and below the surface [1]. These defects have been shown to be produced by energetic particles accelerated from the locale of the electron filament onto the sample by the electric and magnetic fields present in the surrounding area of the metal source [2].

3.3. Morphology / surface topology of Ti contacts

AFM analysis revealed the topography of the samples used in this study. Fig. 6 displays images of Ti contacts obtained using

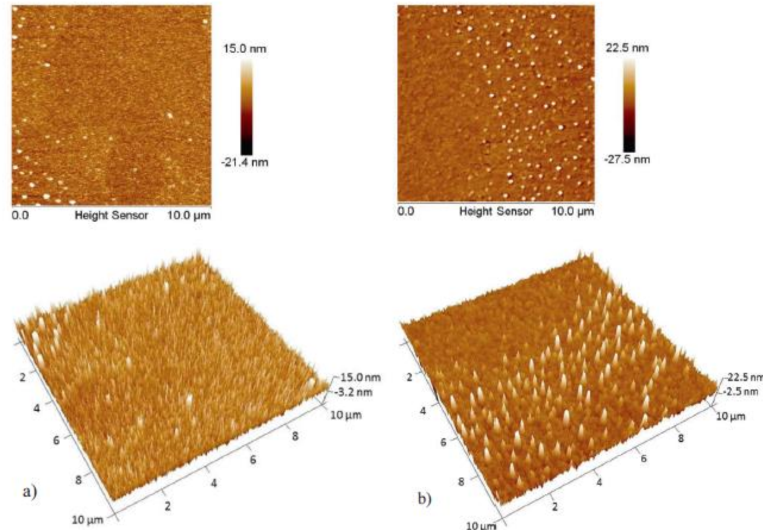

Fig. 6. 10 µm × 10 µm AFM 2-D and 3-D images of (a) the as-deposited sample and (b) after annealing at 400 °C.

ScanAsyst mode. The figure shows (a) the as-deposited sample and (b) the sample after annealing at 400 °C. The surface morphology of the as-deposited Ti/p-Si Schottky barrier diode is fairly rough with a root-mean-square (RMS) roughness of 3.43 nm. The roughness of the as-deposited SBDs may be attributed to damage from the electron beams during metal deposition [1]. The RMS roughness of the diodes increased with increase in annealing temperature. At annealing temperature of 400 °C, the surface morphology degraded slightly with RMS roughness of 4.15 nm. The degraded surface of the SBDs after the annealing may be as a result of outdiffusion of Si into Ti layers [13].

4. Conclusion

We have investigated the thermal stability (in the range 100–400 °C) of defects introduced in p-Si by EBD of Ti contacts as Schottky rectifiers. The Schottky barrier height remained at 0.55 eV after annealing at 400 °C. Series resistance affected the contacts as annealing temperature was increased. Three defects states were observed. H(0.23) and H(0.38) were states observed by other authors after irradiation H(0.23) was attributed to the divacancy of charge state 0/+. The level H(0.38) was associated with the K centre. The identity of H(0.05) is not yet known. AFM revealed that surface roughness increased with increase in annealing temperature. The origin of this surface roughening will be further investigated in future work.

Acknowledgements

The authors would like to thank the South African National Research Foundation (NRF) and the University of Pretoria for financial support. Views and opinions expressed in this article are those of the authors and not of the NRF. The authors would like to thank Dr J.M. Nel for her assistance with AFM analysis.

References

[1] F.D. Auret, P.M. Mooney, J. Appl. Phys. 55 (1984).
[2] C. Christensen, J.W. Petersen, A.N. Larsen, Appl. Phys. Lett. 61 (1992).
[3] H.J. Queisser, E.E. Haller, Science 281 (1998) 945–950.
[4] L. Dobaczewski, P. Kaczor, I.D. Hawkins, A.R. Peaker, Am. Inst. Phys. 76 (1994).
[5] H.T. Danga, F.D. Auret, S.M. Coelho, M. Diale, Phys. B 480 (2016) 206–208.
[6] S.M. Sze, K.K. Ng, Physics of Semiconductor Devices, 3rd ed., John Wiley and Sons (WIE), 2007.
[7] G.P. Burns, J. Appl. Phys. 65 (1989).
[8] P.M. Mooney, L.J. Cheng, M. Sulli, J.D. Gerson, J.W. Corbett, Phys. Rev. B 15 (1977).
[9] F.D. Auret, P.M. Mooney, Am. Inst. Phys. 55 (1983) 984–987.
[10] J.M. Trombetta, G.D. Watkins, Appl. Phys. Lett. 51 (1987).
[11] Y. Zohta, M.O. Watanabe, J. Appl. Phys. 53 (1982).
[12] F.D. Auret, S.M.M. Coelho, J. Nel, W.E. Meyer, Phys. Status Solidi A 209 (2012) 1926–1933.
[13] C. Ramesha, V.R. Reddy, Superlattices Microstruct. 76 (2014) 55–65.

4.1.2 Electron beam exposure

Electron beam exposure (EBE) is a process by which a semiconductor is exposed to EBD conditions without metal deposition. During the process, energetic particles that cause EBD damage are present but interact directly with the semiconductor whereas during EBD this interaction is mostly shielded by the metal being deposited [5]. The main goal of developing the EBE technique was to introduce EBD-induced defects in a controlled method and in easily measureable concentration [6].

In this work nickel (Ni) was used as the contact metal because its melting point (1455°C) is low enough for deposition in the resistive evaporation system, thereby allowing easy comparison between the two techniques. The maximum temperature at which the resistive deposition system at the University of Pretoria can evaporate is 1600°C.

In this study, EBE-induced defects in p-type silicon were studied. EBE-induced defects in n-type silicon have been reported by Danga et al. [7]. This work has been included as an appendix. A detailed comparison of EBE defects introduced in n-Si and p-Si is however beyond the scope of this thesis.

The results of a study on EBE-induced damage in p-type silicon are presented in the paper “Electrical characterisation of electron beam exposure induced defects in silicon” [5],which forms part of this thesis (see next page). In the paper, an electrically active defect in EBE-processed p-Si was studied using conventional and Laplace-DLTS. The defect level observed had an activation energy of H(0.55). This defect has an activation energy similar to that of the I-defect. This defect was also found to be like a defect observed in alpha-particle irradiated Si, which was believed to be boron related. The defect was not observed on contacts fabricated using EBD, which displayed two smaller defects. DLTS depth profiles were used to show that the damage caused by EBE extended deeper into the material compared to EBD damage.

The present author did the sample processing, performed the measurements, processed the data and wrote the paper. S.M.M Coelho and E. Omotoso assisted with electron beam exposure.

Physica B 480 (2016) 206–208

Contents lists available at ScienceDirect

Physica B

journal homepage: www.elsevier.com/locate/physb

Electrical Characterisation of electron beam exposure induced Defects in silicon

Helga T. Danga*, Francois D. Auret, Sergio M.M. Coelho, Mmantsae Diale

Department of Physics, University of Pretoria, Pretoria 0002

ARTICLE INFO

Article history:
Received 15 May 2015
Received in revised form
22 July 2015
Accepted 23 July 2015
Available online 26 July 2015

Keywords:
Silicon
Electron beam exposure
DLTS
Laplace-DLTS

ABSTRACT

The defects introduced in epitaxially grown p-type silicon (Si) during electron beam exposure were electrically characterised using deep level transient spectroscopy (DLTS) and high resolution Laplace-DLTS. In this process, Si samples were first exposed to the conditions of electron beam deposition (EBD) without metal deposition. This is called electron beam exposure (EBE) herein. After 50 minutes of EBE, nickel (Ni) Schottky contacts were fabricated using the resistive deposition method. The defect level observed using the Ni contacts had an activation energy of H(0.55). This defect has an activation energy similar to that of the I-defect. The defect level is similar to that of the HB4, a boron related defect. DLTS depth profiling revealed that H(0.55) could be detected up to a depth of 0.8 μm below the junction. We found that exposing the samples to EBD conditions without metal deposition introduced a defect which was not introduced by the EBD method. We also observed that the damage caused by EBE extended deeper into the material compared to that caused by EBD.

© 2015 Elsevier B.V. All rights reserved.

1. Introduction

Electron beam deposition (EBD) of metals in a vacuum system plays an important role in the semiconductor technology industry. This method is useful when it comes to depositing materials with a high melting point which cannot be evaporated by resistive heating because of limitations of the power input [1]. The disadvantage of EBD is that this technique introduces defects in n-type Si close to the metal-silicon interface [2]. These defects influence device performance and alter the barrier heights of the contacts [3].The defects responsible for these barrier modifications are formed when energetic particles reach the semiconductor surface and interact with it, resulting in lattice damage. Depending on the application, these defects may either be beneficial or detrimental for optimum device functioning. In silicon, for example, defect introduction during high energy electron and proton irradiation increases the switching speed of devices [4]. On the other hand, in the case of high open circuit voltage solar cells, degraded device properties have been reported after EBD of contacts [5,6].

The main aim of developing the EBE technique was to see if EBD induced defects could be introduced in a controlled manner. Excessive exposure would reduce the functionality of diodes for further study thus putting a limit on how much damage could be introduced. Energetic particles that cause EBD damage are present during EBE but interact directly with the semiconductor material whereas during EBD this interaction mostly occurs via the metal used as a contact [7]. Silicon(Si) is one of the most important semiconductor materials and it has been studied extensively [8]. This is mainly due to its low cost, thermal stability, and good durability [9]. It is because of these properties that Si is a suitable candidate for exploring the EBE technique.

In this paper we report the defects introduced in epitaxially grown, boron-doped, p-type Si. In addition, we identify the C_i and the I-defect. We demonstrate that when exposing the sample to EBD conditions without depositing any metal, different defects are introduced.

2. Experimental Details

Epitaxially grown boron-doped p-type Si $< 111 >$ grown on p^+ Si substrate was investigated. Before metallisation the samples were first degreased and then dipped in hydrofluoric acid (HF) for 1 minute to etch off the native oxide layer. Directly after cleaning the samples were inserted into the vacuum system. Vacuum pumping was carried out by a dry pump in series with a turbo molecular pump to lower the H_2 concentration. To improve the vacuum, titanium (Ti) was deposited in the chamber with the sample rotated away from the evaporation source. While the pre-deposition vacuum was typically 5×10^{-7} mbar, this soon increased to approximately 3×10^{-6} mbar during the evaporation. As the vacuum conditions vary greatly during EBD, forming gas

* Corresponding author.
E-mail address: helga.danga@up.ac.za (H.T. Danga).

http://dx.doi.org/10.1016/j.physb.2015.07.025
0921-4526/© 2015 Elsevier B.V. All rights reserved.

H15, with a composition of N_2: H_2 of 85%: 15% by volume was also used to raise the pressure in the vacuum chamber to 10^{-4} mbar and kept constant during processing of samples selected for EBE. Electron beam exposure of samples and the fabrication of contacts using electron beam deposition were done by utilising a 10 kV source (MDC model e-Vap 10CVS) with the samples positioned 50 cm above the crucible [5].

During EBE, without metal deposition, the samples were exposed for 50 minutes; while the beam heated a tungsten source using a beam current of 100 mA, this current being insufficient to evaporate tungsten, thus exposing the samples to EB conditions comparable to those experienced during deposition. Ni diodes were used for all the samples prepared for this study as this metal can be evaporated resistively, a process that is known to not introduce defects in concentrations measurable by deep level transient spectroscopy (DLTS) [5]. A control sample was prepared by resistively depositing aluminium (Al) contacts onto p-type epitaxial material without using EB exposure.. A sample with Al contacts irradiated with alpha-particles at a fluence of 5.1×10^{-10} cm^{-2} was also used in this study for comparison. DLTS and high resolution Laplace-DLTS were used to characterise the defects introduced in epitaxially grown p-type Si during EBE and EBD

3. Results and discussion

In this study, the following defects were observed: (H0.59), H (0.55), H(0.52), H(0.33) and H(0.16). The defect level observed using the Nickel contacts after EBE (spectrum (c) in Fig.1) had an activation energy of H(0.55) with an apparent capture cross-section of 6.6×10^{-14} cm^2. This defect had an activation energy similar to the I-defect. Pintilie et al. [10] observed a defect with a similar energy of 0.545 eV with an apparent capture cross-section of 9.0×10^{-14} cm^2.This defect was observed after exposing their samples to high irradiation fluences. The defect level was detected using thermally stimulated current (TSC). The H(0.55) defect is aligned to the defect H(0.52) as shown in Fig.2. This defect was introduced by alpha-particle irradiation. It had an apparent capture cross-section of 1.7×10^{-14} cm^2 and its temperature peak was at 246 °C. Nyamhere et al. measured a defect they referred to as HB4, a defect having an apparent cross-section of 1.3×10^{-13} cm^2. It had an activation enthalpy of 0.54 eV and its peak temperature

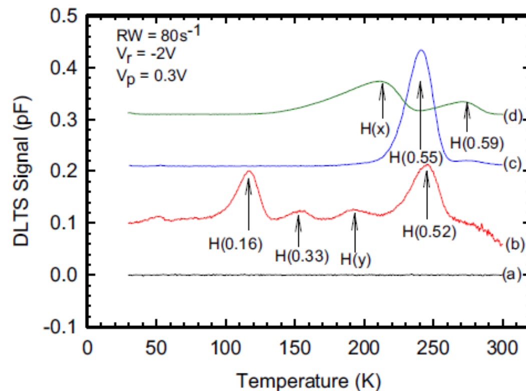

Fig. 1. DLTS spectra for (a) is a control spectrum measured from Al Schottky diodes fabricated using resistive deposition, (b) α-particle irradiated Al Schottky diodes, (c) Ni Schottky diodes fabricated after EBE and (d) Ni Schottky diodes fabricated using the EBD method.

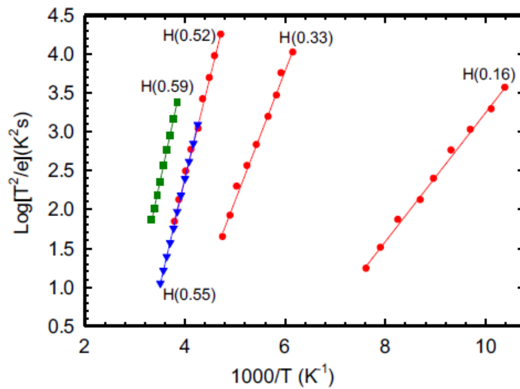

Fig. 2. Arrhenius plots for defects introduced after: samples exposed to electron beam conditions (EBE) thereafter Ni Schottky diodes fabricated (down triangles); α-particle irradiated Al Schottky diodes (circles) and Ni Schottky contacts fabricated using the EBD method (squares).

was at 240 °C. This peak temperature was similar to that of H (0.55), which lay at 242 °C. HB4 was attributed to interstitial boron-on-substitutional boron-hydrogen (B_i-B_s-H) complex [11–14].

For Ni contacts fabricated using EBD, spectrum (d) in Fig.1, we observed the defect level H(0.59). This defect had a similar activation enthalpy and apparent capture cross-section as that of HB5, a defect observed by Nyamhere et al. [14]. In their study of EBD processed induced defects and their annealing behaviour, it was proposed that the breakup of the 0.54 eV defect level was responsible for the introduction of the 0.59 eV level. This defect was boron related [14]. We were unable to resolve the peak H(x) using L-DLTS. This peak could have been a surface state or an extension of a defect.

From the spectrum shown in Fig.1(b), for the alpha-particle irradiated Al contacts, the hole traps observed were: H(0.16), H (0.33) and H(0.52).The defect level H(0.33) was identified as the interstitial carbon (C_i) related defect. It was a result of induced damage and could only be explained by the presence of donor-like traps [7].The capture cross-section was calculated to be 1.6×10^{-19} cm^2 from the Arrhenius plot shown in Fig. 2. Auret et al. observed a defect in p-type silicon with the same activation energy in samples that had been fabricated with titanium contacts using the resistive deposition method [15]. Defects with a similar activation energy (H(0.33)) have been identified in the literature. These are all related to the residual carbon impurity which has been reported to form complexes directly with radiation-produced primary defects or with secondary defects induced by radiation damage. These defects include the interstitial-carbon-interstitial-oxygen ($C_i - O_i$) complex (C(3) centre) [16], the carbon-oxygen-vacancy complex (the K centre) [17,18] and the interstitial-substitutional-carbon complex ($C_s - C_i$)[19–21]. In their study, Asghar et al. observe that the 0.35 eV defect annealed at approximately 400 °C in agreement with the literature of similar defect levels $E_V + 0.38$ and $E_V + 0.33$ [17,18]. These reports suggest that this level originates from the carbon-oxygen-vacancy ($C - O - V$) complex. However, studies by Song et al. [22] strongly suggest this defect to be associated with $C_i - O_i$ complex. This deep level would be expected to be strongly dependant on the material and sample since unintentional carbon and oxygen contamination could vary with the material growth technique used as well as device processing. It seems that H(0.52) is a boron impurity related defect. This defect was attributed to EBD damage. [14]. The identity of H(0.16) has not been established. Resolving the identity of peak H(y) using L-DLTS

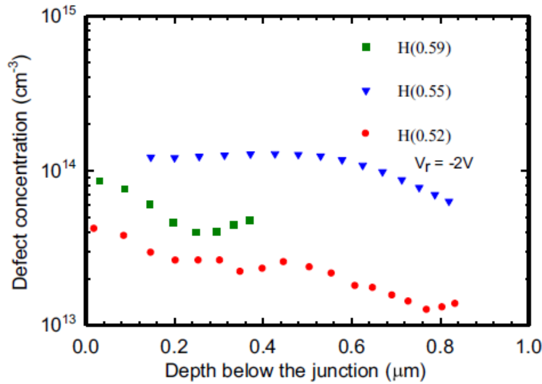

Fig. 3. Depth concentration profiles of H(0.59) a defects introduced by EBD,H(0.55) is a defect introduced during EBE and H(0.52) is a defect level introduced by α-particle irradiation.

proved to be a challenge. It may have been an extension of a neighbouring defect.

The aim of depth profiling was to find the defect concentration as a function of depth for individual defects. Fixed bias-variable pulse Laplace-DLTS depth profiling [6,23] was used to measure the depth distribution of the defects investigated in this study. For each defect, the temperature was kept constant, the reverse bias of -2 V was maintained while varying the filling pulse. Fig. 3 illustrates the results obtained. Depth profiling of the defects showed that as we probed deeper into the bulk away from the junction, the H(0.55) defect decreased from 1×10^{14} cm^{-3} at the metal-semiconductor interface to 6×10^{13} cm^{-3} about 0.8 μm below the interface. The defect level H(0.59) introduced by EBD, decreased from 2×10^{14} cm^{-3} at the interface to about 5×10^{13} cm^{-3}at 0.4 μm below the junction. In the case of the defect level H(0.52), the defect concentration showed a decrease from 4×10^{13} cm^{-3}at the junction to 1×10^{13} cm^{-3} at approximately 0.8 μm below the junction. This implies that the damage caused by EBE extends deeper into the material when compared to EBD. This is because during EBD, the metal deposited shields the semiconductor material from the energetic particles which would otherwise have more energy when interacting with the material.

4. Conclusion

We observed that the EBE process induced a different defect to the one observed in the EBD. H(0.55) for Ni contacts was associated with the I-centre. The defect H(0.59) was observed after EBD. H(0.59) was a boron related defect. The hole traps observed for alpha-particle irradiated Al contacts were: H(0.16), H(0.33) and H(0.52). H(0.33) was identified as the interstitial carbon (C_i) related defect and H(0.52) was identified as a boron impurity related defect. This study revealed that a different defect is introduced during EBE which is not introduced by EBD method. The H(0.55) defect level seems to have been of the same origin as H(0.52), a defect introduced by alpha-particle irradiation. Laplace-DLTS depth profiling revealed that H(0.55) could be detected up to a depth of 0.8 μm. The EBD defect observed was at 0.4μm below the junction. The defect introduced by alpha-particle irradiation extended to a depth of about 0.83 μm.The damage caused by EBE extends deeper into the material compared to EBD but not as deep as alpha-particles. This was attributed to the shielding effect the deposited metal has on the semiconductor material from the energetic particles which would otherwise extend deeper into the material.

Acknowledgements

The authors would like to thank the National Research Foundation of South Africa for the financial support. We also thank Mr P.J Janse van Rensburg for his technical assistance.

References

[1] F.D.Auret, P.M.Mooney, American Institute of Physics 55 (1983).
[2] F.D. Auret, P.M. Mooney, J. App. Phys 55 (1984).
[3] G. Myburg, F.D. Auret, J. Appl. Phys. 71 (1992).
[4] D.C. Swako, J. Bartko, IEEE Nucl. Sci. 30 (1983).
[5] A.W. Blakers, M.A. Green, IEEE Electron Device Letters (1984) 246.
[6] F.D. Auret, S.M.M. Coelho, J. Nel, W.E. Meyer, Phys.Status Solidi A 209 (2012) 1926–1933.
[7] O. Paz, F.D. Auret, Mat. Res. Soc. Symp 25 (1984).
[8] S.M. Sze, Physics of Semiconductor Devices, Second ed., John Wiley and Sons (WIE), 1981.
[9] ⟨http://www.americanphotonics.com/si.php⟩, 2009.
[10] I. Pintilie, M. Buda, E. Fretwurst, G. Lindstom, J. Stahl, Nuclear Instruments and Methods in Physics Research A 556 (2006) 197–208.
[11] O. Feklisova, N. Yarikin, E.B. Yakimov, J. Weber, Physica B (2001) 210–212.
[12] M. Mamor, M. Willander, F.D. Auret, W. Meyer, E. Sveinbjornsson, Phys. Rev. B B63 (2000).
[13] F. Volpi, A.R. Peaker, I. Berebezier, A. Ronda, J. Appl. Phys. 95 (2004).
[14] C. Nyamhere, A.G.M. Das, F.D. Auret, M.H. C., Journal of Physics Conference Series, IOP, 2008.
[15] F.D. Auret, R. Kleinhenz, C.P. Schnider, Appl. Phys. Lett. 44 (1984).
[16] J.M. Trombetta, G.D. Watkins, Appl. Phys. Lett. 51 (1987).
[17] P.M. Mooney, L.J. Cheng, M. Sulli, J.D. Gerson, J.W. Corbett, Phys. Rev. B 15 (1977).
[18] Y.H. Lee, K.L. Wang, A. Jaworowski, P.M. Mooney, L.J. Cheng, J.W. Corbett, Phys. Status Solidi A 57 (1980) 697.
[19] L.C. Kimberling, International Connference On Radiation Effects On Semiconductors, in: N.B. Urli, J.W. Corbett (Eds.), Inst. Phys., Bristol, 1977, p. 221 , Ser.No.
[20] L.C. Kimberling, IEEE Trans. Nucl.Sci. NS-23 (1976) 1497.
[21] M.Asghar, M.Z.Iqbal, N.Zafar, American Institute of Physics 73 (1993).
[22] L.W. Song, X.D. Zhan, B.W. Benson, G.D. Watkins, Physical Review B 42 (1990).
[23] Y. Zohta, M.O. Watanabe, J.Appl. Phys. 53 (1982).

4.2 Radiation-induced defects

Radiation-induced defects originate as a result of processing steps which can introduce radiation damage or by operating in radiation-harsh environments. From a physics point of view the understanding and control of radiation damage is key for process optimisation [8] and production of radiation hard devices for space applications [9].Furthermore, there should be a correspondence between process and irradiation-induced defects, which could lead to better understanding of the fundamental physics involved. This section focuses on alpha-particle irradiation.

4.2.1 Alpha-particle irradiation at room temperature

In this section, results obtained from the electrical characterisation of α-particle induced defects are reported. Aluminium (Al) contacts fabricated on the p-type silicon samples were irradiated by making use of a 5.4 MeV Am-241 radioactive source with a fluence rate of 7×10^6 cm^{-2}s^{-1}. The Al contacts were irradiated for 30 minutes initially at a fluence of 1.3×10^{10} cm^{-2}. The contacts were then exposed for another 90 minutes at 30minute intervals until the total fluence was 5.1 $\times 10^{10}$cm^{-2}. *I-V* measurements, *C-V* measurements and DLTS were done after each irradiation.

An article by the present author entitled “Electrically active defects in p-type silicon after alpha particle irradiation” [10], presents the results of the study. In this work, conventional DLTS revealed five peaks, with the parameters of four of the defects were obtained using Laplace-DLTS.The defect level H(0.10) was tri-vacancy related. H(0.33) was identified as the interstitial carbon (Ci) related defect which was a result of radiation induced damage. H(0.52) was a B-related defect. Absolute deductions about the origin of H(0.16) have not yet been achieved. Due to the proximity of a large peak, the parameters of the fifth peak could not be determined by Laplace-DLTS.

The present author’s contribution to the paper included: planning, sample preparation, electrical characterisation, data analysis and writing of the draft manuscript for proof reading and discussion with the co-authors.

Physica B 535 (2018) 99–101

Contents lists available at ScienceDirect

Physica B

journal homepage: www.elsevier.com/locate/physb

Electrically active defects in p-type silicon after alpha-particle irradiation

Helga T. Danga*, F. Danie Auret, Shandirai M. Tunhuma, Ezekiel Omotoso, Emmanuel Igumbor, Walter E. Meyer

Department of Physics, University of Pretoria, Pretoria 0002, South Africa

ARTICLE INFO

Keywords:
Silicon
Laplace-DLTS
Irradiation

ABSTRACT

In this work, we investigated the defects introduced when boron (B) doped silicon (Si) was irradiated by making use of a 5.4 MeV americium (Am) 241 foil radioactive source with a fluence rate of 7×10^{6} cm^{-2} s^{-1} at room temperature. Deep level transient spectroscopy (DLTS) and Laplace-DLTS measurements were used to investigate the electronic properties of the introduced defects. After exposure at a fluence of 5.1×10^{10} cm^{-2}, the energy levels of the hole traps measured were: H(0.10), H(0.16), H(0.33) and H(0.52) The defect level H(0.10) was tri-vacancy related. H(0.33) was identified as the interstitial carbon (C_i) related defect which was a result of radiation induced damage. H(0.52) was a B-related defect. Explicit deductions about the origin of H(0.16) have not yet been achieved.

1. Introduction

Silicon (Si) is arguably the most important semiconductor material. It has been studied extensively and widely used in commercial products [1]. This is mainly due to its low cost, thermal stability, good durability [2] and reliability of its oxide for use in complementary metal-oxide semiconductor (CMOS) technology [3]. These properties have enabled researchers to make major advances towards reliable and cost-effective silicon-based photonic–electronic integration [4].

The study of radiation-induced defects in semiconductors comprises a significant area of research on materials from the point of view of device applications [5]. For Si, studies using high energy electron irradiation, have been primarily motivated by the strong degradation effects on Si solar cells caused by radiation during space use. Gamma-rays and neutrons have also been used to study defects in Si which are generally produced in electronic devices in nuclear radiation environments such as those provided by nuclear reactors [5]. α-radiation from packaging was well-known as the major source of failure in Si memory devices causing both soft [6] and hard [7] errors. Thus, α-particle-induced defects are a cause of principal concern for the in-use failure of these electronic applications of Si devices. Not many studies on alpha-particle radiation induced defects exist in literature [5] these have primarily focused on n-type material. Takeuchi *et al.* [7] reported on deep level defects produced by α-particle irradiation in the upper half of the band gap of the p-type Si. A detailed and comprehensive characterisation of defects in p-type material in both halves of the band gap is generally lacking in the literature [5]. Furthermore, reports on hole traps are not many due to the struggle in fabricating quality Schottky contacts on p-type Si for consistent electrical characterisation [8].

In this paper we report on defects introduced in B doped p-type Si after irradiation by α-particles at room temperature. The defects were investigated using deep level transient spectroscopy (DLTS) and Laplace-DLTS which are quantitative electrical characterisation techniques highly suitable for point defect studies.

2. Experimental details

Aluminium (Al) Schottky contacts were fabricated on the p-Si samples with indium-gallium eutectic as the ohmic contact. Current-voltage (*I-V*) and capacitance-voltage (*C-V*) measurements were conducted to ascertain the quality of the contacts produced. Thereafter, DLTS measurements were carried out on the samples. The samples were then irradiated with α-particles at room temperature. This was achieved by making use of a 5.4 MeV Am-241 radioactive source with a fluence rate of 7×10^{6} $cm^{-2}s^{-1}$. The Al samples were first irradiated for 30 min at a fluence of 1.3×10^{10} cm^{-2} then the samples were exposed for 120 min at a cumulative fluence of 5.1×10^{10} cm^{-2}. *I-V* measurements, *C-V* measurements and DLTS were done in the 40 – 300 K temperature range at a scan rate of 2 K/min, after each irradiation. High resolution Laplace-DLTS was used to resolve the defects observed. In this study, the Al diodes were made using resistive evaporation which is known not to introduce defects in concentrations that can be measured by DLTS [9].

* Corresponding author.
E-mail address: helga.danga@up.ac.za (H.T. Danga).

http://dx.doi.org/10.1016/j.physb.2017.06.070
Received 21 April 2017; Received in revised form 20 June 2017; Accepted 26 June 2017
Available online 27 June 2017
0921-4526/ © 2017 Elsevier B.V. All rights reserved.

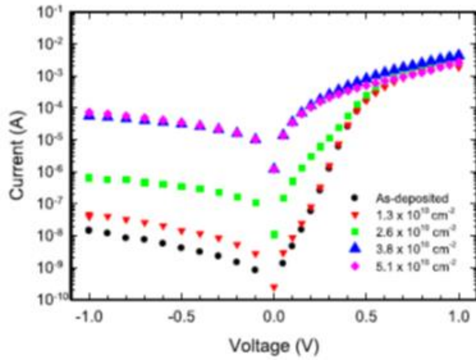

Fig. 1. Semi-logarithmic plot for forward and reverse *I-V* characteristics for the Al/p-Si contacts before and after α-particle irradiation up to a fluence of 5.1×10^{10} cm^{-2}.

3. Results and discussion

3.1. I-V characterisation

The *I-V* characteristics of the Al Schottky contacts prior to and after α-particle irradiation are shown in Fig. 1. The as-deposited samples produced a linear forward *I-V* curve. At this point the thermionic emission model can be used to explain the transport mechanism at the metal-semiconductor interface and can be expressed as

$$I = I_s exp\left(\frac{qV}{nkT}\right)\left[1 - exp\left(\frac{-qV}{kT}\right)\right]$$

Where I is the measured current, I_s is the saturation current, V is the applied voltage, q is the electronic charge, n the ideality factor, k_B is the Boltzmann constant and T is the absolute temperature. The forward-semi-logarithmic *I-V* curves obtained after irradiation deviated from linearity as the time of exposure to irradiation increased. This is ascribed to defects introduced by irradiation which lead to generation recombination current therefore the non-linear curves at low voltages.

Table 1 summarises the diode characteristics obtained from *I-V* and *C-V* measurements. The Schottky barrier height (SBH) was modified as the irradiation fluence increased. The ideality factor increased tremendously from 1.36 to 5.68. which was very large and indicated that the thermionic emission model doses not hold and other mechanisms, e.g. generation recombination dominate [10].

The *I-V* SBH decreased with increasing radiation fluence while the *C-V* SBH increased with increasing radiation fluence. These changes in both *I-V* and *C-V* characteristics were attributed to radiation damage [7]. The reverse leakage current, measured at −1V, increased from 1.44×10^{-8}A before irradiation to 7.15×10^{-5} A after irradiation with a fluence of 5.1×10^{-10} cm^{-2}. This could have been a consequence of interface states present at the metal-semiconductor interface or a non-uniform thin oxide layer at the interface [11].

The free carrier density was obtained from the slope of the $1/C^2$ versus V curve. The free-carrier density was 2.4×10^{15} cm^{-3} before irradiation. The initial radiation exposure decreased the free carrier density to 2.3×10^{15}cm^{-2}. It remained at this value for the subsequent two doses then it decreased to 2.2×10^{15}cm^{-3} at a fluence of 5.1×10^{10} cm^{-2}. We deduce from this that the concentration of deep levels is much less than the carrier density and the sample is therefore suitable for Laplace-DLTS investigations.

Table 1
Parameters obtained from *I-V* and *C-V* measurements as the irradiation fluence increased.

Fluence (cm^{-2})	n	I-V SBH (eV)	C-V SBH (eV)	I_R at -1V (A)	Free carrier density (cm^{-3})
0	1.36	0.81	1.25	1.4×10^{-8}	2.4×10^{15}
1. 3×10^{10}	1.43	0.79	1.20	3.9×10^{-8}	2.3×10^{15}
2. 6×10^{10}	2.55	0.64	1.24	6.7×10^{-7}	2.3×10^{15}
3. 8×10^{10}	4.30	0.52	1.32	5.6×10^{-5}	2.3×10^{15}
5. 1×10^{10}	5.68	0.51	1.30	7.2×10^{-5}	2.2×10^{15}

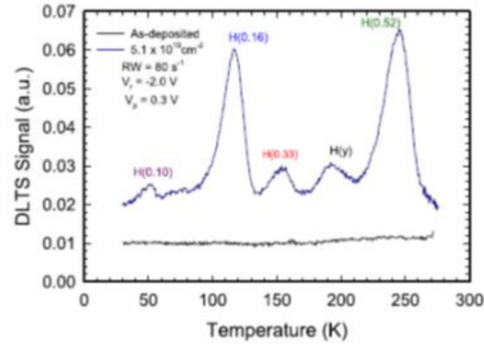

Fig. 2. DLTS spectra illustrating the as deposited sample and defects obtained after α-particle irradiation at a fluence of 5.1×10^{10} cm^{-2}.

3.2. DLTS characterisation

From the spectrum shown in Fig. 2, the hole traps observed were: H(0.11), H(0.16), H(0.33) and H(0.52). In this nomenclature, "H" means "hole trap" and the number after H is the activation enthalpy, in eV, obtained from an Arrhenius plot of log (T^2/e_n) vs 1000/T. Here e_n is the emission rate at temperature T. The defect H(0.10) was identified as the tri-vacancy (V_3) related defect. The calculated capture cross-section was 2.5×10^{-16} cm^2 from the Arrhenius plot shown in Fig. 3. Markevich *et al.* [12] identified + 0.106 eV as one of the energy levels of V_3. They observed this defect level after irradiating their samples with 6 MeV electrons and subsequent annealing at 100 °C. These authors also employed ab initio modelling for the identification of the same defect.

The defect level H(0.33) was identified as the interstitial carbon (C_i) related defect. It was a result of induced radiation damage [13]. The apparent capture cross-section was calculated to be 1.6×10^{-19} cm^2. Auret *et al.* [14] observed a defect in p-type silicon with the same activation energy in samples that had been fabricated with titanium contacts using resistive deposition. Defects with similar activation energies have been identified in literature [15]. They are all related

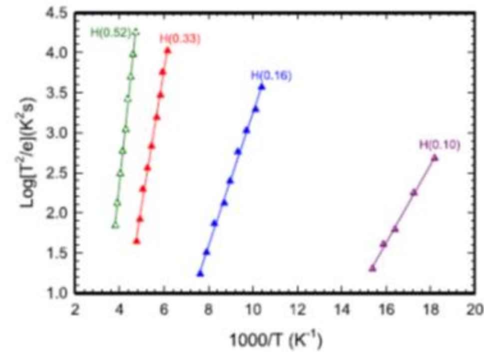

Fig. 3. Arrhenius plots obtained using the L-DLTS technique on Al/p-Si contacts after α-particle irradiation.

to the residual carbon impurity which has been reported to form complexes directly with radiation-induced primary defects or with secondary defects induced by radiation damage. These defects include the interstitial-carbon-interstitial-oxygen (C_i–O_i) complex (C(3) centre) [16], the carbon-oxygen-vacancy complex (K centre) [17,18] and the interstitial-substitutional-carbon complex (C_s–C_i) [5]. In their study, Asghar *et al.* [5] observed that the 0.35 eV defect annealed at approximately 400 °C, in agreement with literature of similar defect levels, E_V+0.38 and E_V+0.33 [17,18]. These reports suggest that the H(0.33) level originates from the carbon-oxygen-vacancy ($C-O-V$) complex. However, studies by Song *et al.* [19] strongly suggest that this defect is associated with C_i–O_i complex. This deep level is probably strongly dependant on the semiconductor and sample since unintentional carbon and oxygen contamination could vary with the material growth technique used as well as device processing [5].

H(0.52) was observed by Volpi *et al.* [20] after wet chemical etching followed by sputter deposition of MBE-grown boron doped silicon. They concluded that the defect was B-related. A similar defect was observed after electron beam deposition (EBD) damage [21]. The apparent capture cross-section of H(0.52) was 1.7×10^{-14} cm^2. H(0.16) was observed by Feklisova *et. al.* [22] it was a radiation induced defect observed in hydrogenated Si after electron irradiation. The capture-cross-section of H(0.16) was 1.8×10^{-17} cm^2. Resolving the peak H(y) using L-DLTS proved to be a challenge. The peak may have been an extension of neighbouring defects or a continuum of defect states.

4. Conclusion

We reported on defects introduced in epitaxially grown B doped p-type Si after irradiation by α-particles at room temperature. The *I-V* characteristics illustrate that the Al contacts rectification properties deteriorated as the irradiation fluence increased. The as deposited sample showed linear forward *I-V* characteristics with the leakage current at 1.4×10^{-8} *A*. The value of the reverse leakage current increased to 7.2×10^{-5} *A* while the forward *I-V* graphs lost their linearity as the irradiation fluence increased. The hole traps observed after alpha-particle irradiation of Al contacts were: H(0.16), H(0.33) and H(0.52). H(0.33) was identified as the interstitial carbon (C_i) related defect and H(0.52) was identified as a B-related defect. We have not yet made any explicit deduction about the origin of H(0.16).

Acknowledgements

This work is based on the research supported by the National Research Foundation of South Africa under grant number 98961. Opinions, findings and conclusions or recommendations are that of the authors, and the NRF accepts no liability whatsoever in this regard. The authors would like to thank the University of Pretoria for financial support. Views and opinions expressed in this article are those of the authors and not of the NRF. We also thank Mr P.J Janse van Rensburg for his technical assistance. The Laplace DLTS software and hardware used here was received from L. Dobaczeweski (Institute of physics, Polish Academy of Science) and A. R. Peaker (Centre for Electronic Materials Devices and Nano-structures, University of Manchester.

References

[1] S.M. Sze, K.K. Ng, Physics of Semiconductor Devices, 3rd ed, John Wiley and Sons (WIE), 2007.
[2] H.T. Danga, F.D. Auret, S.M. Coelho, M. Diale, Phys. B: Condens. Matter 480 (2016) 206–208.
[3] E.Y. Wu, E.J. Nowak, A. Vayshenker, W.L. Lai, D.L. Harmon, IBM J. Res. Dev. 46 (2002) 287–298.
[4] S. Chen, W. Li, J. Wu, Q. Jiang, M. Tang, S. Shutts, S.N. Elliott, A. Sobiesierski, A.J. Seeds, I. Ross, Nat. Photonics (2016).
[5] M. Asghar, M.Z. Iqbal, N. Zafar, J. Appl. Phys. 73 (1993) 4240–4247.
[6] R.C. Baumann, IEEE Trans. Device Mater. Reliab. 5 (2005) 305–316.
[7] K. Takeuchi, K. Shimohigashi, H. Kozuka, T. Toyabe, K. Itoh, H. Kurosawa, IEEE Trans. Electron Devices 37 (1990) 730–736.
[8] C. Nyamhere, F. Cristiano, F. Olivie, E. Bedel-Pereira, Z. Essa, Phys. Status Solidi C 11 (2013) 146–149.
[9] A.W. Blakers, M.A. Green, IEEE Electron Device Lett. (1984) 246.
[10] E.H. Rhoderick, IEE Proc. I-Solid-State Electron Devices 129 (1982) 1.
[11] D.K. Schroder, Semiconductor Material And Device Characterization, A John Wiley & Sons, Inc, 2006.
[12] V. Markevich, A. Peaker, B. Hamilton, S. Lastovskii, L. Murin, J. Coutinho, V. Torres, L. Dobaczewski, B. Svensson, Phys. Status Solidi (a) 208 (2011) 568–571.
[13] O. Paz, F.D. Auret, Mat. Res. Soc. Symp. 25 (1984).
[14] F.D. Auret, R. Kleinhenz, C.P. Schnider, Appl. Phys. Lett. 44 (1984).
[15] L.C. Kimberling, International Connference On Radiation Effects On Semiconductors, Bristol, 1977, pp. 221.
[16] J.M. Trombetta, G.D. Watkins, Appl. Phys. Lett. 51 (1987).
[17] P.M. Mooney, L.J. Cheng, M. Sulli, J.D. Gerson, J.W. Corbett, Phys. Rev. B 15 (1977).
[18] Y.H. Lee, K.L. Wang, A. Jaworowski, P.M. Mooney, L.J. Cheng, J.W. Corbett, Phys. Status Solidi A 57 (1980) 697.
[19] L.W. Song, X.D. Zhan, B.W. Benson, G.D. Watkins, Phys. Rev. B 42 (1990).
[20] F. Volpi, A.R. Peaker, I. Berbezier, A. Ronda, J. Appl. Phys. 95 (2004) 4752–4760.
[21] C. Nyamhere, A.G.M. Das, F.D. Auret, M. Hayes, J. Phys. Conf. Ser., IOP (2008).
[22] O.V. Feklisova, N.A. Yarykin, Semicond. Sci. Technol. 12 (1997) 742–749.

4.2.2 Low temperature alpha-particle irradiation

This section looks at the defects introduced using low temperature irradiation. The reason for undertaking low temperature irradiation is that it allows observation of first generation defects which are not seen after room temperature irradiation. Although low temperature irradiation by electrons has been reported [11-13], it is expected that alpha-particle irradiation would cause more damage because of alpha-particles greater mass [14]. Moreover, alpha particle irradiation is safer to use because of its weak penetrating power and lack of bremsstrahlung.

The present author has written a manuscript entitled "The study of low temperature irradiation induced defects in p-Si using deep-level transient spectroscopy". In this work, irradiation was carried out at cryogenic temperatures. By making use of conventional DLTS, the defect levels were observed were +0.10 eV, +0.14 eV and +0.18 eV. These peaks were attributed to the boron-substitutional vacancy, the mono-vacancy a vacancy related defect respectively

The present author's contribution to the paper included: planning of the experimental set up and assembly, sample preparation, electrical characterisation, data analysis and wrote the draft manuscript for proof reading and discussion with the co-authors.

Nuclear Inst. and Methods in Physics Research B 442 (2019) 28–30

Contents lists available at ScienceDirect

Nuclear Inst. and Methods in Physics Research B

journal homepage: www.elsevier.com/locate/nimb

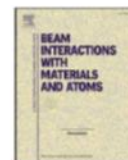

The study of low temperature irradiation induced defects in p-Si using deep-level transient spectroscopy

H.T. Danga*, S.M. Tunhuma, F.D. Auret, E. Igumbor, E. Omotoso, W.E. Meyer

Department of Physics, University of Pretoria, Pretoria 0002, South Africa

ARTICLE INFO

Keywords:
Silicon
Irradiation
Vacancy
DLTS

ABSTRACT

Primary defects introduced in boron-doped silicon by an alpha-particle source with a fluence rate of $7 \times 10^6\,\text{cm}^{-2}\text{s}^{-1}$ at cryogenic temperatures were investigated using deep-level transient spectroscopy (DLTS). The data showed that the defects observed between 35 K and 120 K were not detectable when irradiation was carried out at room temperature. The defect levels were observed at 0.10 eV, 0.14 eV and 0.18 eV above the valence band maximum. These levels were attributed to the boron-substitutional vacancy complex, the mono vacancy and a vacancy-related defect respectively.

1. Introduction

For over 50 years, defects in Si have been investigated, but a clear understanding of their nature and occurrence still lacks. This is because at room temperature some point defects such as interstitials (I) and vacancies (V), are difficult to investigate in Si as they become mobile above cryogenic temperatures [1]. It is of paramount importance to gain a more complete understanding of the properties of point defects and their evolution with temperature. Interstitials and vacancies are difficult to produce in p-type Si but it can be done by irradiating at cryogenic temperatures [2].

Effective defect engineering of electronic materials will depend on a thorough understanding of the generation of electrically active defects, which are responsible for the changes observed in the devices' properties at their operating temperatures [3]. In the case of Si detectors, degradation manifests itself as an increase in leakage current, free carrier concentration removal and a decrease in charge collection efficiency. This makes the radiation tolerance of Si detectors an issue of great concern to which much effort has been devoted in recent years [4].

When compared to n-type semiconductors, there are fewer articles on the subject of Schottky barriers on p-type materials because their barriers are generally so much lower. Moreover, the low impedance of the resulting devices makes measurement difficult. The hurdle in fabricating quality Schottky contacts on p-type Si for reliable electrical characterisation reduces technological interest in the p-type material [5]. This is why there are more studies on implantation-induced defects on electron traps than reports on hole traps [6].

Work on irradiating p-Si at low temperatures has been reported by Zangenberg and Nylandested Larson [1,2]. Immediately after irradiation they observed the vacancy with the trap energy at 0.137 eV, the divacancy at 0.189 eV and two of the three configurations of the boron substitutional vacancy ($B_S - V$) designated by them as AA1 and AA2. The AA1 configuration was found to be at 0.175 eV. The AA2-defect was too unstable and small for thorough analysis. These authors made use of 2 MeV electrons and a temperature range of 20–50 K [1]. Gorelkinskii et al. [7] also reported on low temperature irradiation using H^+ and He^{++} (at 30 MeV and 4.7 MeV, respectively) at 77 K. The samples contained the defect levels H1 (E_V + 0.13 eV), H2 (E_V + 0.20 eV) and H3 (E_V + 0.29 eV) which have been identified as the vacancy (+ +/0), divacancy (+/0) and carbon interstitial trapped by a substitutional carbon ($C_i - C_s$) (+/0).

Deep-level transient spectroscopy (DLTS) has been useful in deducing most of the characteristics of defects introduced in several semiconductors during crystal growth, radiation with different particle types, and by several device fabrication processes [8]. DLTS is a highly sensitive technique, which is capable of detecting impurities at low concentrations and measures their electronic properties such as energy level(s) in the band gap, defect concentration and apparent capture cross sections for electrons and holes [8,9].

In this article, we report on defects introduced in boron-doped p-type Si after irradiation by alpha particles at 35 K. Low temperature irradiation enables us to observe primary defects which are not normally seen after room-temperature irradiation. To the best of our knowledge previous studies have been carried out at temperatures around 77 K using liquid nitrogen based systems or on systems. In this

* Corresponding author.
E-mail address: helga.danga@up.ac.za (H.T. Danga).

https://doi.org/10.1016/j.nimb.2019.01.015
Received 1 September 2018; Received in revised form 30 December 2018; Accepted 9 January 2019
Available online 17 January 2019
0168-583X/ © 2019 Elsevier B.V. All rights reserved.

study, irradiation was carried out in a closed-cycle helium cryostat that can reach 35 K. This allows for measurements in a wider temperature range after irradiation. Previous researchers were limited by instrumentation [10,11]. Moreover, cryogenic temperatures are required to freeze in most primary defects [12].

2. Experimental techniques

Aluminium (Al) Schottky diodes were made on boron-doped *p*-type float zone (FZ) Si wafers with a carrier concentration of $1.9 \times 10^{15}\,\mathrm{cm}^{-3}$. The samples were first cleaned using a three-step degreasing method by making use of trichloroethylene, isopropanol and methanol. Thereafter, the samples were rinsed in deionised water and then etched in hydrofluoric acid to remove the native oxide layer. Flowing nitrogen gas was used to dry the samples before loading them into a resistive evaporation chamber. In this study, the Al diodes were made using resistive evaporation because this method is known not to introduce defects in concentrations that can be detected by DLTS [13].

Indium–gallium eutectic liquid alloy was painted on the other side of the wafer to form the ohmic contact. After contact fabrication, irradiation was performed at a temperature of 35 K with alpha particles. This was achieved by making use of a 5.4 MeV Am-241 radioactive source with a fluence rate of $7 \times 10^{6}\,\mathrm{cm}^{-2}\mathrm{s}^{-1}$. The samples and the alpha-particle source were mounted in a closed-cycle helium cryostat, with the alpha-particle source at room temperature and mounted 10 mm above the sample. Irradiation temperature was controlled using a Lakeshore 332 temperature controller and a heated stage. All samples were irradiated for 132 hours to a fluence of $1.3 \times 10^{13}\,\mathrm{cm}^{-2}$. Deep-level transient spectroscopy (DLTS) was conducted after irradiation.

The samples were kept below 35 K until DLTS measurements were performed in the 35–110 K temperature range at a scan rate of 2 K/min. The quiescent reverse bias was −1 V, the filling pulse amplitude 0.5 V and the filling pulse width 1 ms.

Arrhenius analysis was done according to the equation

$$e_p = \sigma_p \langle v_p \rangle \frac{g_o}{g_1} N_v \exp\left(\frac{E_V - E_T}{k_B T}\right) \quad (1)$$

This equation gives the emission rate as a function of temperature T, where $\langle v_p \rangle$ is the thermal velocity of electrons, $(E_V - E_T)$ is the activation energy. N_v is the effective density of states in the valence band and g_0 and g_1 are the degeneracy terms referring to the states before and after hole emission and k_B is the Boltzmann constant. The signatures (energy level in the band gap, E_T and apparent capture cross section, σ_p) of the induced defects were calculated from the slope and *y*-intercept, respectively using log (e_p/T^2) versus (1000/*T*) Arrhenius' plots, according to the equation [14].

3. Results and discussion

Fig. 1 illustrates the DLTS spectrum obtained shortly after irradiation. The hole traps observed were: H(0.10), H(0.14) and H(0.18), where the number in brackets refers to $E_V - E_T$. As is often the case with radiation induced defects [15–17], the peaks were on a skewed baseline. The skewed baseline is often attributed to a continuum of defect states on the surface of the material induced by particle irradiation [18]. This baseline made Laplace-DLTS impossible.

The defect level H(0.10) was identified as the metastable $B_S - V$ in the B configuration [1]. This defect has two other configurations, i.e. configurations A1 and A2 which were not observed in this experiment [1,19].The apparent capture cross-section of H(0.10) was calculated to be $1.7 \times 10^{-14}\,\mathrm{cm}^2$ from the Arrhenius plot shown in Fig. 2.

H(0.14) was identified as the mono vacancy [1]. The apparent capture cross-section was $1.1 \times 10^{-14}\,\mathrm{cm}^2$. Watkins et al. found the trap to be at E_V + 0.13 eV [20]. In a theoretical paper by Antonelli et al. [21], two configurations of the single vacancy were reported. One is a metastable configuration which could be similar to the AA1-defect measured by Zangenberg et al., the other, a stable configuration of the vacancy [1].These configurations were not observed in this work.

The defect level H(0.18) was identified as a divacancy-related

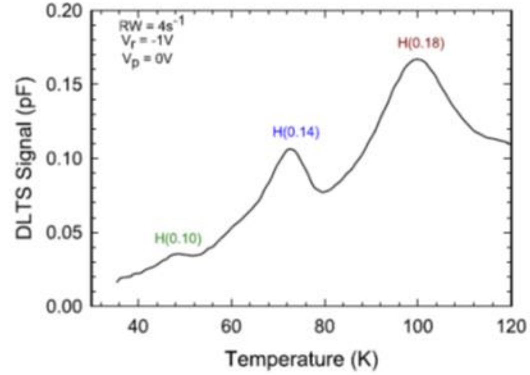

Fig. 1. DLTS spectrum showing the defects obtained soon after alpha-particle irradiation at a fluence of $3 \times 10^{13}\,\mathrm{cm}^{-2}$.

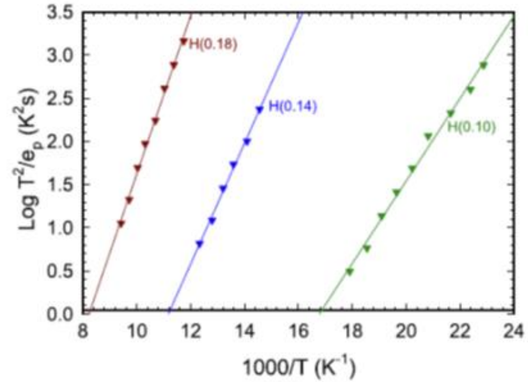

Fig. 2. Arrhenius plots of the DLTS peaks shown in Fig. 1.

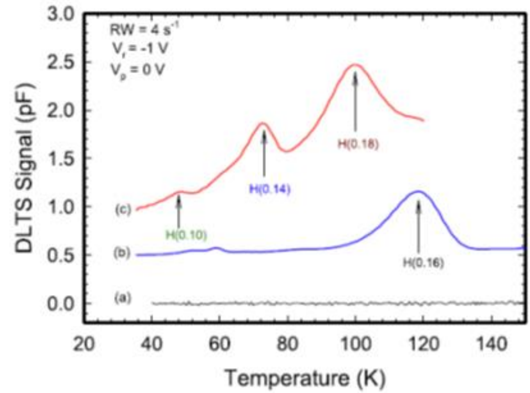

Fig. 3. DLTS spectra illustrating (a) the as-deposited sample, (b) room temperature alpha-particle irradiation and (c) low temperature alpha-particle irradiation.

Table 1
List of parameters obtained from Arrhenius plots.

Defect	DLTS parameters in this work		Comment	Literature
	$E_T \pm 0.3$ (eV)	$\sigma_p \pm 5\%$ (cm^2)		
$B_S - V$	0.10	1.7×10^{-14}	B configuration	0.105 eV [1] 0.11 eV [2]
V	0.14	1.1×10^{-14}	$(+/++)$ charge states	0.137 eV [1] 0.13 eV [12]
V_2	0.18	5.6×10^{-15}	$(0/+)$ charge states	0.189 eV [1] 0.19 eV [22] 0.20 eV [7]

defect. This defect had an apparent capture cross-section of $5.6 \times 10^{-15}\,\text{cm}^2$. A similar defect at 0.189 eV was observed by Zangenberg et al. [1,2]. Trauwaert et al. observed a defect at the H (0.19) level in both Czochralski (Cz) and FZ material with a capture cross-section between $5.0 \times 10^{-16}\,\text{cm}^2$ and $1.0 \times 10^{-15}\,\text{cm}^2$ using conventional Arrhenius analysis. This defect was attributed to the donor level of the Si divacancy [22]. Gorelkinskii et al. performed irradiation experiments using H^+ and H^{++} at 77 K. These researchers observed the $V(++/0)$, V_2, and C_i which they referred to as H1, H2 and H3 respectively. These authors observed an electron trap they called E1in their experiments. However, they did not observe the metastable defect $B_S - V$ because of the temperature ranges they conducted their measurements in.

Fig. 3 shows a comparison between room temperature irradiation and low temperature irradiation, spectra (b) and (c) respectively. Spectrum (a) is a reference spectrum of an unirradiated sample. Fig. 3 shows that when irradiation is carried out at room temperature, the defects introduced during low-temperature irradiation are not observed. While one defect at 0.16 eV is measured in the 35–115 K range after irradiation at room temperature, 3 defects are measured in the same temperature range after irradiation at 35 K. This is because the vacancies and interstitials produced upon irradiation at room temperature, recombine or react to form secondary defects [23]. The defects measured in this work are listed in Table 1 with their characteristic signatures (E_T, σ_p) and data from literature.

4. Conclusion

Defects introduced in boron-doped p-type silicon after low-temperature irradiation by alpha particles were observed. Irradiation was carried out at 35 K in a closed cycle cryostat. This allowed the observation of the H(0.10), H(0.14) and H(0.18) defects. The defect H (0.10) was identified as the configuration B of the $B_S - V$ defect, H (0.14) was identified as the mono vacancy and H(0.18) was identified as a divacancy-related defect. Defects observed after low temperature alpha-particle irradiation were not observed after room temperature alpha-particle irradiation measured in the same temperature range. Due to a skewed baseline, Laplace-DLTS measurements were not successful.

Acknowledgements

The authors would like to thank the South African National Research Foundation (NRF) and the University of Pretoria for financial support. Views and opinions expressed in this article are those of the authors and not of the NRF. We also thank Mr P.J. Janse van Rensburg and Mr M.J. Legodi for their technical assistance. The Laplace DLTS software and hardware used here was received from L. Dobaczeweski (Institute of physics, Polish Academy of Science) and A. R. Peaker (Centre for Electronic Materials Devices and Nano-structures, University of Manchester.

References

[1] N.R. Zangenberg, A.N. Larsen, On-line DLTS investigations of vacancy related defects in low-temperature electron irradiated, boron-doped Si, Appl. Phys. A – Mater. Sci. Process. 80 (2005) 1081.

[2] N. Zangenberg, J.-J. Goubet, A.N. Larsen, On-line DLTS investigations of the mono- and di-vacancy in p-type silicon after low temperature electron irradiation, Nucl. Instrum. Methods Phys. Res. B 186 (2002) 71–77.

[3] I. Pintilie, G. Lindstroem, A. Junkes, E. Fretwurst, Radiation-induced point- and cluster-related defects with strong impact on damage properties of silicon detectors, Nucl. Instrum. Methods Phys. Res. 611 (2009) 52–68.

[4] J. Coutinho, V.P. Markevich, A.R. Peaker, B. Hamilton, S.B. Lastovskii, L.I. Murin, B.J. Svensson, M.J.R.R. Briddon, Electronic and dynamical properties of the silicon trivacancy, Phys. Rev. B 86 (2012).

[5] B.L. Smith, E.H. Rhoderick, Schottky barriers on p-type silicon, Solid-State Electron. 14 (1971) 71–75.

[6] C. Nyamhere, F. Cristiano, F. Olivie, E. Bedel-Pereira, Z. Essa, Electrical and optical characterization of extended defects induced in p-type Si after Si ion implantation, Phys. Status Solidi C 11 (2014) 146–149.

[7] Y.V. Gorelkinskii, K.A. Abdullin, B.N. Mukashev, T.S. Turmagambetov, Self-interstitial and relate defects in irradiated silicon, Phys. B: Condens. Matter 404 (2009) 4579–4582.

[8] F.D. Auret, P.N.K. Deenapanray, Deep level transient spectroscopy of defects in high-energy light-particle irradiated Si, Crit. Rev. Solid State Mater. Sci. 29 (2004) 1–44.

[9] S.M. Tunhuma, M. Diale, M.J. Legodi, J.M. Nel, T.T. Thabete, F.D. Auret, Defects induced by solid state reactions at the tungsten-silicon carbide interface, J. Appl. Phys. 123 (2018).

[10] K.A. Abdulin, Y.V. Gorelkinskii, B.N. Mukashev, S.Z. Tokmoldin, Clustering of defects and impurities in hydrogenated single-crystal silicon, Semiconductors 36 (2002) 239–249.

[11] B.N. Mukashev, K.A. Abdullin, Y.V. Gorelkinskii, Interactions of primary defects with impurities in silicon, Nucl. Instrum. Methods Phys. Res. B 186 (2002) 83–87.

[12] G.D. Watkins, Intrinsic defects in silicon, Mater. Sci. Semicond. Process. 3 (2000) 227–235.

[13] H.T. Danga, F.D. Auret, S.M. Tunhuma, E. Omotoso, E. Igumbor, W.E. Meyer, Electrically active defects in p-type silicon after alpha-particle irradiation, Phys. B: Condens. Matter 535 (2018) 99–101.

[14] A.R. Peaker, V.P. Markevich, I.D. Hawkins, B. Hamilton, K.B. Nielsen, K. Gościński, Laplace deep level transient spectroscopy: embodiment and evolution, Phys. B: Condens. Matter 407 (2012) 3026–3030.

[15] S.M. Tunhuma, F.D. Auret, M. Legodi, M. Diale, Electrical Characterisation of 5.4 MeV Alpha-Particle Irradiated; Low Doped, n-Type Gallium Arsenide, South African Institute of Physics, Port Elizabeth, 2015.

[16] P.J.V. Rensburg, F.D. Auret, V. Matias, A. Vantomme, Electrical characterization of rare-earth implanted GaN, Phys. B: Condens. Matter 404 (2009) 4411–4414.

[17] S.M. Tunhuma, F.D. Auret, M.J. Legodi, J. Nel, M. Diale, Electrical characterization of defects introduced during sputter deposition of tungsten on n type 4H-SiC, Mater. Sci. Semicond. Process. 81 (2018) 122–126.

[18] J.D. Eshelby, The continuum theory of lattice defects, Solid State Phys. 3 (1956) 79.

[19] J. Adey, R. Jones, D.W. Palmer, P.R. Briddon, S. Öberg, Theory of boron-vacancy complexes in silicon, Phys. Rev. B 71 (2005).

[20] G.D. Watkins, J.H. Troxell, Negative-U properties for point defects in silicon, Phys. Rev. Lett. 44 (1980) 593–596.

[21] A. Antonelli, E. Kaxiras, D.J. Chadi, Vacancy in silicon revisited: structure and pressure effects, Phys. Rev. Lett. 81 (1998) 2028–2091.

[22] M.-A. Trauwaert, J. Vanhellemont, H.E. Maes, A.-M.V. Bavel, G. Langouche, P. Clauws, Low temperature anneal of electron irradiation induced defects in p type silicon, Mater. Sci. Technol. 14 (1998) 1295–1298.

[23] C. Claeys, E. Simoen, Radiation Effects in Advanced Semiconductor Materials and Devices, Springer, Berlin, 2002.

4.3 General discussion

In this study, a total of thirteen defects were observed. The detailed characteristics of the defects have been discussed in the previous sections. In this section, the possible reasons of the results obtained are discussed. Section 4.3.1 discusses the differences due to different contact metals used in the devices fabricated using EBD. Section 4.3.2 discusses the differences between the room and low temperature alpha-particle radiation.

4.3.1 Differences in defects formed during EBD of Ti and Ni

In any deposition process, the surface chemistry and morphology play important roles in determining the structure and properties of the deposit. For deposition of metals onto silicon, the experimental conditions should be such that oxide formation is avoided and the surface should be stable during the deposition process [15]. Despite the dip in HF Si rapidly re-grows the oxide layer [16]. Ti seems not affected by the oxide layer compared to Ni looking at the *I-V* characteristics shown in figure 4-1.Cowley [17] also came to the same conclusion. Figure 4.1 shows the *I-V* characteristics of the two devices. Ni produced a leaky diode with a bigger series resistance compared to the Ti contact. Defects can be introduced into the Si substrate during the deposition process. Deep levels associated with such defects may play a role in determining the barrier height if they are formed at or near the interface. These defects may serve as recombination-generation centres giving rise to excess current which causes deviations from ideal forward and reverse current characteristics [18].

Ti forms silicides with Si at the room temperature [19]. There is also the formation of Si rich and Ni rich silicides during thin-film deposition [20]. Ti seems more reactive with Si compared to Ni because it forms more silicide phases than Ni [19]. These differences could be attributed to the catalytic nature of Ni [16]. There is speculation that the aforementioned facts could be reason for the observed differences in the characteristics of the Ti and Ni contacts.

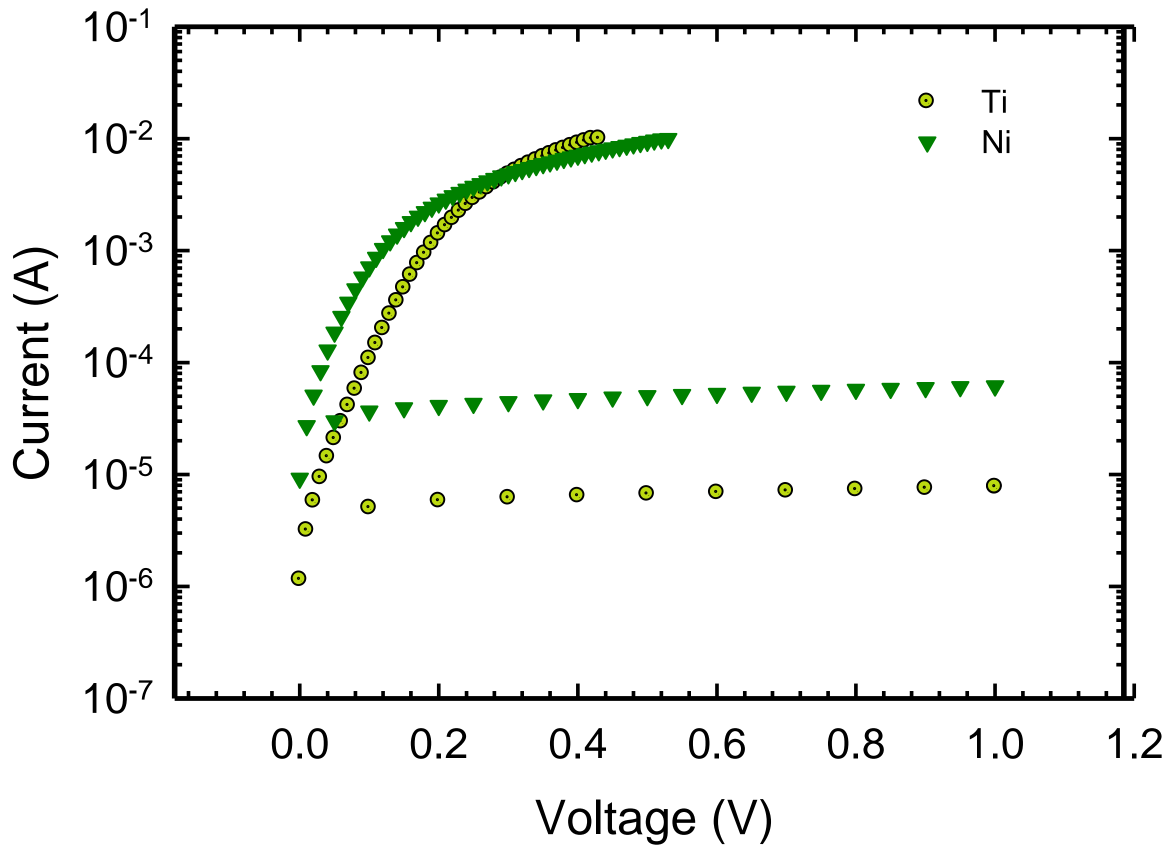

Figure 4-1 :The forward and reverse bias I-V characteristics of Ti/Si and Ni/Si Schottky contacts fabricated using EBD.

Figure 4.3 shows Arrhenius plots of all defects observed in this study. Comparing Ti and Ni EBD deposited contacts. It is clear that the two systems induce a different set of defects. In fact, while the Ti device exhibited three defects, Ni showed only one. Figure 4.2 shows the spectra of the two devices. The Ni spectrum showed two peaks with smaller heights than the Ti peaks. Although Ni showed two peaks one of them was very broad and unstable (H(y)), as a result, Laplace–DLTS could not resolve the identity of this peak.

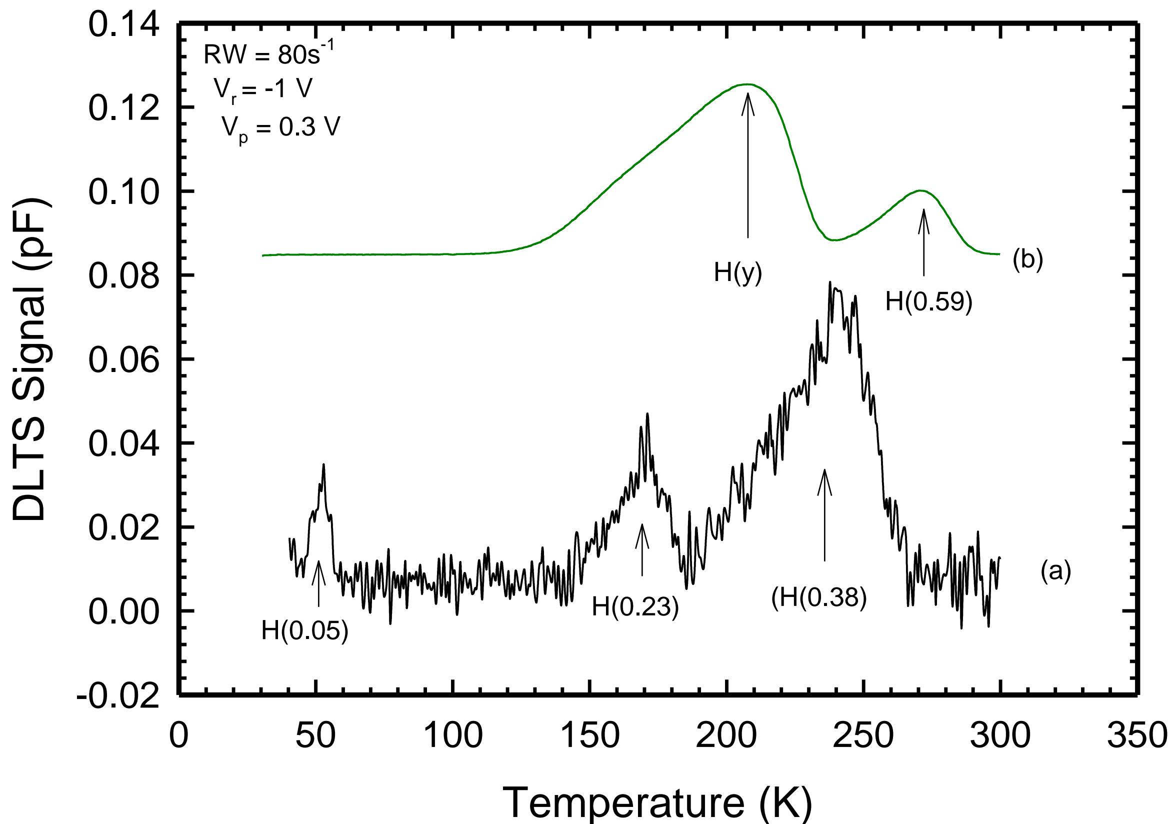

Figure 4-2: The DLTS spectra of (a) Ti/Si Schottky contacts and (b) Ni/Si Schottky contacts.

4.3.2 Alpha- particle irradiation

In this study, seven defects were measured, four after room temperature irradiation and three after low temperature irradiation. Figure 4-3 shows the Arrhenius plots of the defects observed after room temperature and low temperature irradiation. The Arrhenius plotted using black circles are those observed after room temperature alpha-particle irradiation. The red squares are the defects measured after low temperature irradiation. In the room temperature study only one vacancy-related defect was observed whereas in the low temperature study, three vacancy-related defects were observed. This is because at room temperature the vacancies and interstitials recombine so there is no permanent damage whereas during low temperature irradiation, the displaced lattice atoms do not possess enough kinetic energy to recombine. Only the interstitials are mobile at these low temperatures and all other defects are frozen in [12].

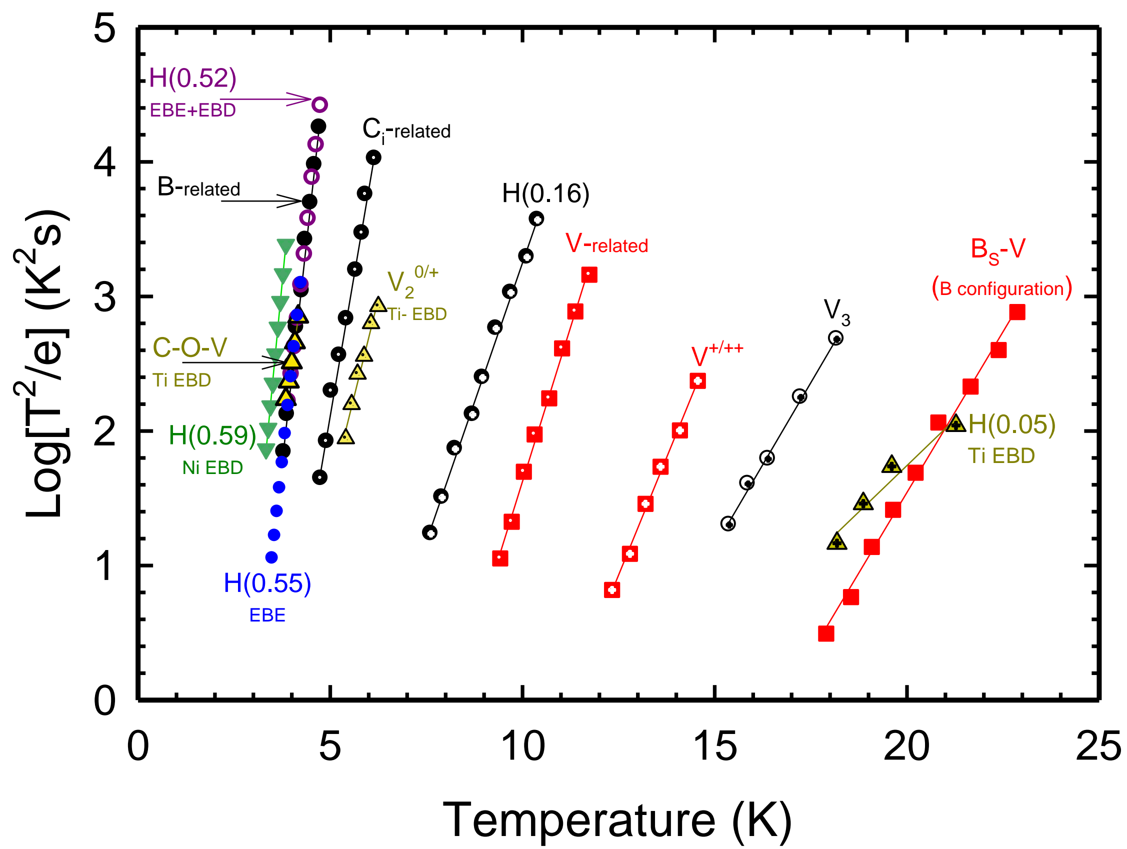

Figure 4-3: All defects measured in the current study using conventional and Laplace – DLTS.

References

[1] S.M.M. Coelho, *Electrical characterization of process induced defects in germanium,* in: Physics, University of Pretoria, Pretoria, 2015, pp. 173.

[2] F.D. Auret, S.A. Goodman, *Radiation and processed induced defects in GaN* in: M.O. Manasreh (Ed.) *III-V Nitride Semiconductors: Defects and Structural Properties* Elsevier, Amsterdam, 2000, pp. 448.

[3] R.C. Newman, *Defects in silicon*, Reports on Progress in Physics, **45** (1982) 1163.

[4] H.T. Danga, F.D. Auret, S.M.Tunhuma, E. Omotoso, E. Igumbor, W.E. Meyer, *Thermal stability of defects introduced by electron beam deposition in p-type silicon*, Nuclear Instruments and Methods in Physics Research, **409** (2017) 46-49.

[5] H.T. Danga, F.D. Auret, S.M.M. Coelho, M. Diale, Electrical *Characterisation of electron beam exposure induced Defects in silicon,* Physica B: Condensed Matter, **480** (2016) 206-208.

[6] S.M.M. Coelho, F.D. Auret, P.J.J.v. Rensburg, J.M. Nel, , *Electrical characterization of defects introduced in n-Ge during electron beam deposition or exposure,* Journal of Applied Physics, **114** (2013).

[7] H.T. Danga, F.D. Auret, S.M. Tunhuma, E. Omotoso, E. Igumbor, W.E. Meyer, *Electrical characterisation of electron beam exposure induced defects in epitaxially grown n-type silicon*, in: J.M. Andrew (Ed.) 6th International Conference on Women in Physics, IOP, Birmingham, United Kingdom, 2018.

[8] C. Claeys, E. Simoen, Radiation *Effects in Advanced Semiconductor Materials and Devices*, Springer, Berlin, 2002.

[9] G. Lindstrom, M. Ahmed, S. Albergo, P. Allport, D. Anderson, L. Andrice, M.M. Angarano, V. Augelli, N. Bacchetta, P. Bartalini, R. Bates, U. Biggeri, *Radiation hard silicon detectors*-developments by the RD48 (ROSE) collaboration, Nuclear Instruments and Methods in Physics Research A, **466** (2001) 308-326.

[10] H.T. Danga, F.D. Auret, S.M.Tunhuma, E. Omotoso, E. Igumbor, W.E. Meyer, *Electrically active defects in p-type silicon after alpha-particle irradiation,* Physica B: Condensed Matter, **535** (2018) 99-101.

[11] N. Zangenberg, J.-J. Goubet, A.N. Larsen, *On-line DLTS investigations of the mono- and di-vacancy in p-type silicon after low temperature electron irradiation*, Nuclear Instruments and Methods in Physics Research B, **186** (2002) 71–77.

[12] N.R. Zangenberg, A.N. Larsen, *On-lineDLTS investigationsof vacancy related defects in low-temperature electron irradiated,boron-doped Si*, Applied Physics A - Materials Science & Processing, 80 (2005) 1081.

[13] Y.V. Gorelkinskii, K.A. Abdullin, B.N. Mukashev, T.S. Turmagambetov, *Self-interstitial and relate defects in irradiated silicon*, Physica B: Condensed Matter, **404** (2009) 4579-4582.

[14] A.T. Paradzah, F.D. Auret, M.J. Legodi, E. Omotoso, M. Diale, *Electrical characterization of 5.4 MeV alpha-particle irradiated 4H-SiC with low doping density*, Nuclear Instruments and Methods in Physics Research Section B: Beam Interactions with Materials and Atoms, **356** (2015) 112-116.

[15] G. Oskam, J.G. Long, A. Natarajan, P.C. Searson, *Electrochemical deposition of metals onto silicon*, Journal of Physics D: Applied Physics, **31** (1998) 1927–1949.

[16] S.H. Hsieh, J.M. Hsieh, W.J. Chen, C.C. Chuang, *Electroless nickel deposition for front side metallization silicon solar cells,* Materials, 10 (2017).

[17] A.M. Cowley, *Titanium-silicon Schottky barrier diodes*, Solid-State Electronics, **12** (1969) 403.

[18] M.O. Aboelfotoh, K.N. Tu., *Schottky-barrier heights of Ti and $Tisi_2$ on n-type and p-type Si (100)* Physical Review B, **34** (1986) 2311.

[19] M.d. Giudice, J.J.Joyce, M.W. Ruckman, J.H. Weaver, *Silicide formation at the Ti/Si(111) interface:Room-temperature reaction and Schottky-barrier formation*, Physical Review B **35** (1987) 6213.

[20] J. Grunthaner, F.J. Grunthaner, *XPS study of the chemical structure of the nickel/silicon interface*, Journal of Vacuum Science and Technology, **17** (1980) 924.

5 Conclusion

The research in this thesis is a selection of the investigations done by means of the conventional and Laplace-DLTS techniques. Conclusions explicit to each of the experimental sections are given in the included papers. In this section, the conclusions pertaining to the characterisation of process and radiation induced defects using DLTS are summarised.

5.1 Electron beam deposition and electron beam exposure induced defects

Process induced defects are "a necessary evil" during device fabrication. However, having knowledge of how these defects are formed and their characteristics can be beneficial to the field of defect engineering.

EBD induced three defects in p-type silicon, albeit at very low concentration. Two of the defects were identified as the 0/+ charge state of the divacancy and the V-O-C complex. The identity of the third defect is yet to be known. Annealing removed two EBD induced defects, but one defect remained even after annealing at 400°C. Annealing not only affected the electrical characteristics of the contacts but also the surface topology of the contacts was altered during the heat treatment. AFM showed that the surface roughness increased with increase in temperature.

The EBE damage was at a higher concentration and extended deeper into the material than EBD damage–almost as deep as alpha-particle irradiation-induced damage. The defect concentration of the EBD defect was significantly less than the concentration of EBE. Interestingly, EBD and EBE introduced different defects in p-type silicon. One defect induced by EBE was similar to an alpha-particle induced defect, but this defect was not observed in EBD material. None of the EBD induced defects corresponded to alpha-particle irradiation-induced defects.

Although EBE was originally conceived as a method to investigate EBD-induced defects in more detail, after the EBE experiment only one peak was observed and this peak was not seen in EBD samples. The defect observed was identified as the I-defect. There is speculation that this may have been caused by the effects of the metal chosen to make the Schottky contacts of the EBE samples, in this case, nickel.

5.2 Room- and low-temperature alpha-particle induced defects

In this thesis radiation studies show that the defects observed during low temperature irradiation are not seen when irradiation is carried out at room temperature. After room temperature irradiation, four peaks were characterised using Laplace DLTS. Defects associated with the tri-vacancy, C_i-O_i complex, a boron-related defect were observed. The identity of one of the radiation induced defects is yet to be known.

Low temperature irradiation induced three defects which were observed in the temperature range 35-120 K. The defects were identified as the B_s-V, the vacancy and a vacancy-related defect. The resolution of the peaks using Laplace-DLTS was a challenge due to the skewed base line.

5.3 Future work

The low temperature irradiation experiment should be repeated using the Van de Graaff accelerator, which would irradiate the sample with collimated monochromatic particles at a much higher flux would lead to interesting comparative results. Furthermore, this should also simplify the measurement procedure.

Further investigation of the effects of nickel on p-Si should be carried out for a better understanding of its influence on the electrical characteristics of the material and the basic physics involved.

AIP Conference Proceedings

Electrical characterization of electron beam exposure induced defects in epitaxially grown n-type silicon

Cite as: AIP Conference Proceedings **2109**, 080003 (2019); https://doi.org/10.1063/1.5110130
Published Online: 03 June 2019

H. T. Danga, F. D. Auret, S. M. Tunhuma, E. Omotoso, E. Igumbor, and W. E. Meyer

ARTICLES YOU MAY BE INTERESTED IN

Quantum effects in nanostructures
AIP Conference Proceedings **2109**, 030003 (2019); https://doi.org/10.1063/1.5110065

From thermoelectricity to phonoelectricity
Applied Physics Reviews **6**, 021305 (2019); https://doi.org/10.1063/1.5031425

Conformality in atomic layer deposition: Current status overview of analysis and modelling
Applied Physics Reviews **6**, 021302 (2019); https://doi.org/10.1063/1.5060967

AIP Conference Proceedings **2109**, 080003 (2019); https://doi.org/10.1063/1.5110130 **2109**, 080003

© 2019 Author(s).

Electrical Characterization of Electron Beam Exposure Induced Defects in Epitaxially Grown n-type Silicon

H. T. Danga[1, a)], F. D. Auret[1], S. M. Tunhuma[1], E. Omotoso[1], E. Igumbor[1], and W. E. Meyer[1]

[1]*University of Pretoria, Lynnwood Road, Pretoria 0002, South Africa*

[a)]helga.danga@up.ac.za

Abstract. In this paper, we report on defects introduced in epitaxially grown n-type silicon (Si) during electron beam exposure. The defects observed were electrically characterized using deep-level transient spectroscopy (DLTS) and high-resolution Laplace DLTS. In this process, Si samples were first exposed to the conditions of electron beam deposition (EBD) without depositing a metal. In this paper, this process is called electron beam exposure (EBE). After 50 minutes of EBE, gold Schottky contacts were fabricated using a resistive deposition method. The defect levels E(0.11) and E(0.17) seem to be associated with the carbon interstitial-substitutional pair C_iC_s. The C_iC_s-defect is a bistable defect with an amphoteric character in two defect configurations: A and B. The transition from configuration A to B and vice versa is made possible by a simple bond-switching transformation. A defect level E(0.21) was observed, but the defect's structure is not clear. E(0.41) and E(0.45) were also observed, associated with a divacancy and a phosphorous interstitial, respectively. E(0.47) and E(x) were observed, but their structures are still a subject of speculation.

INTRODUCTION

Electron beam deposition (EBD) of metals in a vacuum system is important in the semiconductor technology industry [1, 2]. This method is useful for depositing materials that have a high melting point and therefore cannot be evaporated by resistive heating because of limitations of the power input. The disadvantage of EBD is that this technique introduces defects in n-type silicon (Si) close to the metal-silicon interface [3]. These defects influence device performance and alter the barrier heights of the contacts. The defects responsible for these changes are formed when energetic particles reach the semiconductor surface and interact with it, causing lattice damage [2, 4]. Depending on the application of the device, these defects may either be useful or detrimental for optimum functioning [4]. This investigation is important because it is known that the low-energy ions used in the EBD process introduce defects at and close to the metal-semiconductor junction [5]. Understanding the physical properties and occurrence of defects will potentially lead to improved device designs [6]. The main aim of developing the electron beam exposure (EBE) technique was to see whether EBD-induced defects could be introduced in a controlled manner. Excessive exposure would reduce the functionality of diodes for further study, thus putting a limit on how much damage could be introduced. Energetic particles that cause EBD damage are present during EBE but interact directly with the semiconductor material, whereas during EBD this interaction mostly occurs via the metal used as a contact [2]. Auret and colleagues did a similar study in which they compared their results to defects created by EBD and high energy electron irradiation. In the current work, we concentrate on defect formation by EBE on n-type Si.

EXPERIMENTAL PROCEDURE

Epitaxially grown P-doped n-type Si <111> grown on a highly doped Si substrate was investigated. Before metallization, the samples were first degreased and then dipped in hydrofluoric acid for 1 minute to etch off the native oxide layer. Immediately after cleaning, the samples were inserted into a vacuum system. Vacuum pumping was

Women in Physics
AIP Conf. Proc. 2109, 080003-1–080003-4; https://doi.org/10.1063/1.5110130
Published by AIP Publishing. 978-0-7354-1841-7/$30.00

carried out by a dry pump in series with a turbo molecular pump to lower the H_2 concentration. To improve the vacuum, tungsten (W) was deposited in the chamber with the sample rotated away from the evaporation source. The predeposition vacuum was typically 5×10^{-7} mbar, which was increased to approximately 3×10^{-6} mbar during the evaporation process. Because the vacuum conditions vary greatly during EBD, forming gas H15, with a composition of N_2:H_2 of 85%:15% by volume, was also used to raise the pressure in the vacuum chamber to 10^{-4} mbar and keep it constant during processing of samples selected for EBE. Electron beam exposure of samples and the fabrication of contacts using electron beam deposition were done using a 10 kV source (MDC model e-Vap 10CVS) with the samples positioned 50 cm above the crucible [3].

During EBE without metal deposition, the samples were exposed for 50 minutes; while the beam heated a tungsten source using a beam current of 100 mA, which is insufficient to evaporate tungsten, thus exposing the samples to electron beam conditions comparable to those experienced during deposition. Gold (Au) diodes were used for all the samples prepared for this study because this metal can be evaporated resistively, a process that is known to not introduce defects in concentrations measurable by deep-level transient spectroscopy (DLTS) [3]. A control sample was prepared by resistively depositing Au contacts onto n-type epitaxial material without using EBE. DLTS and high-resolution Laplace DLTS were used to characterize the defects introduced in epitaxially grown n-type Si during EBE.

RESULTS AND DISCUSSION

Figure 1 shows the seven defect levels that were observed. "E" means "electron trap," and the number after E is the activation enthalpy in eV. The activation enthalpy and the apparent cross section were calculated from the gradient and the intercept of the Arrhenius plot (shown in Fig. 2), respectively [7]. The defect levels E(0.11) and E(0.17) seem to be associated with the carbon interstitial-substitutional pair C_iC_s [8]. The C_iC_s defect is a bistable defect with amphoteric character in two defect configurations: A and B. The transition from configuration A to B and vice versa is made possible by a simple-bond switching transformation [9]. A defect with the label E(0.21) was observed. Asghar and colleagues [10] have also measured and calculated E(0.21), but the defect's structure is not clear. E(0.41) was associated with a divacancy [8]. E(0.45) was also observed and could be attributed to the E-center [3]. E(0.47) was observed, but the defect's structure is not yet known. E(x) has not yet been resolved. Measurements to identify this defect are ongoing.

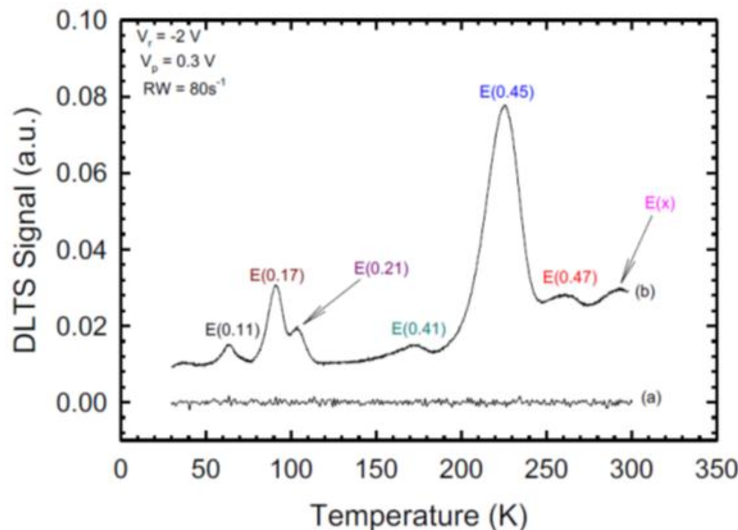

FIGURE 1. DLTS spectra: (a) a control spectrum measured from aluminum Schottky diodes fabricated using resistive deposition, and (b) a spectrum measured from nickel Schottky diodes fabricated after EBE.

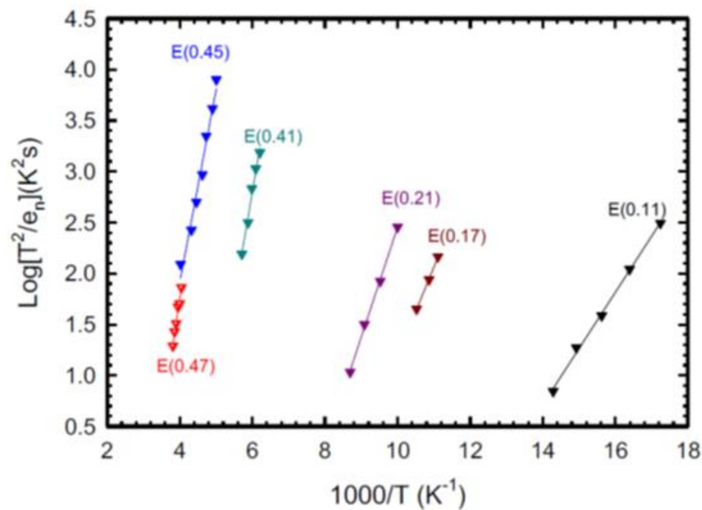

Figure 2. Arrhenius plots for defects introduced after samples were exposed to electron beam conditions (EBE) and then Au Schottky diodes were fabricated.

CONCLUSION

The defect levels E(0.11) and E(0.17) seem to be associated with the carbon interstitial-substitutional pair C_iC_s. The C_iC_s defect is a bistable defect with amphoteric character in two defect configurations: A and B. A defect level E(0.21) was observed, but the defect's structure is not clear. E(0.41) and E(0.45) were also observed, associated with a divacancy and the E-center, respectively. E(0.47) and E(x) were observed, but their structures are still a subject of speculation.

ACKNOWLEDGMENTS

This work is based on the research supported by the National Research Foundation (NRF) of South Africa under grant number 98961. Opinions, findings, and conclusions or recommendations are those of the authors, and the NRF accepts no liability whatsoever in this regard. The authors would like to thank the University of Pretoria for financial support. We also thank Mr. P. J. Janse van Rensburg for his technical assistance. The Laplace DLTS software and hardware used here was received from L. Dobaczeweski (Institute of Physics, Polish Academy of Science) and A. R. Peaker (Centre for Electronic Materials Devices and Nano-structures, University of Manchester)."

REFERENCES

1. S. M. M. Coelho, F. D. Auret, P. J. Janse van Rensburg, and J. M. Nel, "Electrical characterization of defects introduced in n-Ge during electron beam deposition or exposure," Journal of Applied Physics **114**(17), 173708 (2013).
2. H. T. Danga, F. D. Auret, S. M. M. Coelho, and M. Diale, "Electrical characterisation of electron beam exposure induced defects in silicon," Physica B: Condensed Matter **480**, 206–208 (2016).
3. F. D. Auret, S. M. M. Coelho, J. M. Nel, and W. E. Meyer, "Electrical characterization of defects introduced in n-Si during electron beam deposition of Pt," Physica Status Solidi (A) **209**(10), 1926–1933 (2012).

4. F. D. Auret, S. M. M. Coelho, M. Hayes, W. E. Meyer, and J. M Nel, "Electrical characterization of defects introduced in Ge during electron beam deposition of different metals," Physica Status Solidi (A) **205**(1), 159–161 (2008).
5. F. D. Auret, S. M. M. Coelho, G. Myburg, P. J. Janse van Rensburg, and W. E. Meyer, "Electronic and annealing properties of the E 0.31 defect introduced during Ar plasma etching of germanium," Physica B: Condensed Matter **404**(22), 4376–4378 (2009).
6. S. M. Tunhuma, F. D. Auret, M. J. Legodi, and M. Diale, "The fine structure of electron irradiation induced EL2-like defects in n-GaAs," Journal of Applied Physics **119**(14), 145705 (2016).
7. F. Danie Auret and Prakash N. K. Deenapanray, "Deep level transient spectroscopy of defects in high-energy light-particle irradiated Si," Critical Reviews in Solid State and Materials Sciences **29**(1), 1–44 (2004).
8. H. K. Nielson, "Capacitance transient measurements on point defects in silicon and silicon carbide," PhD Thesis, KTH Royal Institute of Technology, Stockholm, Sweden, 2005.
9. L. W. Song, X. D. Zhan, B. W. Benson, and G. D. Watkins, "Bistable interstitial-carbon–substitutional-carbon pair in silicon," Physical Review B **42**(9), 5765 (1990).
10. M. Asghar, M. Zafar Iqbal, and N. Zafar, "Study of alpha-radiation-induced deep levels in p-type silicon," Journal of Applied Physics **73**(9), 4240–4247 (1993).